PAUL SCHERRER INSTITUT

PSI Bericht Nr. 12-04
November, 2012
ISSN 1019-0643

Department Logistics
Division for Radiation Safety and Security

Aeroradiometric Measurements in the Framework of the Swiss Exercise ARM11

Benno Bucher, Gernot Butterweck, Ladislaus Rybach,
Georg Schwarz and Sabine Mayer

PAUL SCHERRER INSTITUT

PSI Bericht Nr. 12-04
November, 2012
ISSN 1019-0643

Department Logistics
Division for Radiation Safety and Security

Aeroradiometric Measurements in the Framework of the Swiss Exercise ARM11

Benno Bucher[1], Gernot Butterweck[2], Ladislaus Rybach[3], Georg Schwarz[1], Sabine Mayer[2]

[1] Swiss Federal Nuclear Safety Inspectorate (ENSI), Industriestrasse 19, 5200 Brugg, Switzerland
[2] Division Radiation Safety and Security, Paul Scherrer Institute (PSI), 5232 Villigen PSI, Switzerland
[3] Institut for Geophysics, Swiss Federal Institute of Technology Zürich (ETHZ), 8092 Zürich, Switzerland

Paul Scherrer Institut
5232 Villigen PSI
Switzerland
Tel. +41 56 310 21 11
Fax +41 56 310 21 99
www.psi.ch

Abstract

The measurement flights of the exercise ARM11 were performed between September 19th and 22nd under the direction of G. Scharding of the National Emergency Operations Centre (NEOC) and coordination by the Expert Group for Aeroradiometrics (FAR).
According to the alternating schedule of the annual ARM exercises, the environs of the nuclear power plants Gösgen (KKG) and Mühleberg (KKM) were inspected. No elevated radioactivity was detected in the environs of KKG and KKM.
The measurements over tunnel portals and excavated rock deposits of the New Rail Link through the Alps (NRLA) construction yielded no indication of anomalous radiological data due to the project.
Areas measured on behalf of the Federal Office for Public Health (FOPH) depicted no unusual activity concentrations.
At some of the sites, the difference of removal of ^{137}Cs deposited by the Chernobyl accident between paved and forested areas could be observed. A comparison at some sites to measurements performed nearly 20 years ago yielded ^{137}Cs activity concentrations slightly lower than would be expected from radioactive decay alone.
Elevated activity concentrations of natural radionuclides at some of the sites could be traced to the underlying geological structure.
An exercise together with emergency responders of Canton Ticino on an area of 100 m x 150 m demonstrated the limitations in spatial resolution of aeroradiometric measurements. If the position of radioactive sources is known with an uncertainty smaller than the field of view of the aeroradiometric detector, the deployment of the aeroradiometry system cannot render additional spatial information of the source locations.

CONTENTS

TABLES

FIGURES

1 INTRODUCTION

Swiss airborne gamma spectrometry measurements started in 1986. Methodology and software for calibration, data acquisition and mapping were developed at the Institute of Geophysics of the Swiss Federal Institute of Technology Zurich (ETHZ), where also the maesuring equipment was built. Between 1989 and 1993 the environs of Swiss nuclear installations were measured annually on behalf of the Swiss Federal Nuclear Safety Inspectorate (ENSI). This schedule was changed to biannual inspections in 1994, together with an organisational inclusion of the airborne gamma-spectrometric system into the Emergency Organisation Radioactivity (EOR) of the Federal Office for Civil Protection (FOCP). The deployment of the airborne gamma-spectrometric system is organized by the National Emergency Operations Centre (NEOC). Aerial operations are coordinated and performed by the Swiss Air Force. The gamma-spectrometric equipment is stationed at the military airfield of Dübendorf. The gamma-spectrometry system can be airborne within four hours.
Responsibility for scientific support, development and maintenance of the aeroradiometric measurement equipment passed from ETHZ to the Radiation Metrology Section of the Paul Scherrer Institut (PSI) in 2003 in cooperation with ENSI. General scientific coordination and planning of the annual measuring flights is provided by the Expert Group for Aeroradiometrics (FAR). FAR was a working group of the Swiss Federal Commission for NBC-protection (ComNBC) and consists of experts from all Swiss institutions concerned with aeroradiometry. FAR was re-organized as an expert group of the NEOC in 2008. Starting with 2011, the report on the results of the national aeroradiometric exercise is published in english instead of german language to facilitate easier access to international readers.
Additional information can be found at http://www.far.ensi.ch/.

1.1 Measuring System

The measuring system consists of four NaI-detectors with a total volume of 16.8 l. The spectrometer includes for each detector a 256-channel analyser with automatic gain control. The measurement control, data acquisition and storage are performed with an industrial grade personal computer. A second, identically configured PC is present in the electronics rack (Fig. 1) as redundancy. Under normal operation conditions, this PC is used for real-time evaluation and mapping of the data.The positioning uses GPS (Global Positioning System) in the improved EGNOS (European Geostationary Navigation Overlay Service) mode. Together with spectrum and position, air pressure, air temperature and radar altitude are registered.The measuring system is mounted in an Aérospatiale AS 332 Super Puma helicopter of the Swiss Air Force (Fig. 2). This helicopter has excellent navigation properties and allows emergency operation during bad weather conditions and nighttime. The detector is mounted in the cargo bay below the centre of the helicopter. The cargo bay is covered with a lightweight honeycomb plate to minimise photon absorption losses.

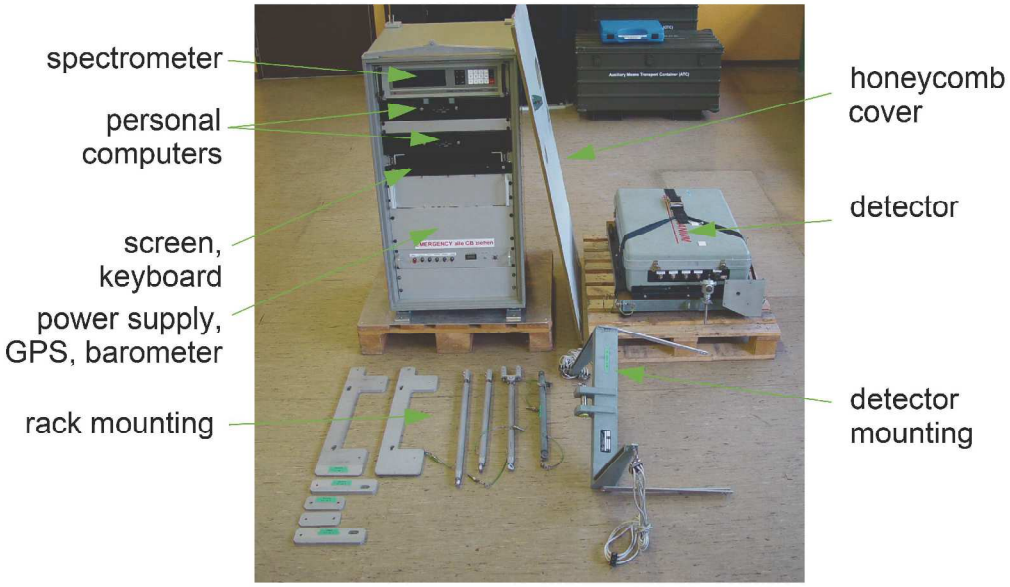

Figure 1: Measurement system of the Swiss team.

Figure 2: Super Puma helicopter of the Swiss Air Force.

1.2 Measuring flights

The advantage of aeroradiometric measurements lies in the high velocity of measurements in a large area, even over rough terrain. Uniform radiological information of an area is obtained from a regular grid of measuring points. This grid is composed from parallel flight lines which are 100 m to 500 m apart, dependent on the scope of the measurement. The flight altitude above ground is kept constant during the measuring flight. Typical values lie between 50 m and 100 m above ground. The

spectra are recorded in regular time intervals of typical one second, yielding an integration over 28 meters of the flight line at a velocity of 100 km/h.

1.3 Data evaluation

The data evaluation follows the methodology described in Schwarz (1991). Since the year 2000, a software developed by the Research Group for Geothermics and Radiometry of the Institute of Geophysics of the Swiss Federal Institute of Technology Zürich (ETHZ) with on-line mapping options (Bucher, 2001) is used.
Starting with this report, data from a minimum of two measured spectra per grid cell are averaged for the production of the maps to reduce artefacts due to poor counting statistics in a single spectrum.
Further introduced are maps of the count rate in the high Man-Made-Gross-Counts (MMGC) energy window as an indicator, where the highly sensitive MMGC ratio has a higher probability for false positive signals. The MMGC ratio is a useful tool for determining areas of potential concern. On the other hand, it can lead to misinterpretations due to its high sensitivity. Already a small underestimation of the count rate in the high MMGC energy window due to counting statistics can lead to false positive readings. Therefore, maps of the raw count rate in the high MMGC energy window with reversed colour scale (red colour denotes unusual low values of the count rate) can assist in locating the probability of a false positive MMGC indication.

2 RESULTS OF THE MEASURING FLIGHTS DURING THE EXERCISE ARM11

Flight parameters and data of ARM11 are listed in Tables 1 and 2. Flight velocity of all measuring flights was around 30 m/s. The counting interval of the spectra was one second.

Table 1: Flight parameters of the exercise ARM11.

Location	Line spacing [m]	Area [km^2]	Ground clearance [m]	Direction [Degree]
KKM	125	79	90	60/240
KKG	125	70	90	90/270
Reussdelta	125	5	90	50/230
Sedrun	125	5	90	80/260
Pizzo Ometto	125	6	90	55/235 140/320
Rasa	125	2	90	90/270
Sigirino	125	6	90	135/315
Chiasso	125	21	90	90/270
Novazzano - Genestrerio	125	6	90	135/315
Croglio	125	2	90	135/315
Novaggio	125	1	90	115/295
Vezia	125	2	90	0/180
Rodi	125	4	90	120/300
Faido - Portal	125	4	90	125/305
Faido - Deposit	125	5	90	160/340
Bodio	125	4	90	125/305
Biasca	125	7	90	10/190
Monte Ceneri	variable	2	variable	variable
Camorino	125	6	90	60/240
Piz Giuv	250	29	90	90/270 165/345
Affoltern (ZH)	125	4	90	135/315

Table 2: Flight data of the exercise ARM11.

Location	Flight number	Date	Effective measuring time [s]	Length of run [km]
KKM	2011005	19.9.2011	7076	311
KKG	2011006	19.9.2011	6549	279
Reussdelta	2011007	20.9.2011	680	30
Sedrun	2011011	20.9.2011	1326	36
Pizzo Ometto	2011012	20.9.2011	2254	36
Rasa	2011013	20.9.2011	521	11
Sigirino	2011014	20.9.2011	1164	38
Chiasso	2011015	21.9.2011	3300	156
Novazzano - Genestrerio	2011016	21.9.2011	1036	37
Croglio	2011017	21.9.2011	336	11
Novaggio	2011018	21.9.2011	248	6
Vezia	2011019	21.9.2011	260	9
Rodi	2011020	21.9.2011	587	21
Faido - Portal	2011021	21.9.2011	857	25
Faido - Deposit	2011022	21.9.2011	657	26
Bodio	2011023	21.9.2011	542	24
Biasca	2011024	21.9.2011	1151	46
Monte Ceneri	2011027, 2011028, 2011029	22.9.2011	1704	54
Camorino	2011030	22.9.2011	870	36
Piz Giuv	2011031	22.9.2011	5560	120
Affoltern (ZH)	2011032	22.9.2011	619	25

The flights of the exercise ARM11 were performed with a Super Puma helicopter of the Swiss Air Force between September 19th and 22nd. The exercise was directed by G. Scharding (NEOC). Personnel of the military unit Stab BR NAZ performed the measurements supported by experts from ENSI and PSI.

2.1 Recurrent measurement areas around KKM and KKG

According to a biannual rotation of routine measurements, the environs of the nuclear power plants Mühleberg (KKM) and Gösgen (KKG) were inspected in 2011. KKM was in shut-down during the flights due to its annual revision. Thus, the signal in the dose rate map (Fig. 10) is weak. The map of the Man-Made-Gross-Count (MMGC) ratio (Fig. 11) shows a clear peak over the plant premises. The MMGC ratio is the quotient of the count rate in the energy interval between 400 keV and 1400 keV to the count rate in the energy interval between 1400 keV and 3000 keV. The photon spectrum over the plant premises (Fig. 3) lacks the high-energy photon radiation of the radionuclide ^{16}N originating from the main steam duct in the power house which is observed during operation of the reactor. Nevertheless, the photon spectrum shows the emissions of ^{60}Co at 1173 keV and 1333 keV, together with an increased count rate at lower energies due to Compton-scattered radiation of ^{60}Co. Therefore, the premises of KKM show also increased values in the map of the ^{137}Cs activity concentration (Fig. 12). The source of the ^{60}Co radiation were radioactive components, which were stored temporarily on the power plant premises during maintenance shutdown.
The Map of the ^{137}Cs activity concentration (Fig. 12) shows normal background readings outside of the premises of KKM.

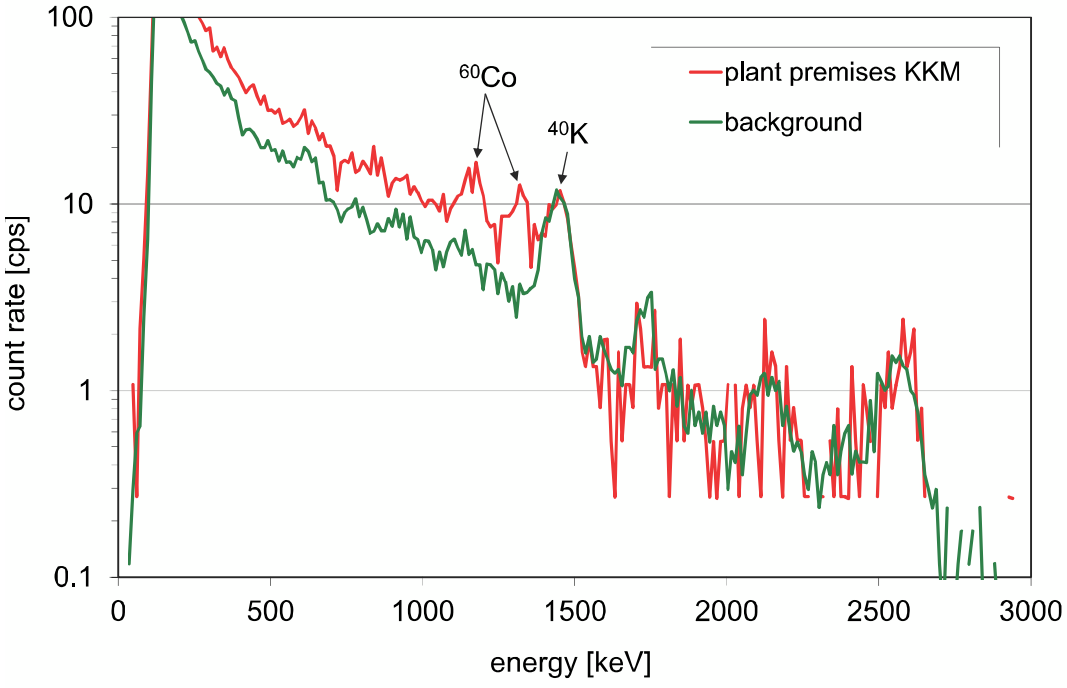

Figure 3: Photon spectrum over the KKM power plant premises compared to the areas outside.

At the pressurized reactor of the nuclear power plant Gösgen (KKG), the main steam stays in the well shielded reactor building. Therefore, KKG shows neither in the dose rate map (Fig. 13) nor in the map of the MMGC ratio (Fig. 14).

The MMGC ratio records elevated values (Fig. 14) next to the railway line at coordinates x=640000 m and y=244850 m. Following the reasoning outlined in paragraph 1.3, the map of the raw count rate in the high MMGC energy window is shown in figure 15. For this map, the usual colour scale is reversed, so that a red colour denotes unusual low values of the count rate. The probability of a false positive MMGC indication is larger in the red areas of the count rate map.
Comparison of details of both maps (Fig. 16 and 17) leads to the result that an unusually low count rate in the high MMGC energy interval is not the cause of the elevated MMGC ratio.
With the exception of the natural radionuclides ^{40}K and ^{208}Tl, the photon spectrum over the coordinate with the elevated MMGC ratio depicts no peaks which could be associated with a specific radionuclide (Fig. 4). The whole range below 750 keV shows increased count rates, thus causing additionally an increased signal in the ^{137}Cs energy window leading to a slightly elevated activity concentration in the ^{137}Cs map (Fig. 18).
A commercial irradiation facility is located at the coordinate under consideration. The photon spectrum leads to the assumption, that scattered radiation of the applied accelerators was observed. The detail of the dose rate map (Fig. 19) shows in this area no significantly elevated values.
Apart from this point, the map of the ^{137}Cs activity concentration (Fig. 20) shows normal background readings in the whole area.

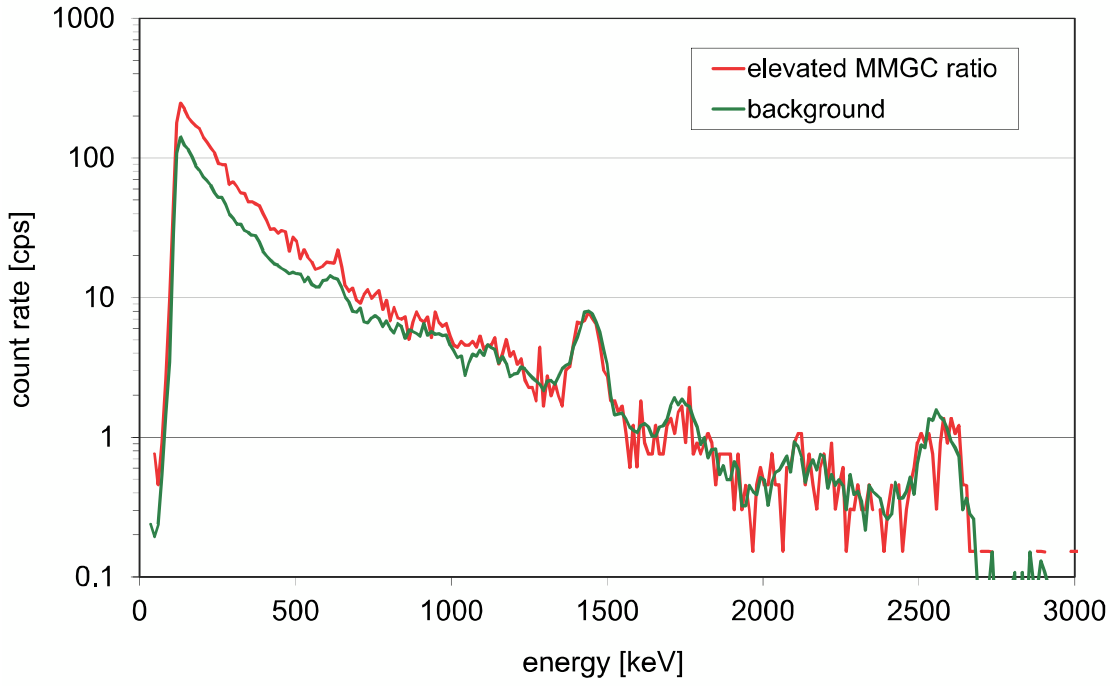

Figure 4: Photon spectrum over the coordinate with elevated MMGC ratio near KKG compared to the background.

2.2 Portals and excavated rock deposits of NRLA

The New Rail Link through the Alps (NRLA) requires large construction projects, especially the Gotthard and Ceneri base tunnels. As rock layers with elevated concentrations of uranium, thorium and potassium may be tunnelled, radioactivity has to be monitored for industrial safety and safe recycling of excavated rocks.

2.2.1 Reuss delta

The only distinct feature of the dose rate map over the NRLA landfills in the delta of the Reuss river at Lake Luzern is the reduction of dose rate due to photon absorption in water (Fig. 21).

2.2.2 Sedrun

Values of the terrestrial dose rate are slightly elevated in the eastern part of the measurement area (Fig.22). The increased values are outside of the zone affected from the NRLA earthworks. The maps of the natural radionuclides ^{40}K and ^{232}Th (Figs. 23 and 24) suggest that the increased values of the terrestrial dose rate originates from these nuclides. No indication of elevated amounts of artificial radionuclides was detected.

2.2.3 Sigirino

A landfill with material from the NRLA excavations is located near the village of Sigirino. The terrestrial dose rate (Fig. 25) shows slightly increased values over a part of the landfill. Elevated values of the ^{137}Cs activity concentration are located over forested areas, while the inhabited regions with buildings and roads show distinctly lower concentrations (Fig. 26). The increased values of the terrestrial dose rate in the western part of the measured area do not correspond with the pattern of ^{137}Cs distribution, but are reflected in the distribution of the natural radionuclides ^{40}K (Fig. 27) and ^{232}Th (Fig. 28). This indicates that the excavated rock in the landfill exhibits slightly larger amounts of natural radionuclides than the surrounding natural rock formations.

2.2.4 Vezia (Breganzona)

The target of the measurement near Vezia was the southern portal of the NRLA Ceneri Tunnel. Unfortunately, the flight was not performed as planned and the actual measured area is located about 2 km south of the portal over Breganzona, Massagno and Sorengo. The map of total dose rate (Fig. 29) depicts no peculiarities.

2.2.5 Faido - Portal and Deposits

For the reduction of construction time of the NRLA Gotthard base tunnel, an auxiliary tunnel was driven at Faido. The construction site is located in the northern part of the measurement area. Some of the excavated rock from the auxiliary tunnel at Faido was deposited south of the construction site. The vicinity of the Faido tunnel portal and deposits was inspected aeroradiometrically during the exercise

ARM11. The total dose rate (Fig. 30) follows the distribution of the natural radionuclides. The activity concentrations of the natural radionuclides ^{40}K (Fig. 32) and to a lesser extent ^{232}Th (Fig. 33) exhibit increased values in the south-eastern part of the measured area. These elevated values are found outside of the NRLA construction site over granite gneiss rock formations, similar to the findings at the adjacent Rodi area (Chapter 2.4.3).
The activity concentration of ^{137}Cs shows slightly elevated values over forested areas (Fig. 31).

2.2.6 Bodio and Biasca
The southern portal of the NRLA Gotthard base tunnel at Bodio and landfill with excavated rock near Biasca were inspected with an aeroradiometric measurement. The map of the terrestrial dose rate shows slightly elevated values in the northern part of the Bodio measurement area and in the south-eastern part of the Biasca measurement area (Fig. 34). With the exception of elevated values in the eastern part of the Biasca measurement area, the activity concentration of ^{137}Cs is distributed evenly (Fig. 35). The pattern observed in the terrestrial dose rate reflects the distribution of the natural radionuclides ^{40}K (Fig. 36) and ^{232}Th (Fig. 37). The area with increased values in the Biasca measurement area exceeds the region of the landfill. A closer look on the geological map (Fig. 36) shows that the higher values fit a post glacial rock slide, which can be thus considered the source of the elevated values.

2.2.7 Camorino
The target of the measurement near Camorino was the northern portal of the NRLA Ceneri Tunnel. The map of the dose rate (Fig. 38) shows homogeneous readings typical for the alpine region. With the exception of slightly elevated ^{137}Cs activity concentrations at the forested slopes of the valley (Fig. 39), the measurement results were also unobtrusive.

2.2.8 Affoltern a. A.
Some of the excavated rock from the NRLA Gotthard base tunnel was deposited near Affoltern am Albis. The dose rate map (Fig. 40) shows homogeneous and low values throughout the measurement area.

2.3 Pizzo Ometto

The total dose rate map of the measured area at Pizzo Ometto (Fig. 41) reflects the alpine topography of the region. The terrestrial dose rate (Fig. 42) with elevated values over Pizzo Leone and in the western part of the inspected area reproduces the pattern in the activity concentration of the natural radionuclides ^{40}K (Fig. 45) and ^{232}Th (Fig. 47). Those again are closely correlated to the rock formations in the area. Figure 46 shows that lower values of ^{40}K are encountered over a calc silicate inclusion in the surrounding gneiss.
Southern Switzerland was affected by deposition of radionuclides emitted during

the Chernobyl accident resulting in an elevated ^{137}Cs concentration in soil (Fig. 43). Part of the measured area at Pizzo Ometto was already inspected in 1999 (Fig. 44). During the time interval between 1999 and 2011, the ^{137}Cs activity concentration is reduced by radioactive decay, yielding in 2011 an expected value of 75% of the values measured in 1999. Calculating average activity concentration and standard deviation inside a polygon measured in both campaigns yields 148 ± 35 Bq/kg for the 1999 exercise and 103 ± 32 Bq/kg for the 2011 exercise. The measured reduction to 69% of the 1999 value in 2011, which is only slightly smaller than the expected reduction due to the radioactive decay, suggests that no major activity dislocation processes are in operation.
A high ^{137}Cs concentration of about 800 Bq/kg was referred in the report of the Swiss aeroradiometric exercise 1999 for a hot spot at coordinates (x=694997 m, y=109898 m). The measuring flight in 2011 could not confirm a hot spot of this activity concentration at these coordinates. The activity concentration reported in 1999 was derived from a single spectrum measured at the south-eastern precipice of Pizzo Ometto next to even higher value of 1888 Bq/kg, which was discarded due to a ground clearance larger than accepted. Figure 5 shows the measured ^{137}Cs activity concentration along the flight line including the hot spot. The dotted parts of the line mark non-valid data points with a radar height above ground larger than 200 m.
The topographical correction used in the data evaluation uses values of the digital height model DHM25 with a resolution of 25 m. The DHM25 model has the largest deviation to the recent and more precise digital terrain model SwissAlti3D just at the location of the hot spot. This leads to the conclusion, that the value measured in 1999 could be overestimated due to the correction with a digital terrain model inadequate at this point of the flight line.

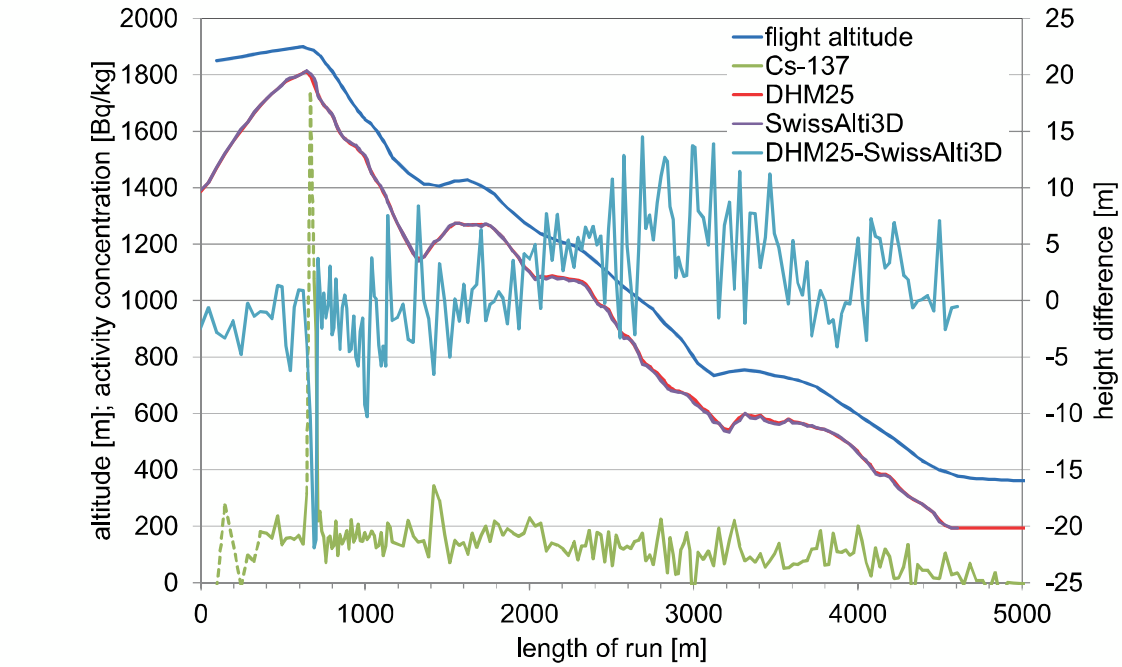

Figure 5: ^{137}Cs activity concentration measured at Pizzo Ometto in 1999, measured flight altitude, altitudes from the digital height models DHM25 and SwissAlti3D and their difference.

2.4 Reference areas of FOPH

These locations are used as reference areas for environmental measurements performed by the Federal Office of Public Health (FOPH). A summary of the measurement results is given in Figure 6. Detailed results are described in chapters 2.4.1, 2.4.2 and 2.4.3.

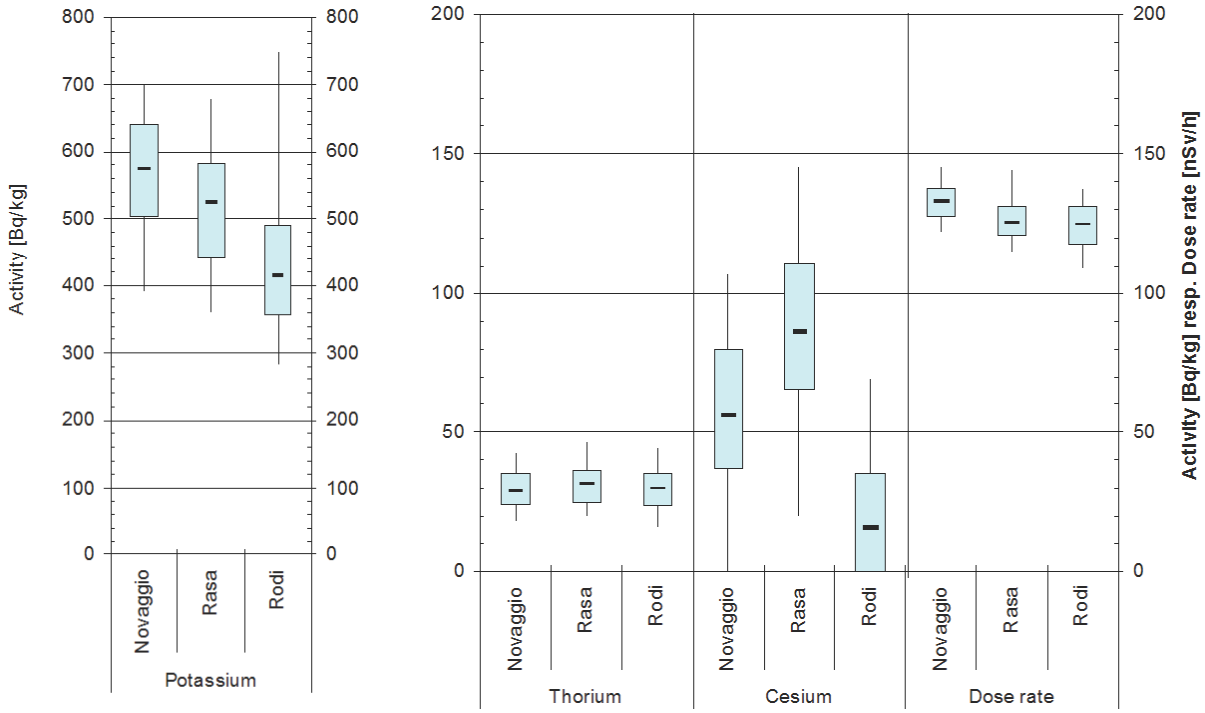

Figure 6: Statistical distribution of the results in the three reference areas of FOPH. Depicted are the 5% and 95% quantils (vertical lines), the first and third quartil (box) and the median value for activity concentrations of ^{40}K, ^{232}Th and ^{137}Cs and of the dose rate.

2.4.1 Rasa

Right next to the measuring area at Pizzo Ometto, the vicinity of Rasa was inspected. The maps of dose rate (Fig. 48), terrestrial component of the dose rate (Fig. 49) and the natural radionuclides ^{40}K (Fig. 52) and ^{232}Th (Fig. 53) show homogeneous values in the measured area. The map of the ^{137}Cs activity concentration (Fig. 50) shows still the fallout of the Chernobyl accident, with the highest values located over forested areas. The area was inspected already in the year 1998, when higher values of ^{137}Cs activity concentrations were measured in the whole area (Fig 51). The ratio of the average ^{137}Cs activity concentrations measured in the overlapping area of both surveys yields that 49% of the activity found in 1998 remain. Radioactive decay between 1998 and 2011 alone would have rendered a ratio of 74% ^{137}Cs remaining.

2.4.2 Novaggio

Like Rasa, the measured area near Novaggio is used as a reference location for environmental measurements performed by the Federal Office of Public Health (FOPH). The dose rate map (Fig. 54) and all other radiological data show unremarkable values in this region.

2.4.3 Rodi

The ^{137}Cs activity in the measured area is low and uniformly distributed (Fig. 57). The activity concentration of the natural radionuclides (Figs. 58 and 59) and to a lesser extent the total dose rate (Fig. 55) and its terrestrial component (Fig. 56) are elevated in the middle of the northernmost flight line. As can be seen from the geological map of the area (Fig. 60), this pattern conforms to the distribution between alluvial deposits (white) and granite gneiss (pink).

2.5 Chiasso

The environs of Chiasso was measured in continuation of airborne gammaspectrometric measurements over cities and towns of Switzerland. The maps of total dose rate (Fig. 61) and its terrestrial component (Fig. 62) show slightly elevated values at the coordinate (x = 721568, y = 76556). The increase of the dose rate at this point is caused by higher values of both the artificial radionuclide ^{137}Cs (Fig. 63) and the natural radionuclides ^{40}K (Fig. 64), ^{232}Th (Fig. 65) and ^{238}U. ^{238}U is detected analysing the photon emissions of the radon decay product ^{214}Bi. As this radionuclide is also present in the air surrounding the helicopter, a quantitative mapping of soil activity concentration is not expedient as the separation of airborne and soil components leads to a significant uncertainty in the calculated uranium contents. Figure 7 shows the photon spectrum over the point with elevated terrestrial dose rate. The Photon peaks of ^{137}Cs, ^{40}K, ^{214}Bi (uranium-radium decay series) and ^{208}Tl (thorium decay series) are recognizable.

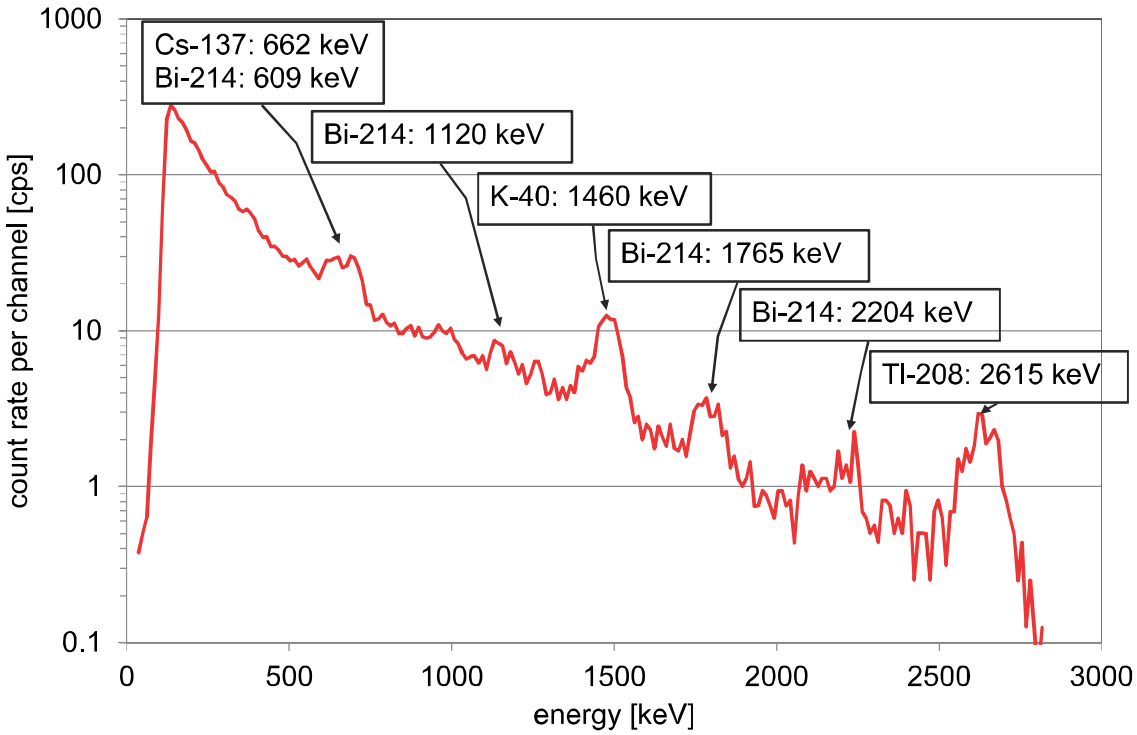

Figure 7: Photon spectrum measured at the coordinate (x = 721568, y = 76556).

2.6 Municipal waste landfill sites

Two landfills with municipal waste were inspected during the exercise ARM11.

2.6.1 Genestrerio and Novazzano

The measuring area between Genestrerio and Novazzano includes a municipal waste disposal site north of the coordinate (x = 719000, y = 79000). The waste disposal site is unremarkable in dose rate (Fig. 66).

2.6.2 Croglio

South of Croglio a closed municipal waste landfill site of 700‘000 m^3 with centre at coordinates (x = 709400, y = 92400) was inspected. The dose rate map (Fig. 67) displays no elevated values over the landfill site. At the forested north-eastern part of the measurement area, increased ^{137}Cs activity concentrations compared to the inhabited river valley can be observed (Fig. 68). The fallout from the Chernobyl accident in 1986 was washed since then from buildings and paved areas by precipitation, thus reducing the initial activity faster compared to forested regions.

2.7 Search exercise for radioactive sources at Monte Ceneri

The aeroradiometric measurements at Monte Ceneri were included in an emergency drill of first responders of Canton Ticino. The exercise simulated an accident of a lorry carrying radioactive material. Figure 8 shows the layout of the exercise scenario, which included that radioactive sources were expelled from the lorry due to the impact. Test sources were supplied by PSI and hidden near the simulated accident location. Radiation protection personnel of PSI assured safety and security during the exercise. The exercise area, sized approximately 100 m x 150 m, was far below the target dimensions commonly requesting the application of airborne gamma spectrometry. Thus, tests of different search strategies applicable to small search areas were performed.

The standard search procedure applied since the exercise ARM07 targets a high flight line density in a low altitude above ground, both dependent of the terrain inspected. An optimum flight line density is achieved by finding the maximum flight velocity at which safety and constant ground clearance can still be maintained.

This strategy failed at Monte Ceneri, because the time gain due to the higher velocity on the flight line was rendered obsolete by the increased time necessary for slowing and turning the helicopter. Thus, the manual approach used prior to 2007 was deemed more efficient. The operators analyse the radiological maps on-line and direct the pilots to points where more information is requested. The flight velocity of this strategy is low and may cause more damage on the ground due to the downdraft of the helicopter. For this reason, the minimal ground clearance was set to 100 m.

Figure 8: Simulated accident scenario of the exercise at Monte Ceneri.

Figure 69 shows flight lines and the total dose rate measured during the accident exercise. The actual exercise area was too small for the helicopter to turn and thus the flight lines extend into the surrounding region. The real extent of the exercise area, together with the placed radioactive sources is depicted in figure 70. As can be seen, the usual grid spacing of 125 m which is usually employed for mapping is too coarse to separate the location of the different sources. In figure 71 the grid cell size is reduced to 25 m to gain additional information on the location of the sources. Nevertheless, it should be noted that the field of view of the detector at each measuring point still represents roughly a circle with a diameter of 300 m, thus covering the whole exercise area. The MMGC ratio (Fig. 72), which is a very sensitive parameter in the detection of artificial radionuclides shows high values throughout the exercise area. A re-scaling of the colour code of the MMGC ratio (Fig. 73) did not facilitate a more detailed location of the radioactive sources placed in the exercise area. During the exercise, the measuring team reported three suspected radioactive sources at the coordinates (x = 713 094, y = 110 857), (x = 713 015, y = 110 884) and (x = 713 136, y = 110 937) to the ground teams. The location of placed radioactive sources was determined with a handheld GPS-receiver, yielding the coordinates listed in Table 3. Four of these sources have an activity of 50 MBq, which is well below the detection limit of the airborne gamma-spectrometry system. The source coordinates (yellow circles) are plotted together with the coordinates estimated from the aeroradiometric data (red circles) in an aerial view of the exercise

area (Fig. 74). As can be seen, neither do the source coordinates suspected from the aeroradiometric data coincide with the real source locations (Table 3), nor do the latter agree with the aerial view. The simulated accident and thus the lorry was located in the centre of the south-western leg of the road, thus the position determined with the hand-held GPS is shifted about 50 m north east.
The small size of the exercise area of 100 m x 150 m demonstrates the resolution limitations of the aeroradiometric system. The results show clearly, that in the case of source positions known to an uncertainty around 100 m, deployment of the aeroradiometric system does not yield additional information on the position of the sources.

Table 3: Radioactive sources placed in the exercise area at Monte Ceneri.

Coordinate [m]		Nuclide	Activity [MBq]
x	y		
713142	110796	^{60}Co	50
713151	110821	^{60}Co	50
713128	110883	^{60}Co	300
713144	110950	^{137}Cs	500
713086	110844	^{60}Co	50
713061	110897	^{60}Co	100
713107	110885	^{60}Co	50

2.8 Piz Giuv

The terrestrial component of the dose rate, consisting of the total dose rate reduced by the cosmic component, depicts elevated values in the south-western part of the measurement area located adjacent to the north-east of Piz Giuv (Fig. 75). This elevation of the terrestrial dose rate was already observed in 1998 (Fig. 76) in the same location. The areas with elevated terrestrial dose rates correspond with an increased activity concentration of the natural radionuclide ^{232}Th (Figs. 77 and 78). The pattern of the elevated activity concentration of ^{232}Th coincides with material from a post-glacial mountain slide depicted in the geological map (Fig. 79) as grey dotted area.
The photon spectrum averaged over the area with elevated ^{232}Th-concentrations (Fig. 9) shows a mixture of peaks associated with radionuclides of the ^{232}Th- and ^{238}U-decay series. This indicates also elevated concentrations of ^{238}U in the post glacial mountain slide.

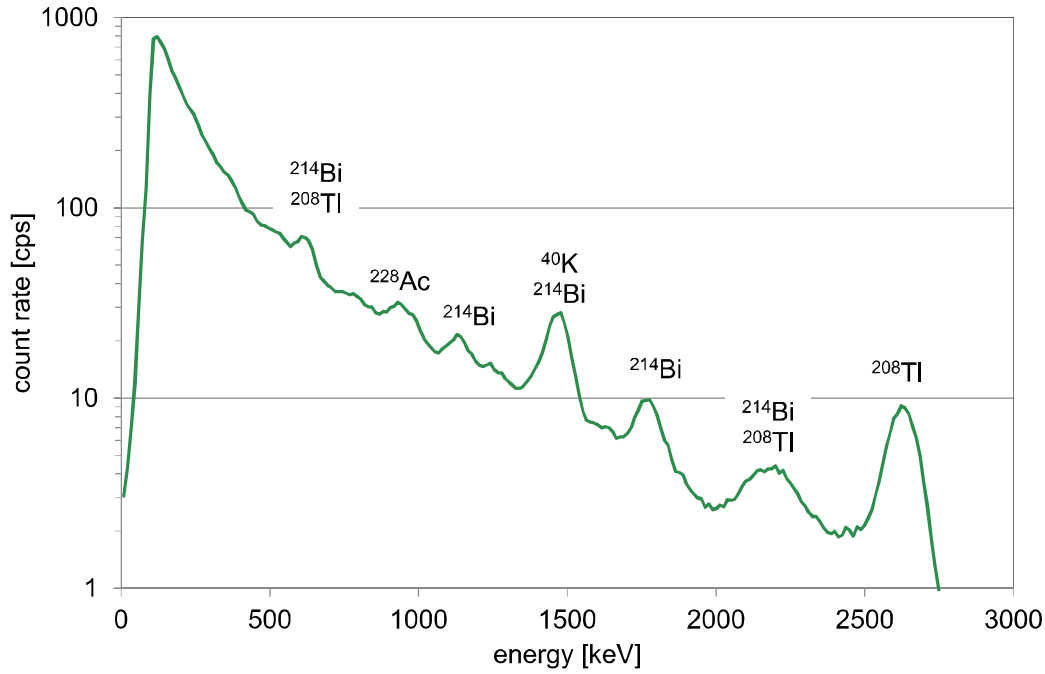

Figure 9: Average photon spectrum over the area with increased ^{232}Th-concentrations at Piz Giuv.

3 CONCLUSIONS

Like in previous years no elevated radioactivity was detected in the environs of the nuclear power plants KKG and KKM.
The measurements over tunnel portals and excavated rock deposits of the NRLA construction yielded no indication of anomalous radiological data due to the project.
Areas measured on behalf of the Federal Office for Public Health (FOPH) depicted no unusual activity concentrations.
At some of the sites, the difference of removal of ^{137}Cs deposited by the Chernobyl accident between paved and forested areas could be observed. A comparison at some sites to measurements performed nearly 20 years ago yielded ^{137}Cs activity concentrations slightly lower than would be expected from radioactive decay alone.
Elevated activity concentrations of natural radionuclides at some of the sites could be traced to the underlying geological structure.
An exercise together with emergency responders of Canton Ticino on an area of 100 m x 150 m demonstrated the limitations in spatial resolution of aeroradiometric measurements for locating radioactive sources. If the position of radioactive sources is known with an uncertainty smaller than the field of view of the aeroradiometric detector, the deployment of the aeroradiometry system cannot render additional spatial information of the sources.

4 LITERATURE

Schwarz, G. F.: Methodische Entwicklungen zur Aerogammaspektrometrie. Beiträge zur Geologie der Schweiz, Geophysik Nr.23, Schweizerische Geophysikalische Kommission, 1991.

Bucher, B.: Methodische Weiterentwicklungen in der Aeroradiometrie. Dissertation Nr. 13973, ETH Zürich, 2001.

5 PREVIOUS REPORTS

Schwarz, G. F., Klingelé, E. E., Rybach, L.: Aeroradiometrische Messungen in der Umgebung der schweizerischen Kernanlagen. Bericht für das Jahr 1989 zuhanden der Hauptabteilung für die Sicherheit der Kernanlagen (HSK). Interner Bericht, Institut für Geophysik, ETH Zürich, 1990.

Schwarz, G. F., Klingelé, E. E., Rybach, L.: Aeroradiometrische Messungen in der Umgebung der schweizerischen Kernanlagen. Bericht für das Jahr 1990 zuhanden der Hauptabteilung für die Sicherheit der Kernanlagen (HSK). Interner Bericht, Institut für Geophysik, ETH Zürich, 1991.

Schwarz, G. F., Klingelé, E. E., Rybach, L.: Aeroradiometrische Messungen in der Umgebung der schweizerischen Kernanlagen. Bericht für das Jahr 1991 zuhanden der Hauptabteilung für die Sicherheit der Kernanlagen (HSK). Interner Bericht, Institut für Geophysik, ETH Zürich, 1992.

Schwarz, G. F., Klingelé, E. E., Rybach, L.: Aeroradiometrische Messungen in der Umgebung der schweizerischen Kernanlagen. Bericht für das Jahr 1992 zuhanden der Hauptabteilung für die Sicherheit der Kernanlagen (HSK). Interner Bericht, Institut für Geophysik, ETH Zürich, 1993.

Schwarz, G. F., Klingelé, E. E., Rybach, L.: Aeroradiometrische Messungen in der Umgebung der schweizerischen Kernanlagen. Bericht für das Jahr 1993 zuhanden der Hauptabteilung für die Sicherheit der Kernanlagen (HSK). Interner Bericht, Institut für Geophysik, ETH Zürich, 1994.

Schwarz, G. F., Rybach, L.: Aeroradiometrische Messungen im Rahmen der Übung ARM94. Bericht für das Jahr 1994 zuhanden der Fachgruppe Aeroradiometrie (FAR). Interner Bericht, Institut für Geophysik, ETH Zürich, 1995.

Schwarz, G. F., Rybach, L.: Aeroradiometrische Messungen im Rahmen der Übung ARM95. Bericht für das Jahr 1995 zuhanden der Fachgruppe Aeroradiometrie (FAR). Interner Bericht, Institut für Geophysik, ETH Zürich, 1996.

Schwarz, G. F., Rybach, L., Bärlocher, C.: Aeroradiometrische Messungen im Rahmen der Übung ARM96. Bericht für das Jahr 1996 zuhanden der Fachgruppe Aeroradiometrie (FAR). Interner Bericht, Institut für Geophysik, ETH Zürich, 1997.

Bucher, B., Rybach, L., Schwarz, G., Bärlocher, C.: Aeroradiometrische Messungen im Rahmen der Übung ARM97. Bericht für das Jahr 1997 zuhanden der Fachgruppe Aeroradiometrie (FAR). Interner Bericht, Institut für Geophysik, ETH Zürich, 1998.

Bucher, B., Rybach, L., Schwarz, G., Bärlocher, C.: Aeroradiometrische Messungen im Rahmen der Übung ARM98. Bericht für das Jahr 1998 zuhanden der Fachgruppe Aeroradiometrie (FAR). Interner Bericht, Institut für Geophysik, ETH Zürich, 1999.

Bucher, B., Rybach, L., Schwarz, G., Bärlocher, C.: Aeroradiometrische Messungen im Rahmen der Übung ARM99. Bericht für das Jahr 1999 zuhanden der Fachgruppe Aeroradiometrie (FAR). Interner Bericht, Institut für Geophysik, ETH Zürich, 2000.

Bucher, B., Rybach, L., Schwarz, G., Bärlocher, C.: Aeroradiometrische Messungen im Rahmen der Übung ARM00. Bericht für das Jahr 2000 zuhanden der Fachgruppe Aeroradiometrie (FAR). Interner Bericht, Institut für Geophysik, ETH Zürich, 2001.

Bucher, B., Rybach, L., Schwarz, G., Bärlocher, C.: Aeroradiometrische Messungen im Rahmen der Übung ARM01. Bericht für das Jahr 2001 zuhanden der Fachgruppe Aeroradiometrie (FAR). Interner Bericht, Paul Scherrer Institut, Villigen, Schweiz, 2002.

Bucher, B., Rybach, L., Schwarz, G., Bärlocher, C.: Aeroradiometrische Messungen im Rahmen der Übung ARM02. Bericht für das Jahr 2002 zuhanden der Fachgruppe Aeroradiometrie (FAR). Interner Bericht, Paul Scherrer Institut, Villigen, Schweiz, 2003.

Bucher, B., Rybach, L., Schwarz, G.: Aeroradiometrische Messungen im Rahmen der Übung ARM03. PSI-Bericht 04-14, ISSN 1019-0643, Paul Scherrer Institut, Villigen, Schweiz, 2004.

Bucher, B., Butterweck, G., Rybach, L., Schwarz, G.: Aeroradiometrische Messungen im Rahmen der Übung ARM04. PSI-Bericht 05-10, ISSN 1019-0643, Paul Scherrer Institut, Villigen, Schweiz, 2005.

Bucher, B., Butterweck, G., Rybach, L., Schwarz, G.: Aeroradiometrische Messungen im Rahmen der Übung ARM05. PSI-Bericht 06-06, ISSN 1019-0643, Paul Scherrer Institut, Villigen, Schweiz, 2006.

Bucher, B., Butterweck, G., Rybach, L., Schwarz, G.: Aeroradiometrische Messungen im Rahmen der Übung ARM06. PSI-Bericht 07-02, ISSN 1019-0643, Paul Scherrer Institut, Villigen, Schweiz, 2007.

Bucher, B., Guillot, L., Strobl, C., Butterweck, G., Gutierrez, S., Thomas, M., Hohmann, C., Krol, I., Rybach, L., Schwarz, G.: International Intercomparison Exercise of Airborne Gammaspectrometric Systems of Germany, France and Switzerland in the Framework of the Swiss Exercise ARM07. PSI-Bericht Nr. 09-07, ISSN 1019-0643, Paul Scherrer Institut, Villigen, Schweiz, 2009.

Bucher, B., Butterweck, G., Rybach, L., Schwarz, G.: Aeroradiometrische Messungen im Rahmen der Übung ARM08. PSI-Bericht Nr. 09-02, ISSN 1019-0643, Paul Scherrer Institut, Villigen, Schweiz, 2009.

Bucher, B., Butterweck, G., Rybach, L., Schwarz, G., Strobl, C.: Aeroradiometrische Messungen im Rahmen der Übung ARM09. PSI-Bericht Nr. 10-01, ISSN 1019-0643, Paul Scherrer Institut, Villigen, Schweiz, 2010.

Bucher, B., Butterweck, G., Rybach, L., Schwarz, G., Mayer, S.: Aeroradiometrische Messungen im Rahmen der Übung ARM10. PSI-Bericht Nr. 11-02, ISSN 1019-0643, Paul Scherrer Institut, Villigen, Schweiz, 2011.

The reports since 1994 can be found and downloaded from the FAR website http://www.far.ensi.ch.

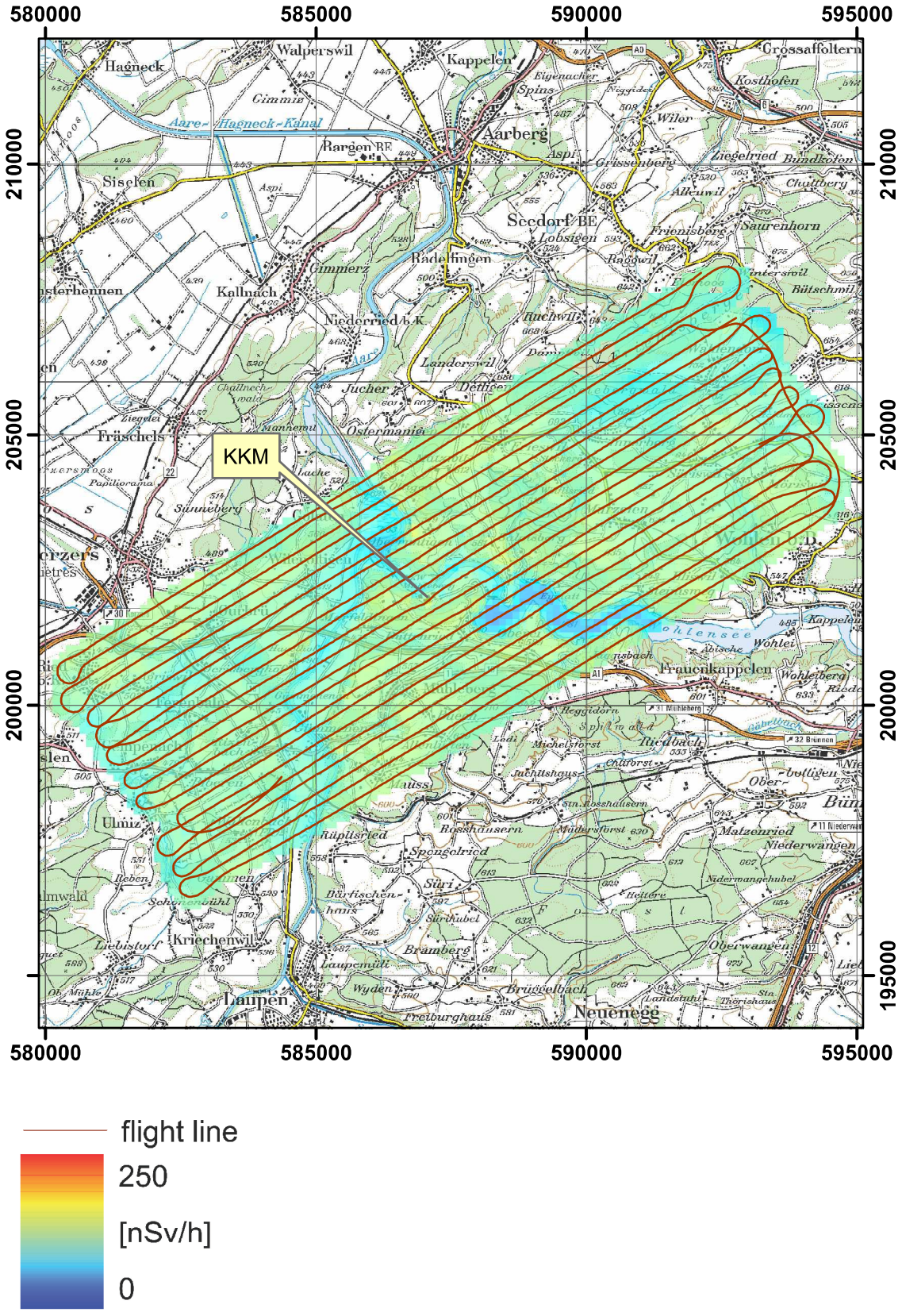

Figure 10: Dose rate in the vicinity of KKM.
PK100 © 2011 swisstopo (JD100043).

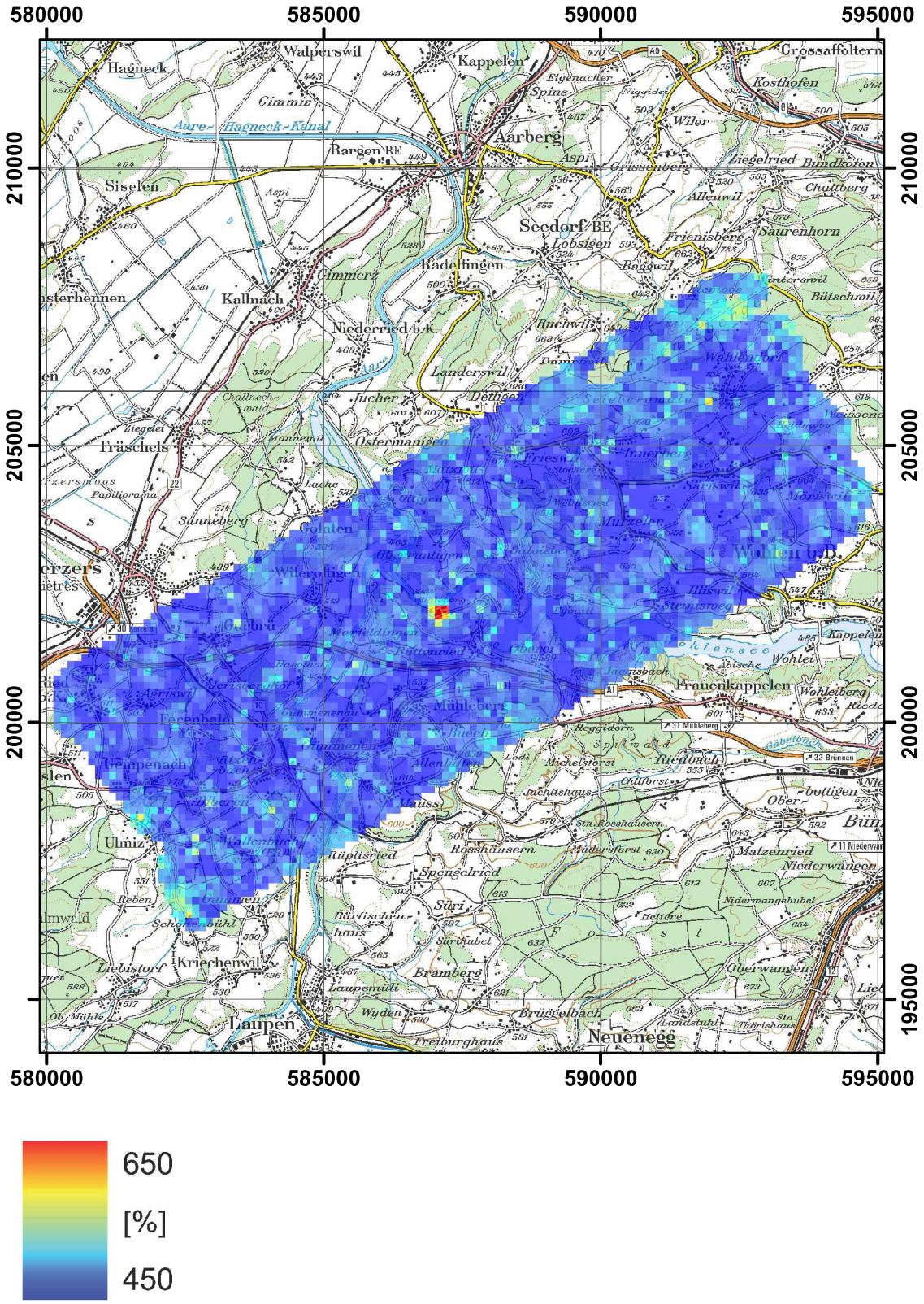

Figure 11: MMGC ratio in the vicinity of KKM.
PK100 © 2011 swisstopo (JD100043).

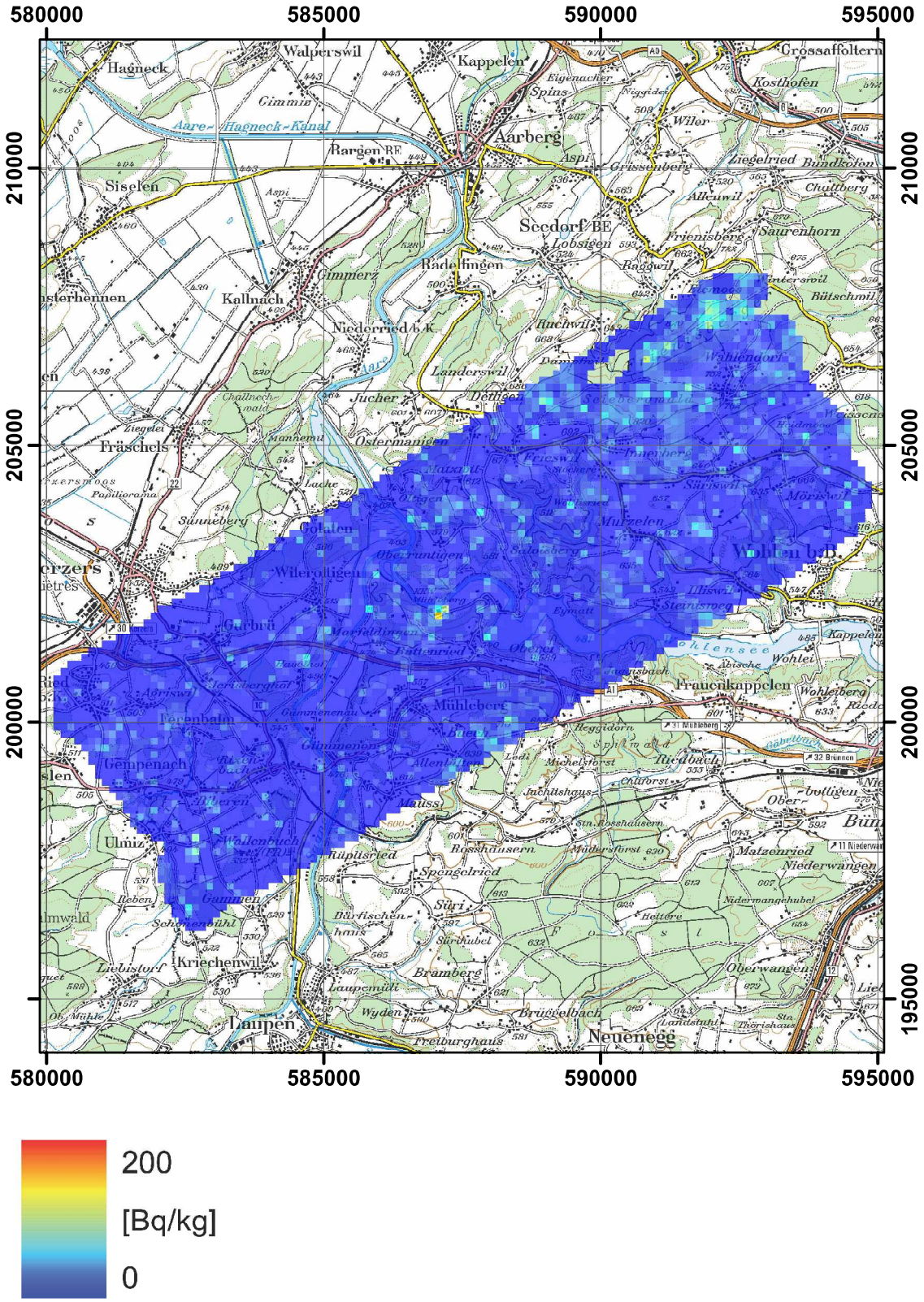

Figure 12: ^{137}Cs activity concentration in the vicinity of KKM. PK100 © 2011 swisstopo (JD100043).

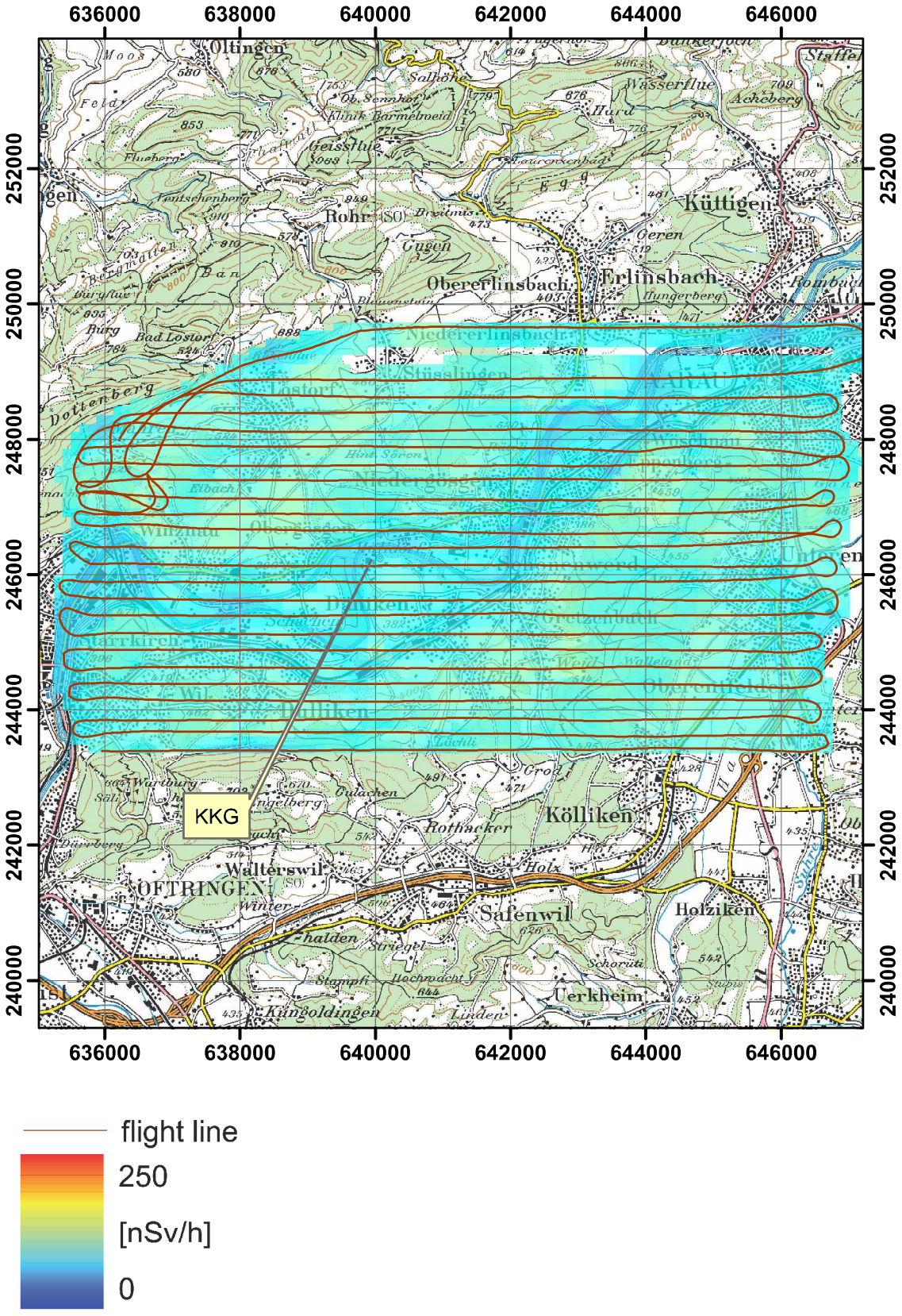

Figure 13: Dose rate in the vicinity of KKG.
PK100 © 2011 swisstopo (JD100043).

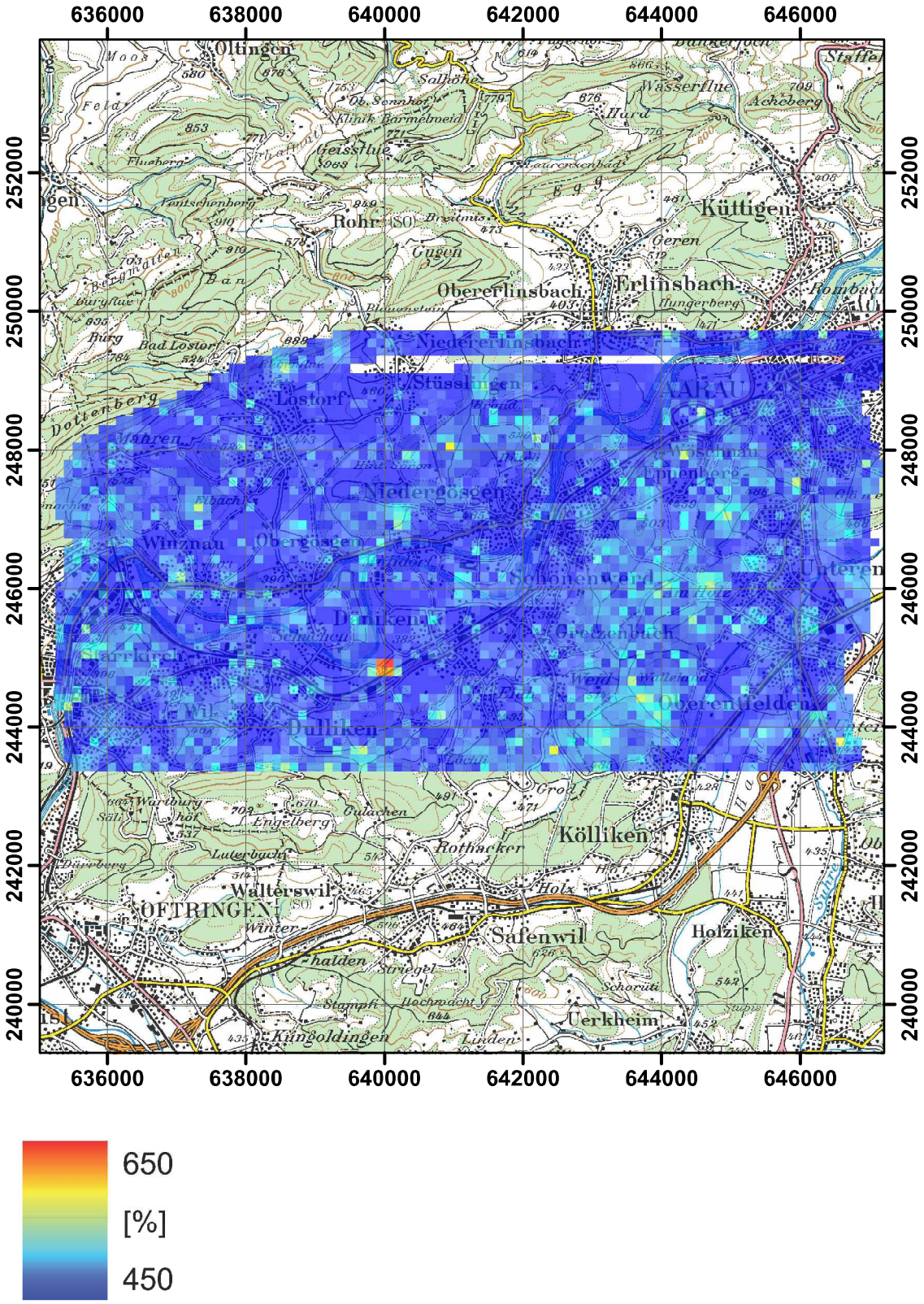

Figure 14: MMGC ratio in the vicinity of KKG.
PK100 © 2011 swisstopo (JD100043).

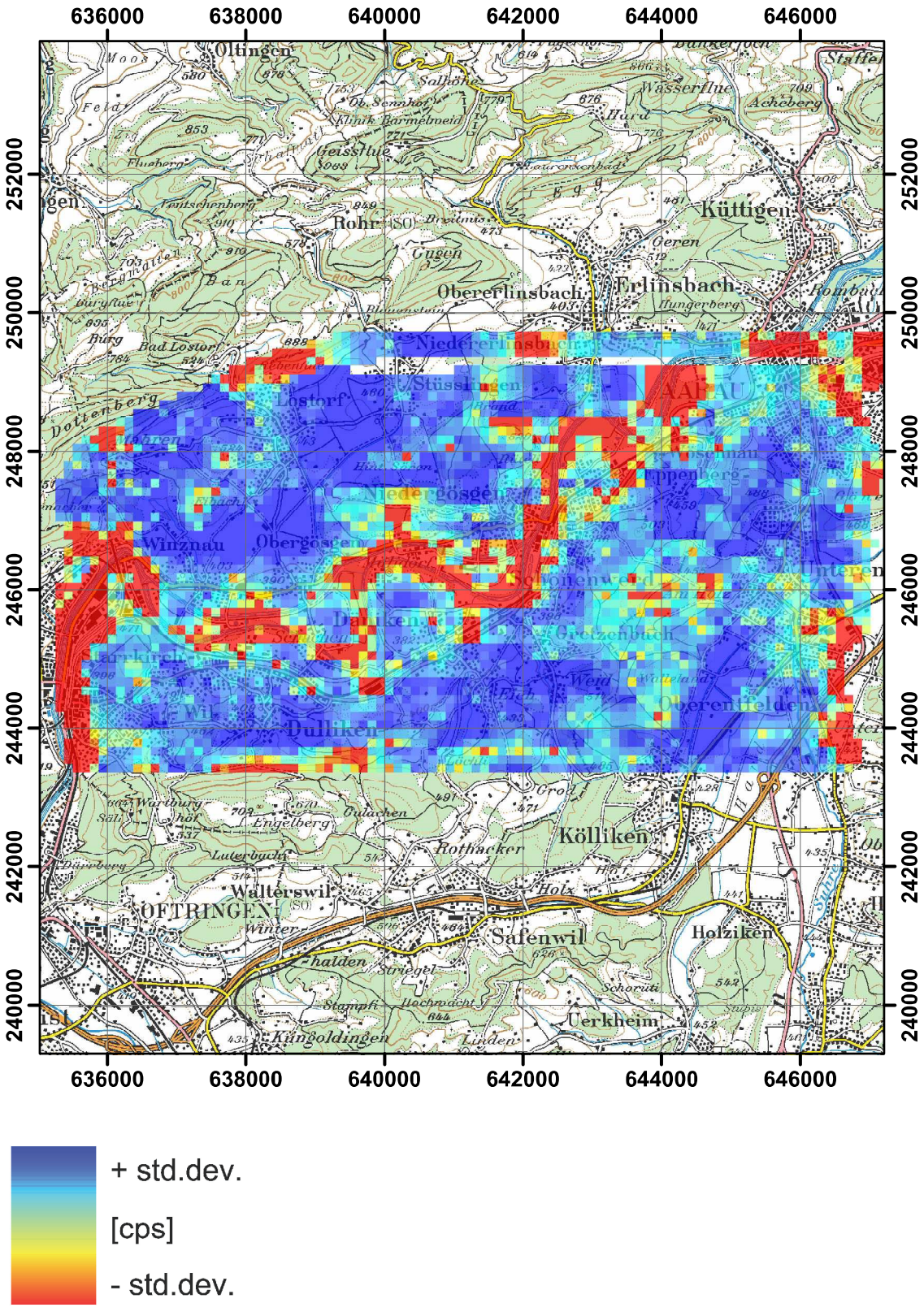

Figure 15: Variation of the raw count rate in the high MMGC energy window in the vicinity of KKG. PK100 © 2011 swisstopo (JD100043).

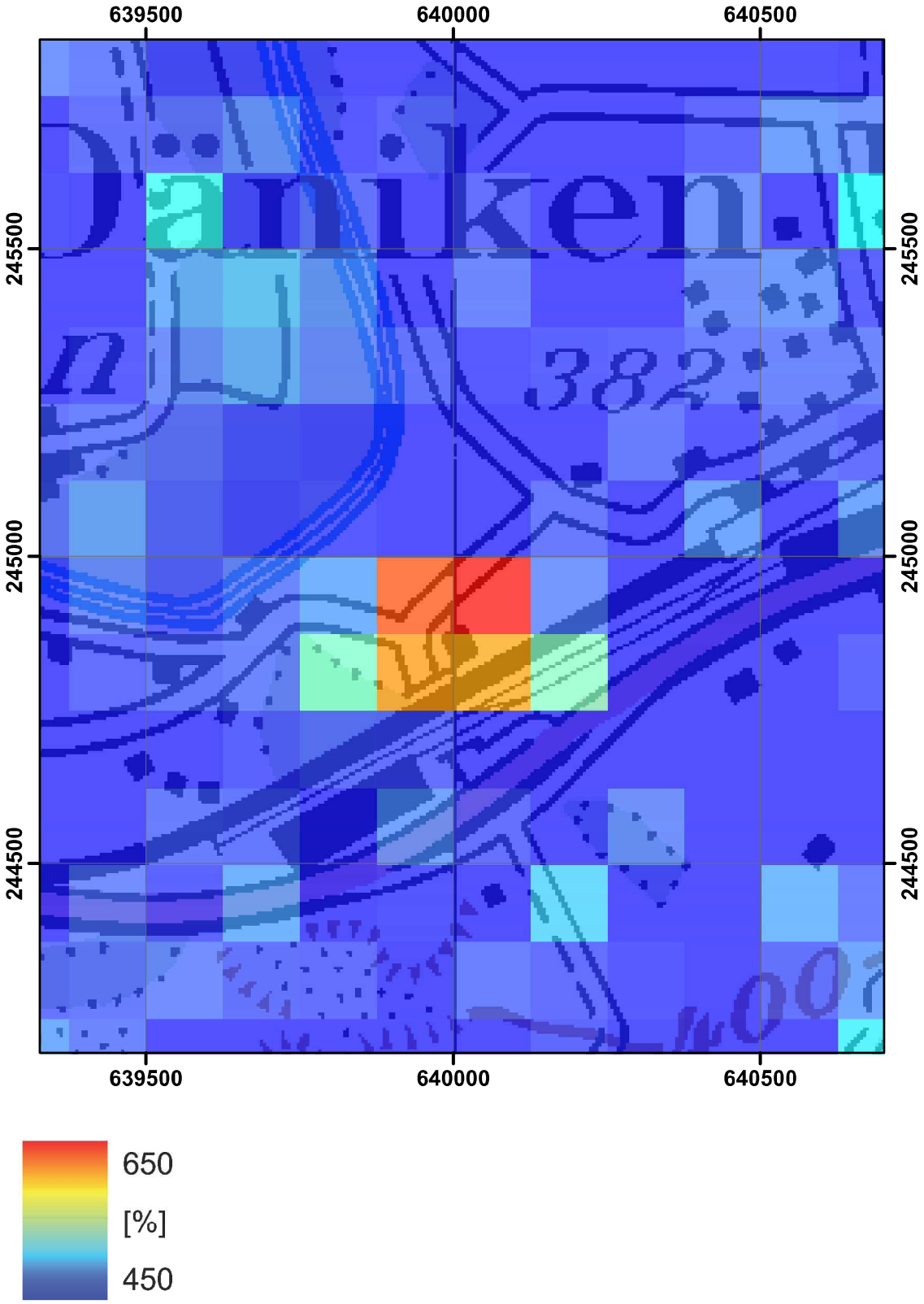

Figure 16: Detail of the map of the MMGC ratio in the vicinity of KKG. PK100 © 2011 swisstopo (JD100043).

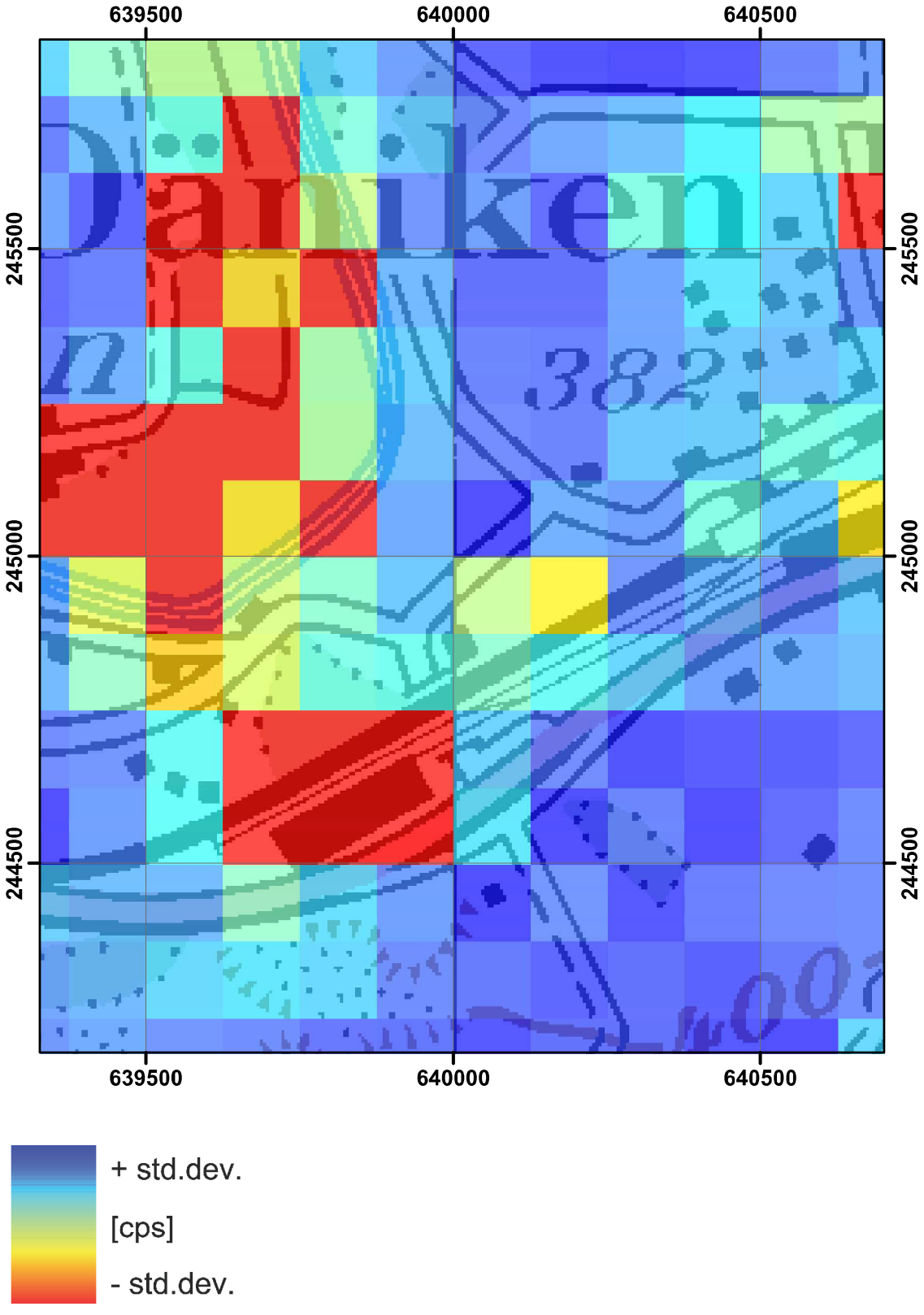

Figure 17: Detail map of the variation of the raw count rate in the high MMGC energy window in the vicinity of KKG.
PK100 © 2011 swisstopo (JD100043).

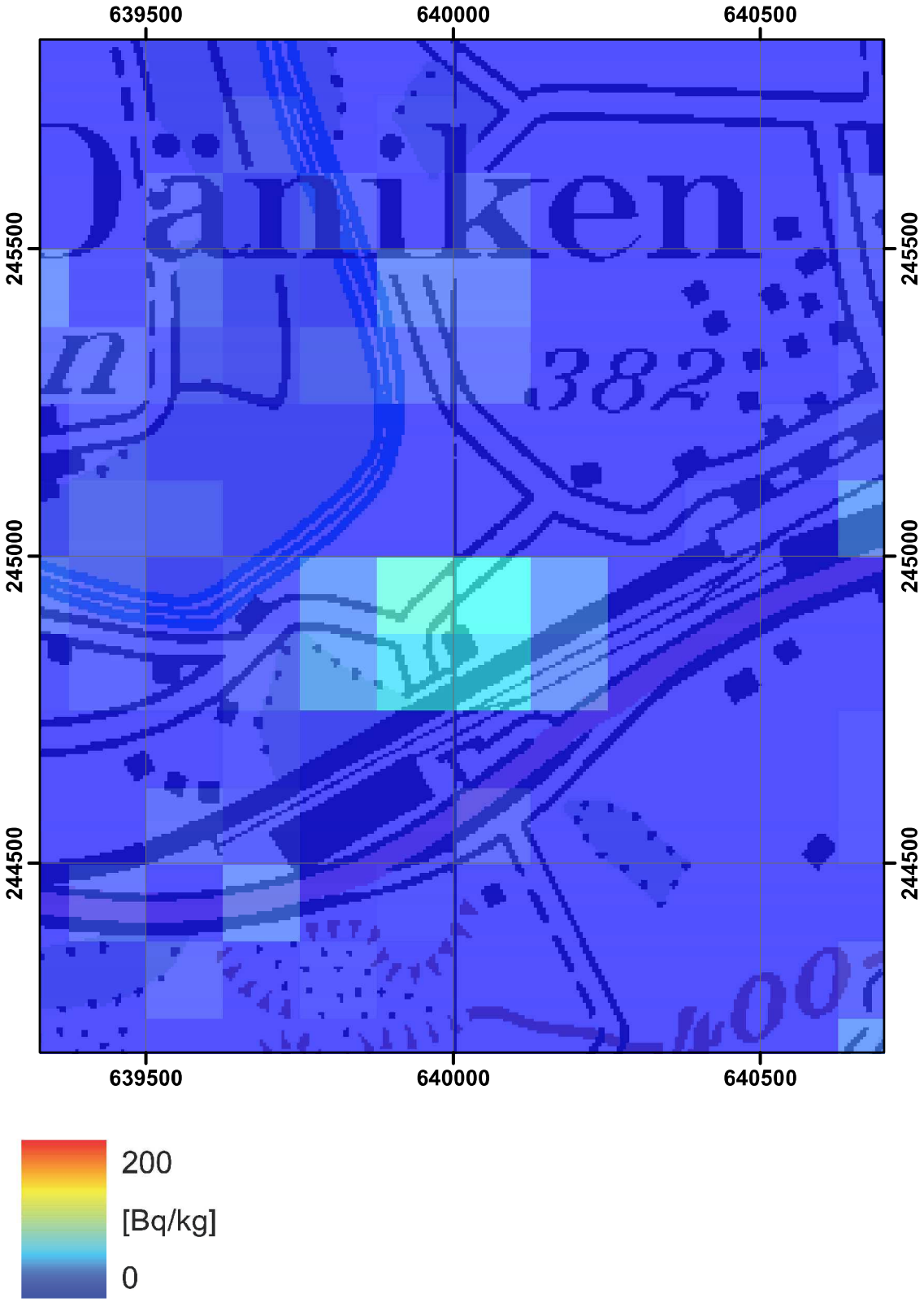

Figure 18: Detail map of the ^{137}Cs activity concentration in the vicinity of KKG. PK100 © 2011 swisstopo (JD100043).

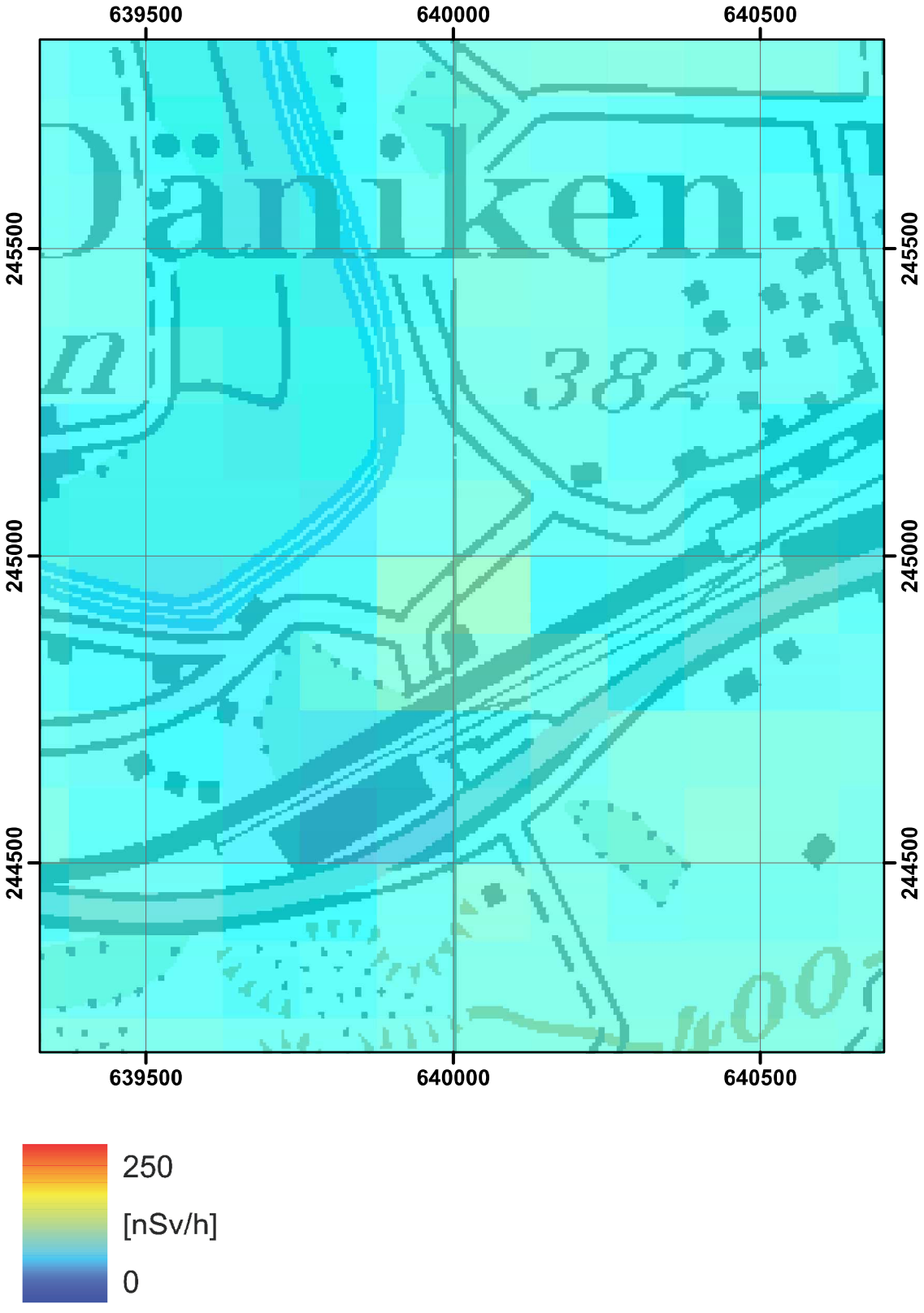

Figure 19: Detail of the dose rate map in the vicinity of KKG.
PK100 © 2011 swisstopo (JD100043).

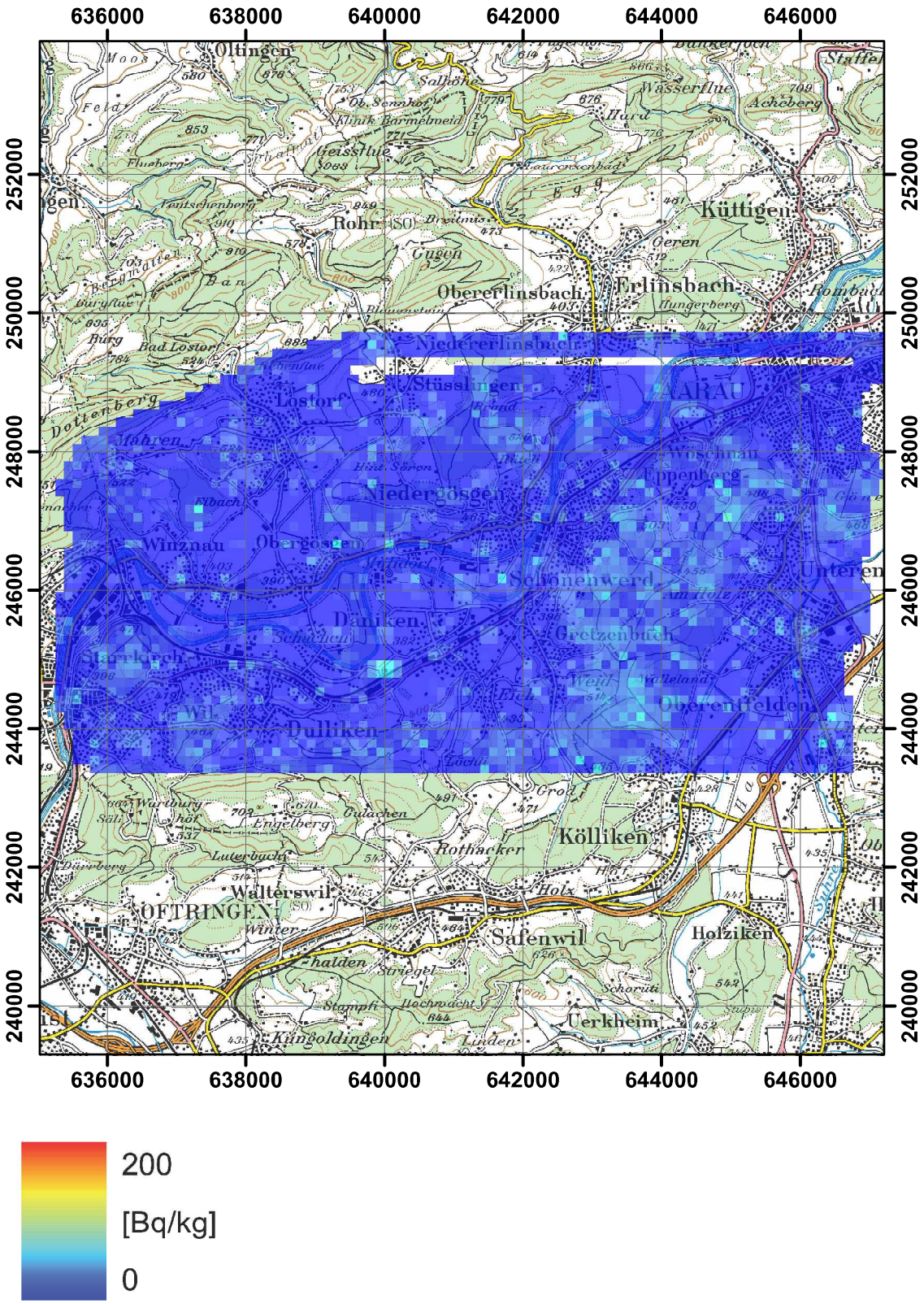

Figure 20: ^{137}Cs activity concentration in the vicinity of KKG.
PK100 © 2011 swisstopo (JD100043).

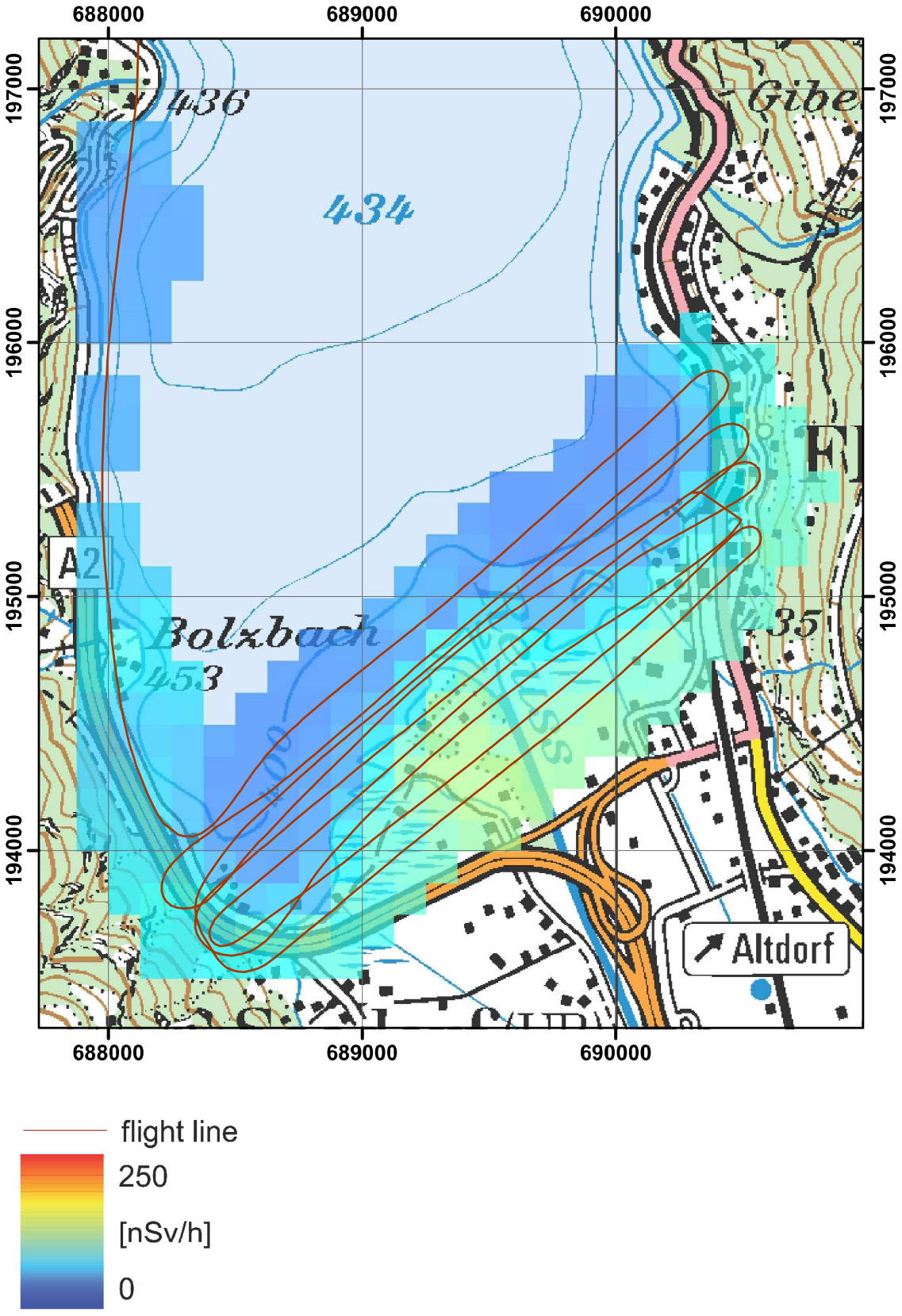

Figure 21: Dose rate in the Reuss delta.
PK100 © 2011 swisstopo (JD100043).

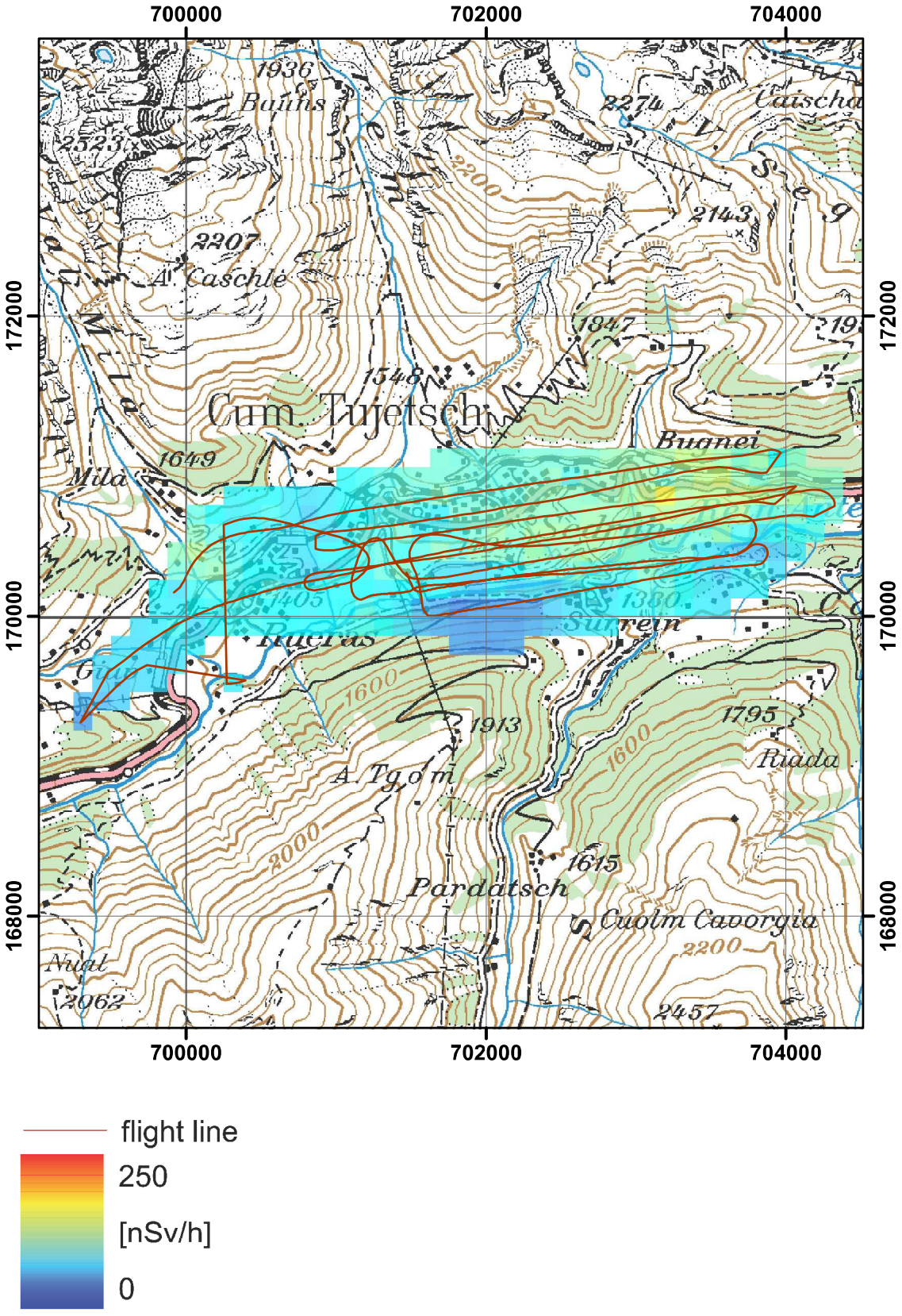

Figure 22: Terrestrial dose rate near Sedrun.
PK100 © 2011 swisstopo (JD100043).

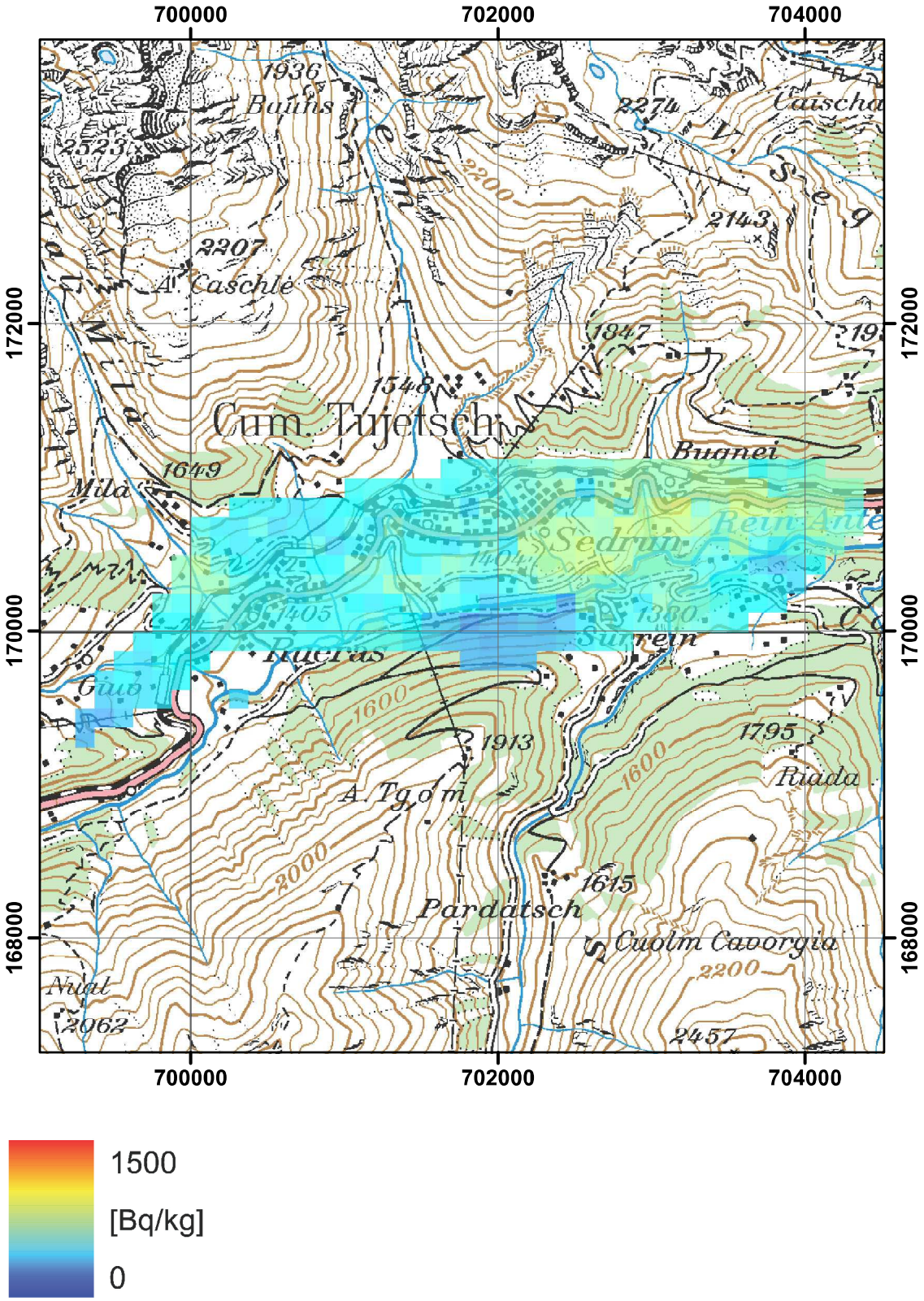

Figure 23: ^{40}K activity concentration near Sedrun.
PK100 © 2011 swisstopo (JD100043).

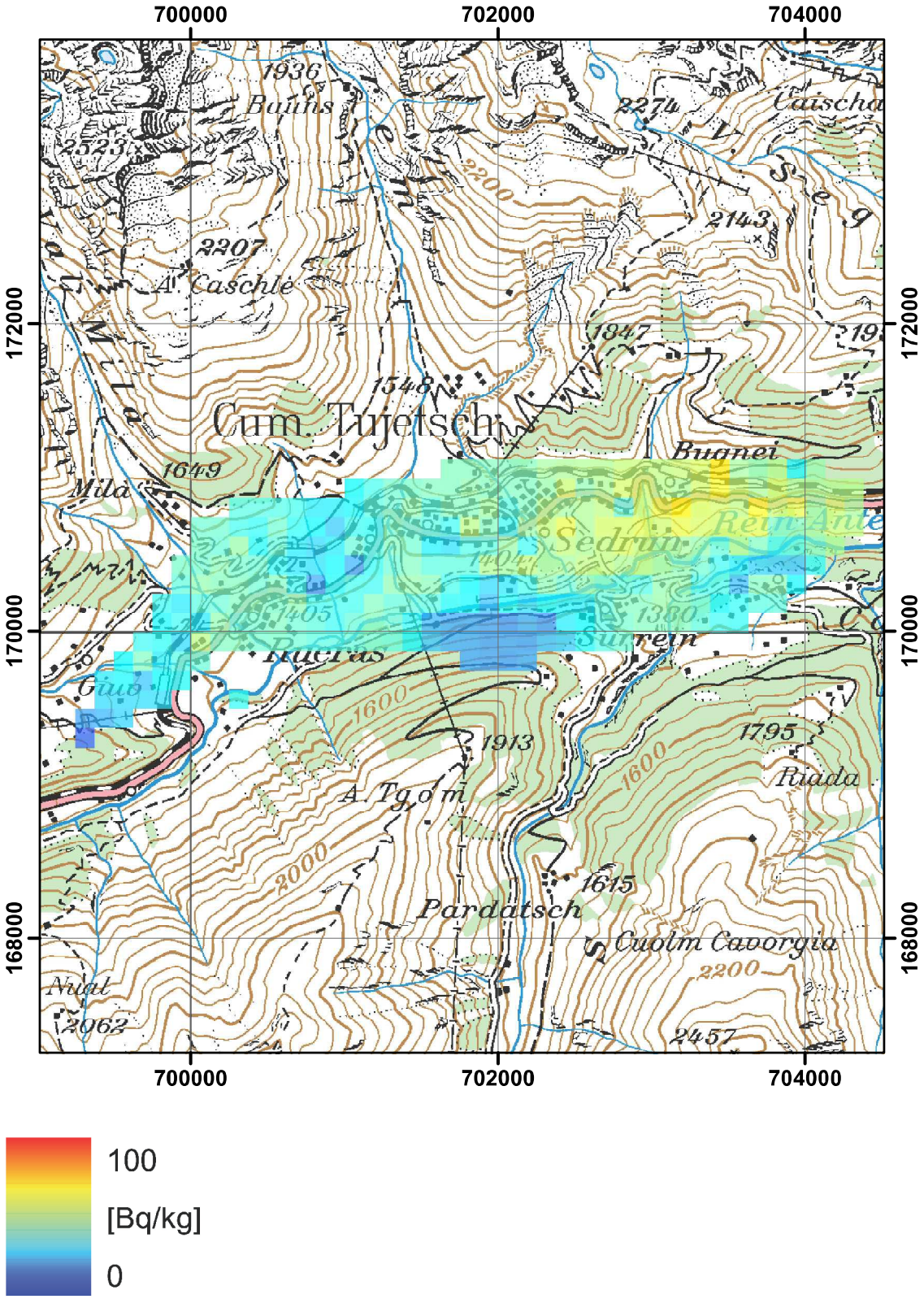

Figure 24: ^{232}Th activity concentration near Sedrun.
PK100 © 2011 swisstopo (JD100043).

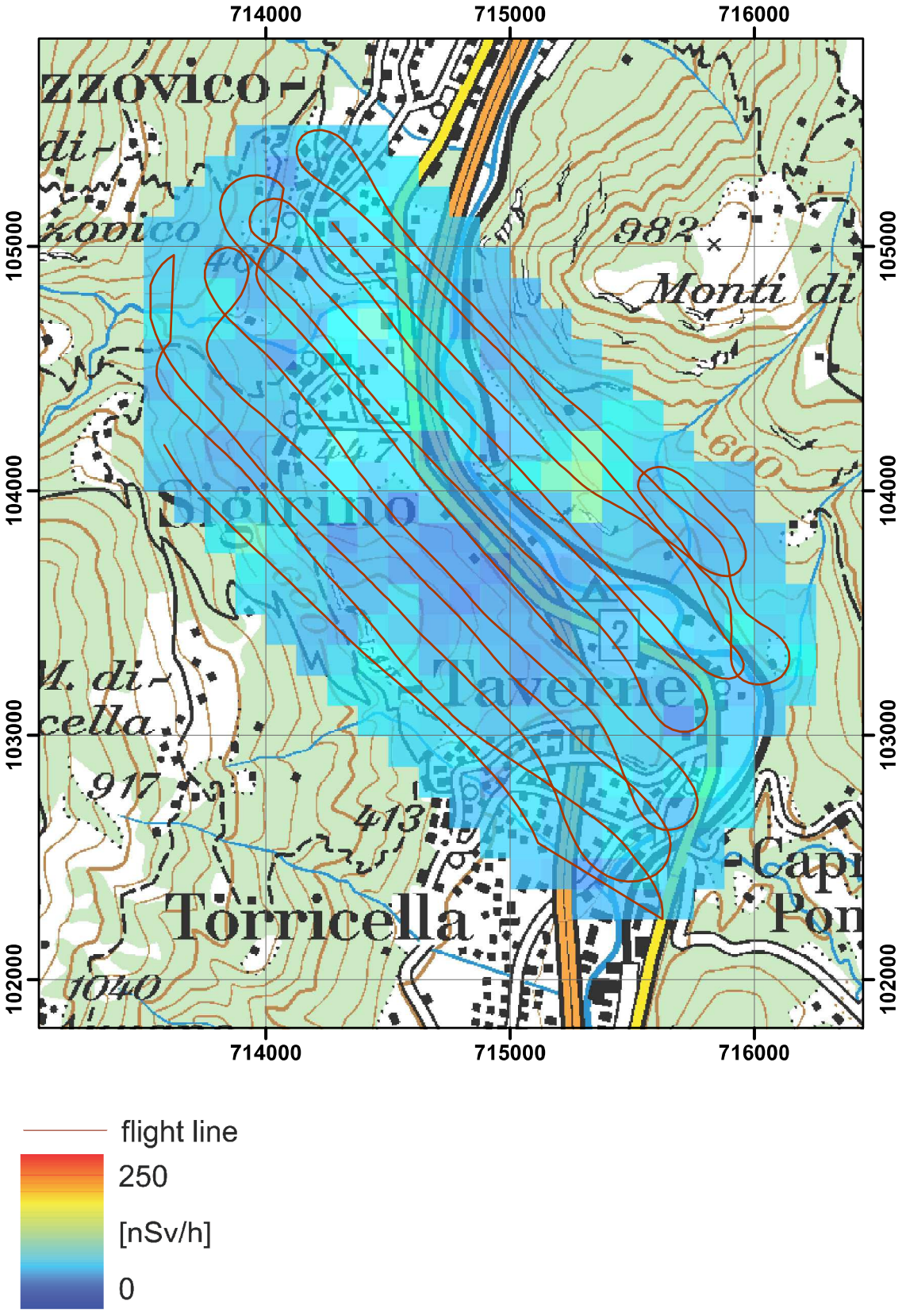

Figure 25: Terrestrial dose rate near Sigirino.
PK100 © 2011 swisstopo (JD100043).

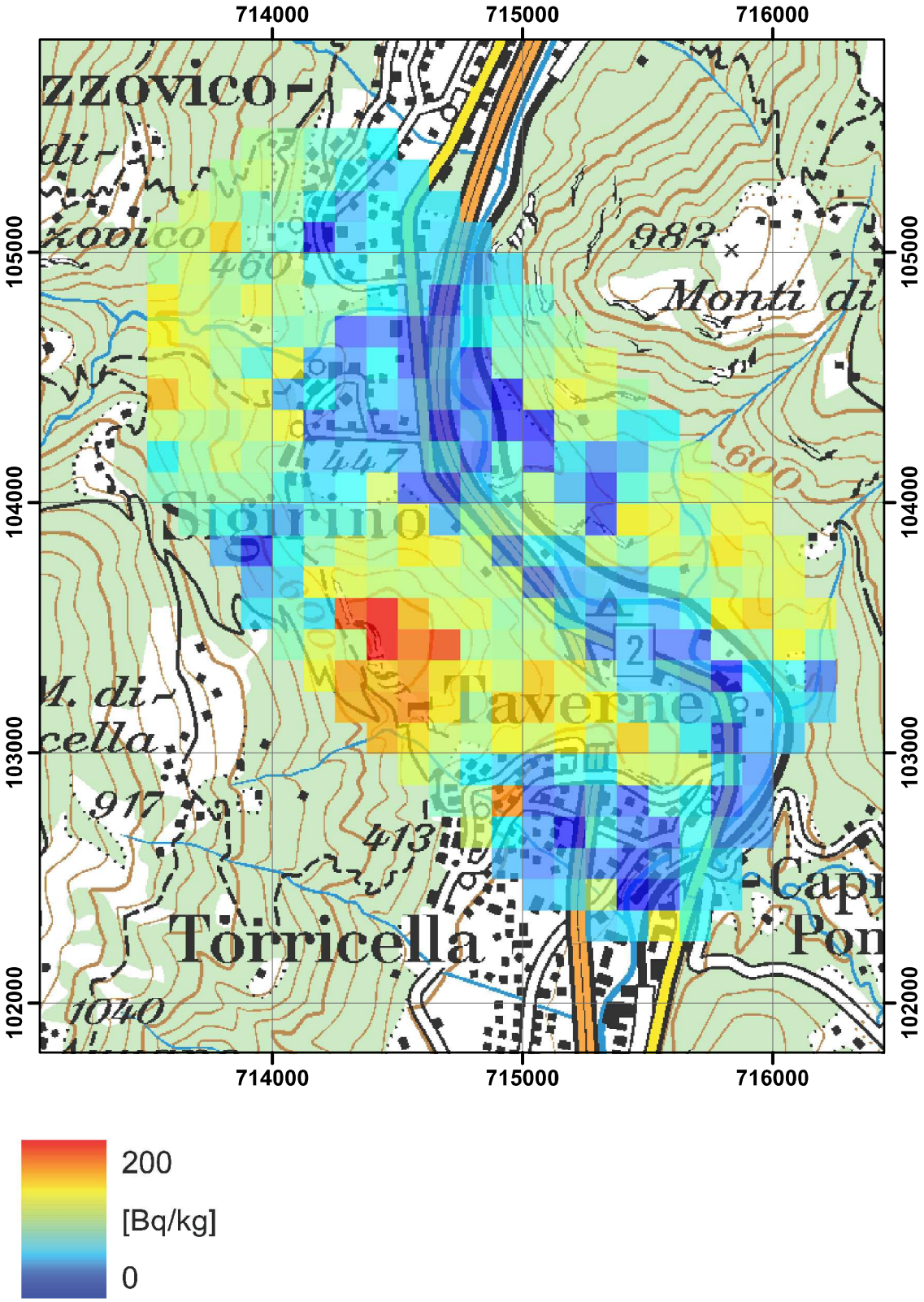

Figure 26: ^{137}Cs activity concentration near Sigirino.
PK100 © 2011 swisstopo (JD100043).

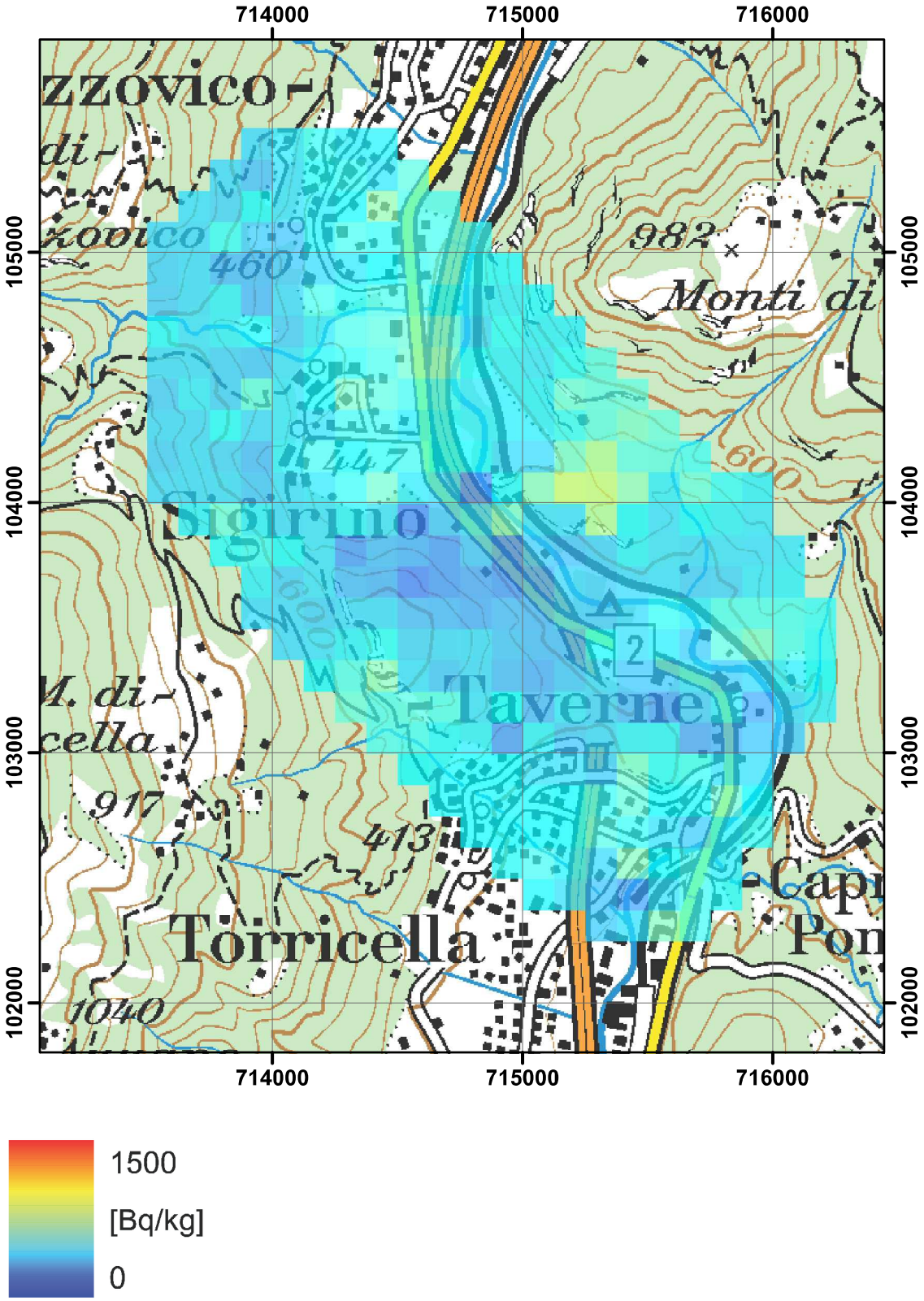

Figure 27: ^{40}K activity concentration near Sigirino.
PK100 © 2011 swisstopo (JD100043).

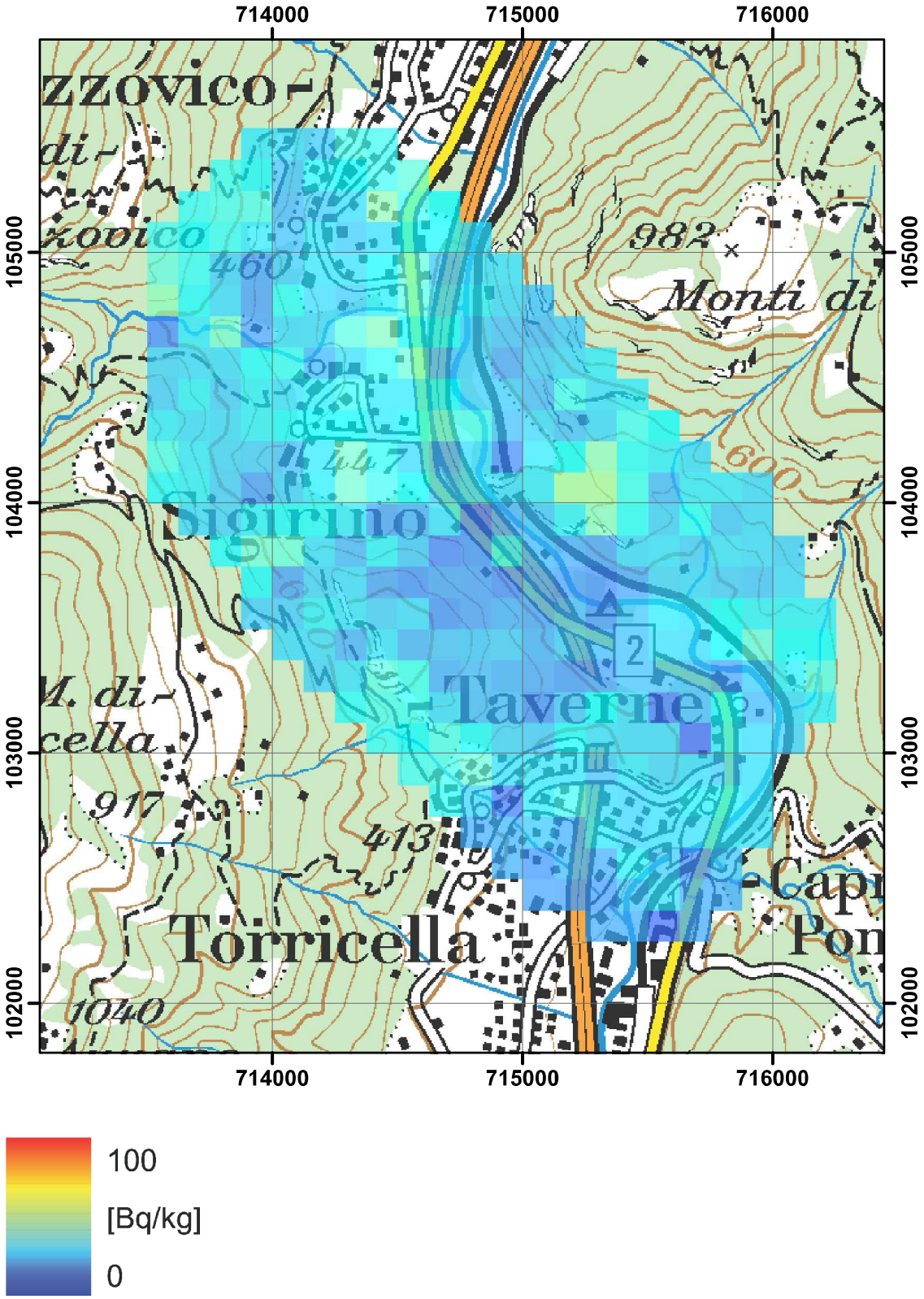

Figure 28: ^{232}Th activity concentration near Sigirino.
PK100 © 2011 swisstopo (JD100043).

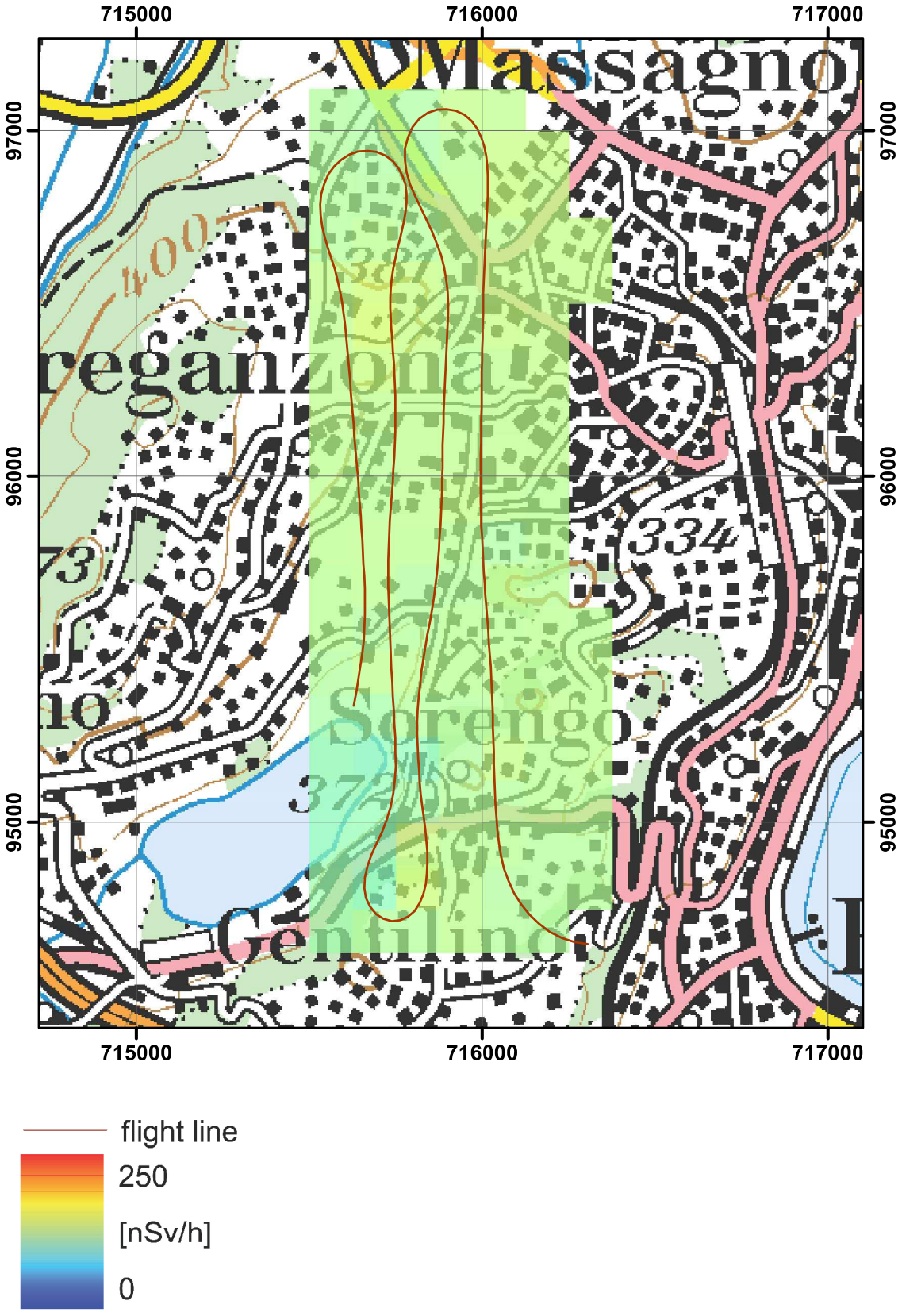

Figure 29: Dose rate near Breganzona.
PK100 © 2011 swisstopo (JD100043).

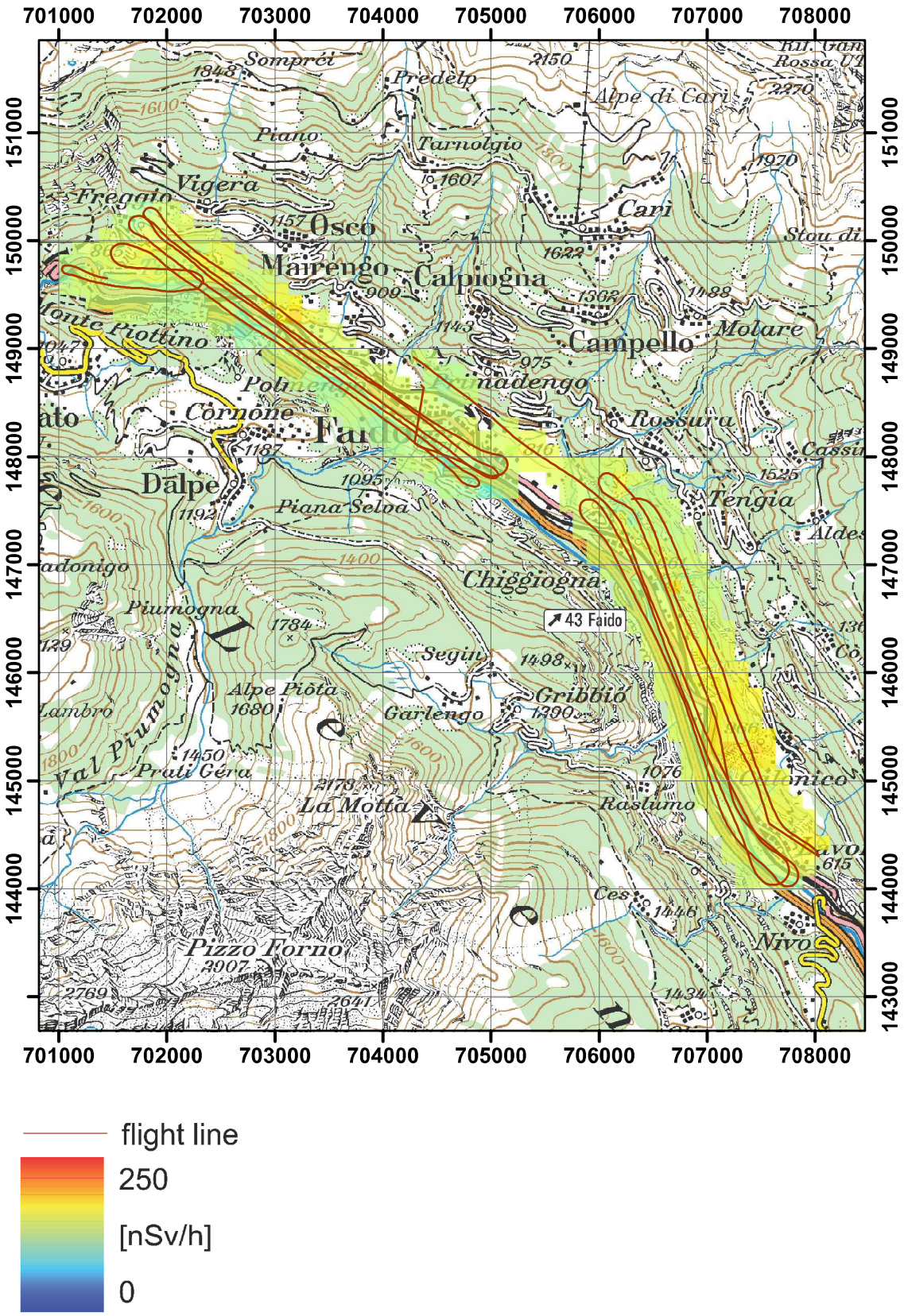

Figure 30: Dose rate at the NRLA sites near Faido.
PK100 © 2011 swisstopo (JD100043).

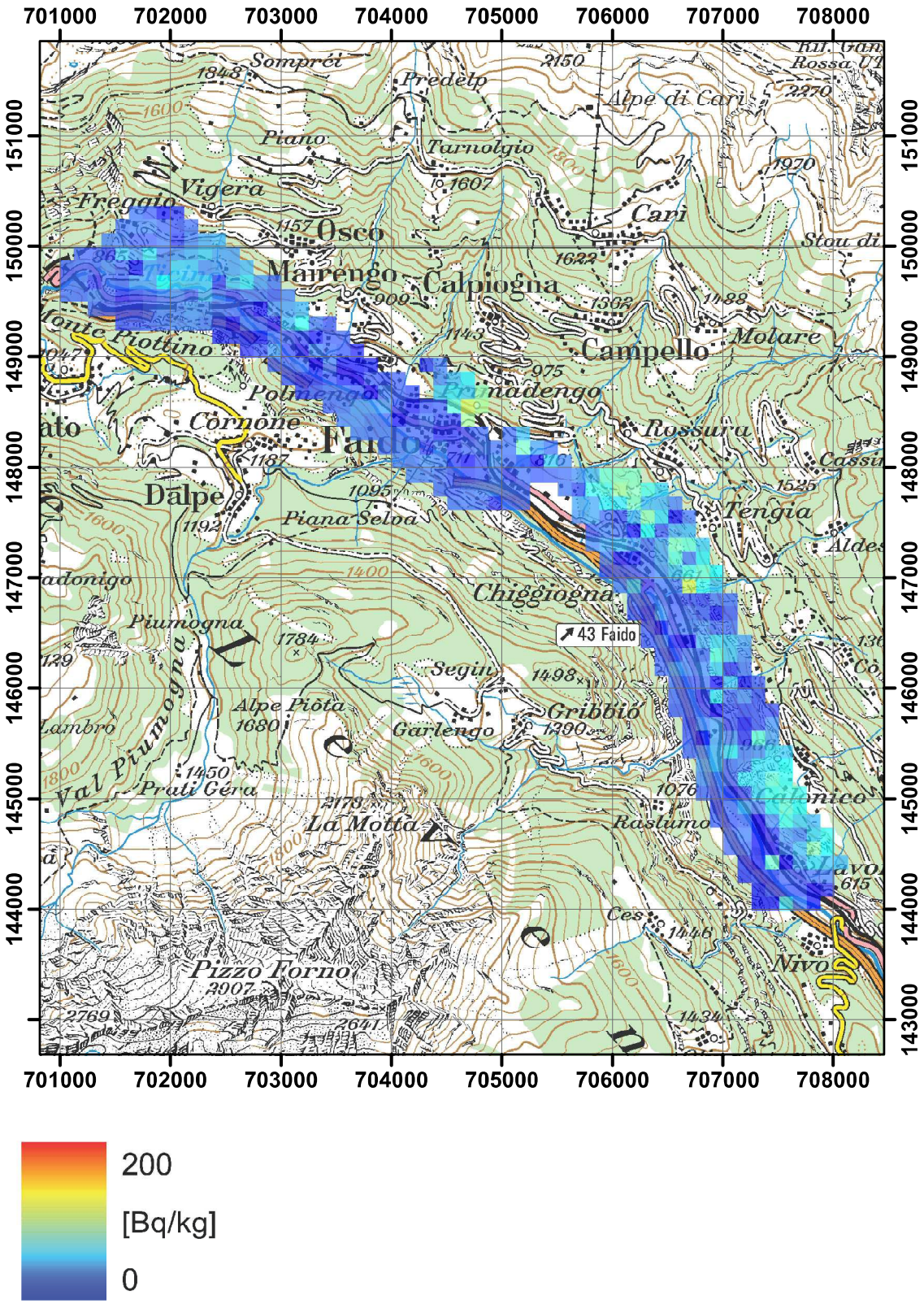

Figure 31: ^{137}Cs activity concentration at the NRLA sites near Faido. PK100 © 2011 swisstopo (JD100043).

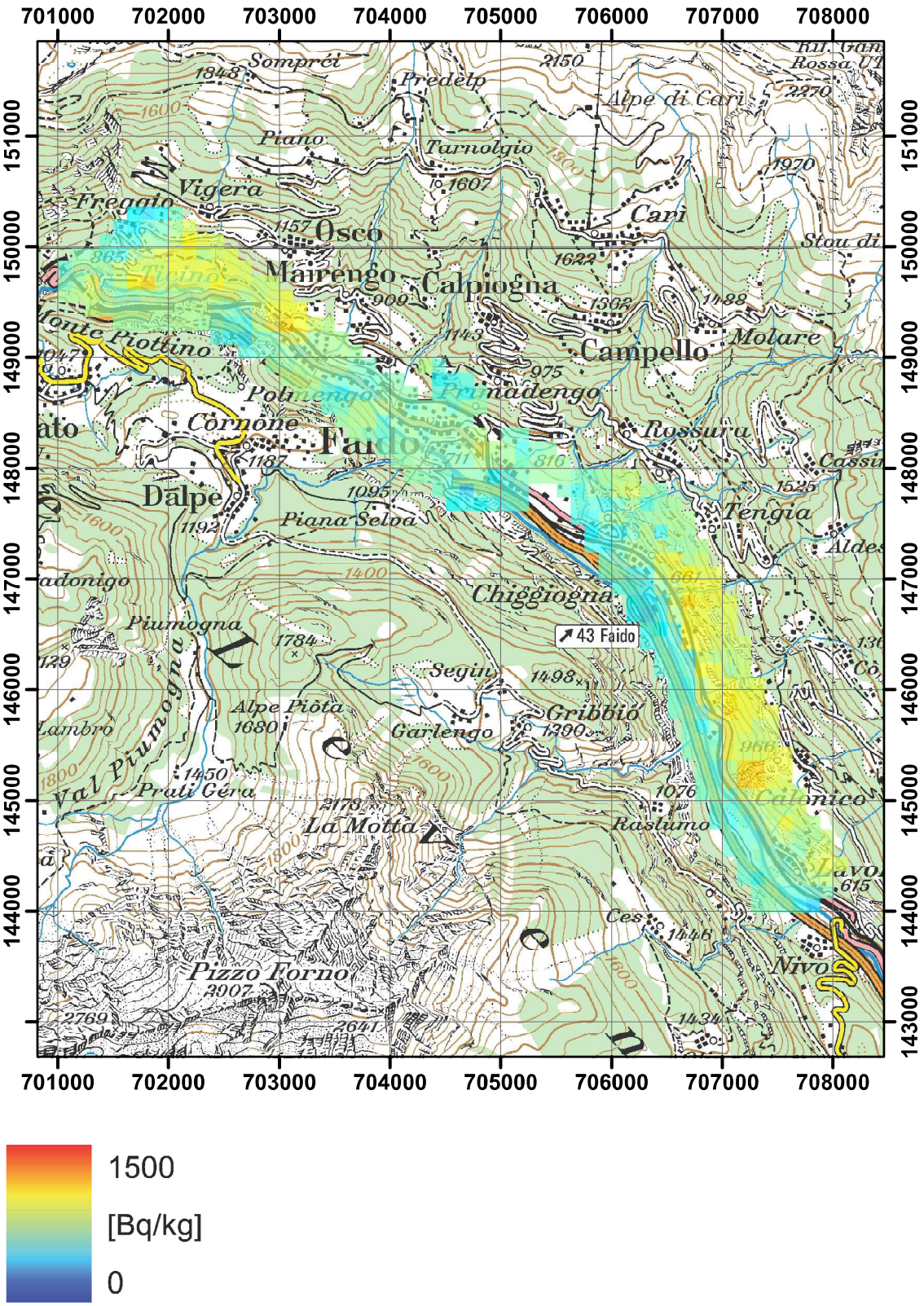

Figure 32: ^{40}K activity concentration at the NRLA sites near Faido. PK100 © 2011 swisstopo (JD100043).

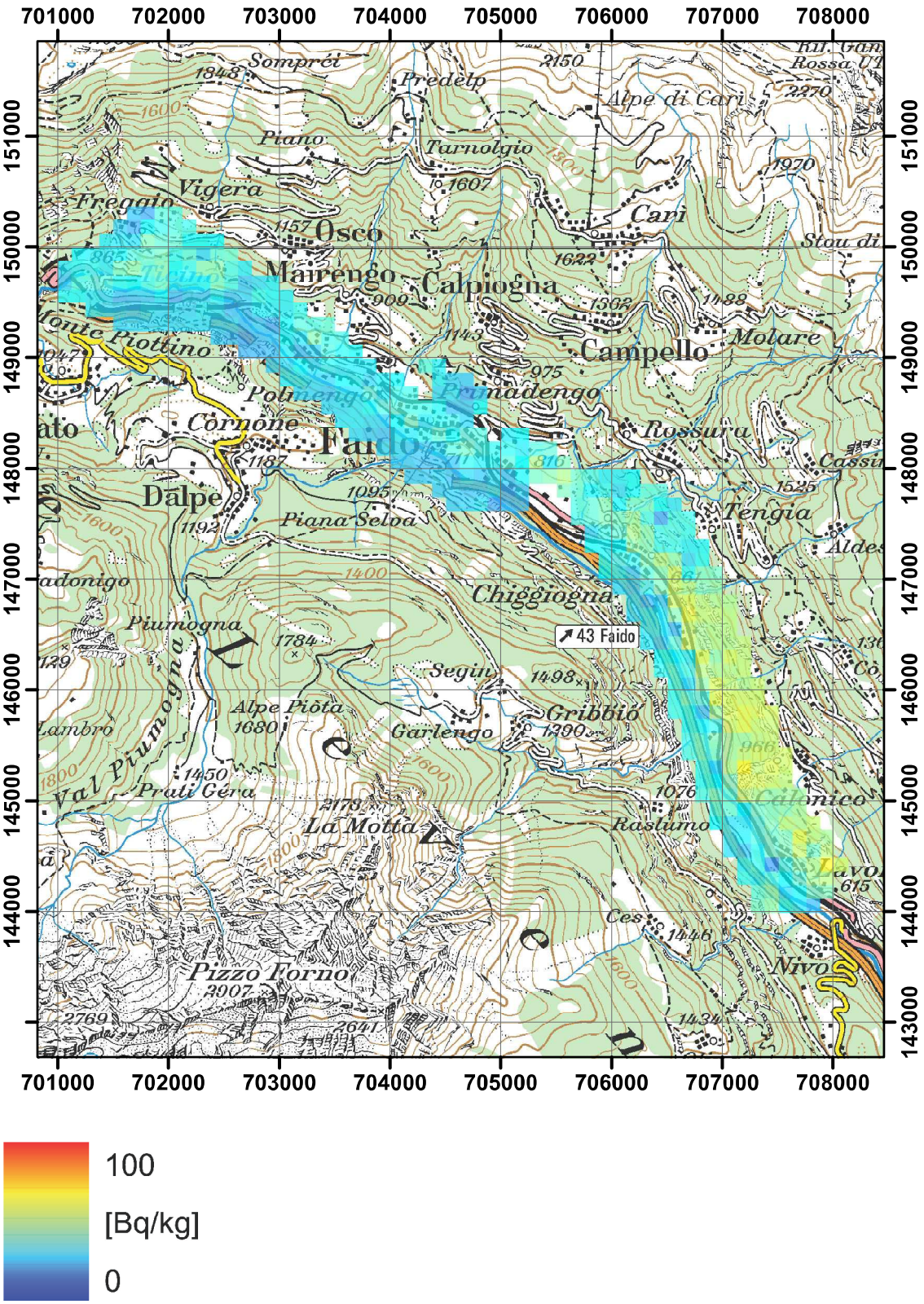

Figure 33: ^{232}Th activity concentration at the NRLA sites near Faido. PK100 © 2011 swisstopo (JD100043).

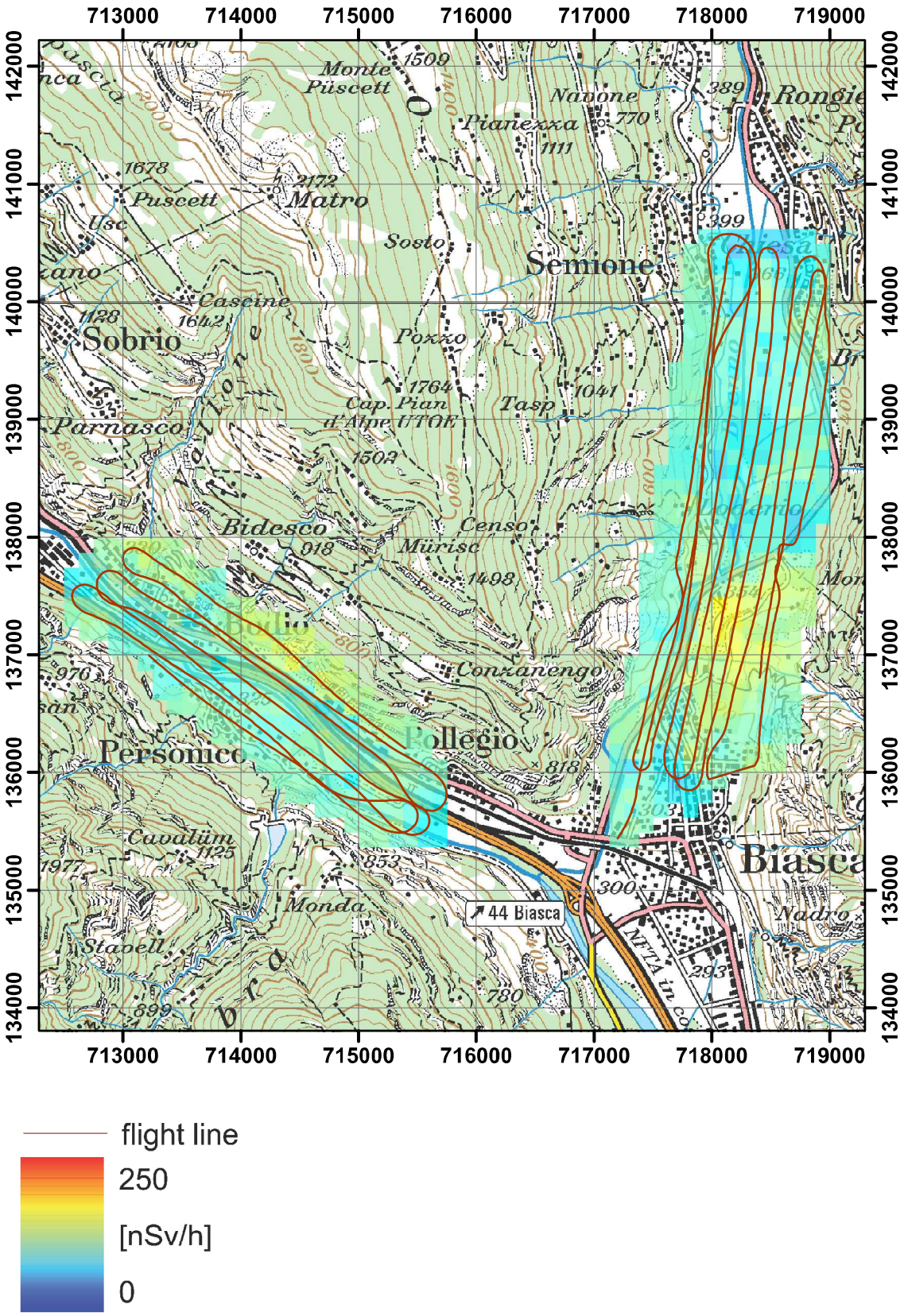

Figure 34: Terrestrial dose rate at the NRLA sites near Bodio and Biasca. PK100 © 2011 swisstopo (JD100043).

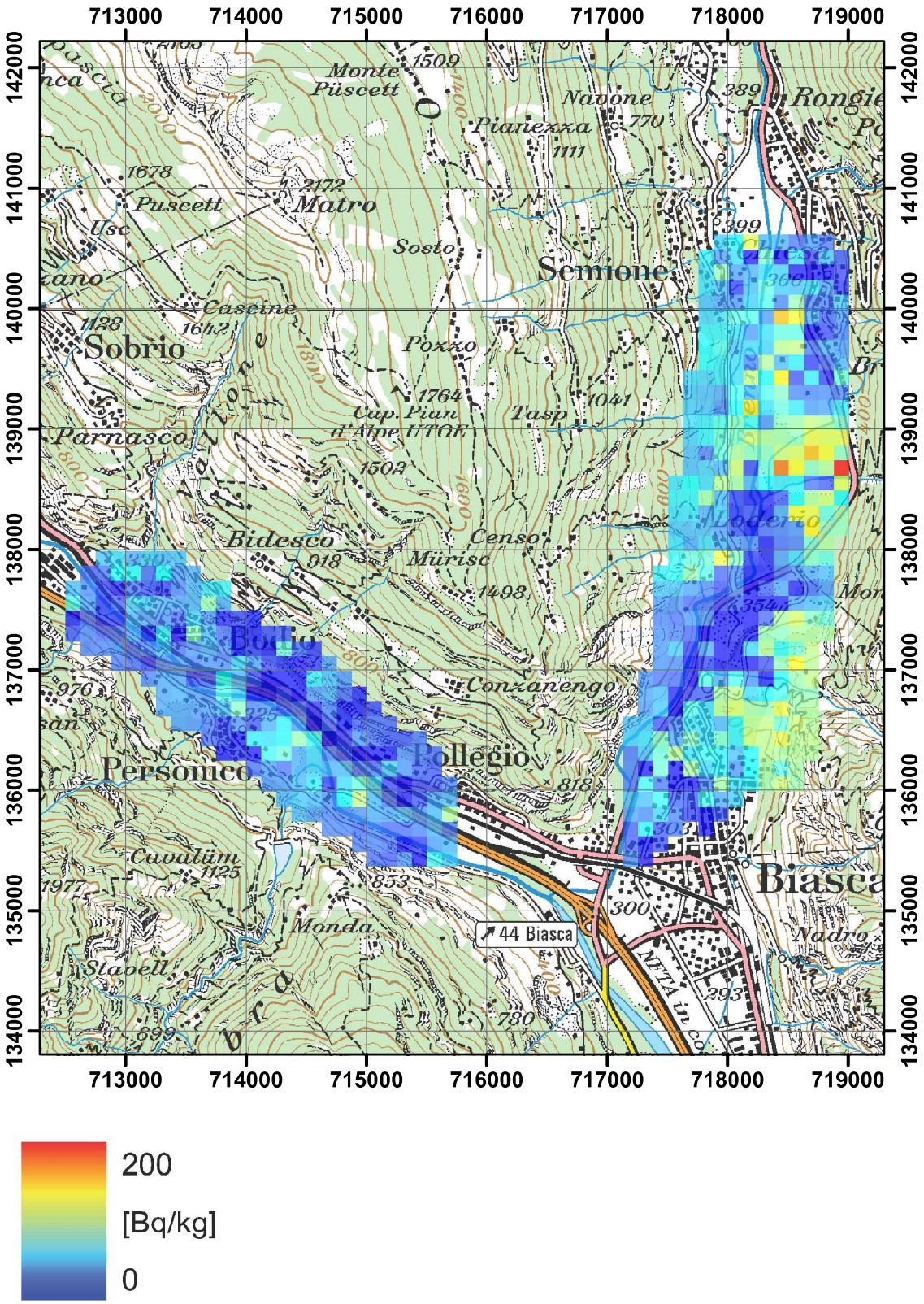

Figure 35: ^{137}Cs activity concentration at the NRLA sites near Bodio and Biasca. PK100 © 2011 swisstopo (JD100043).

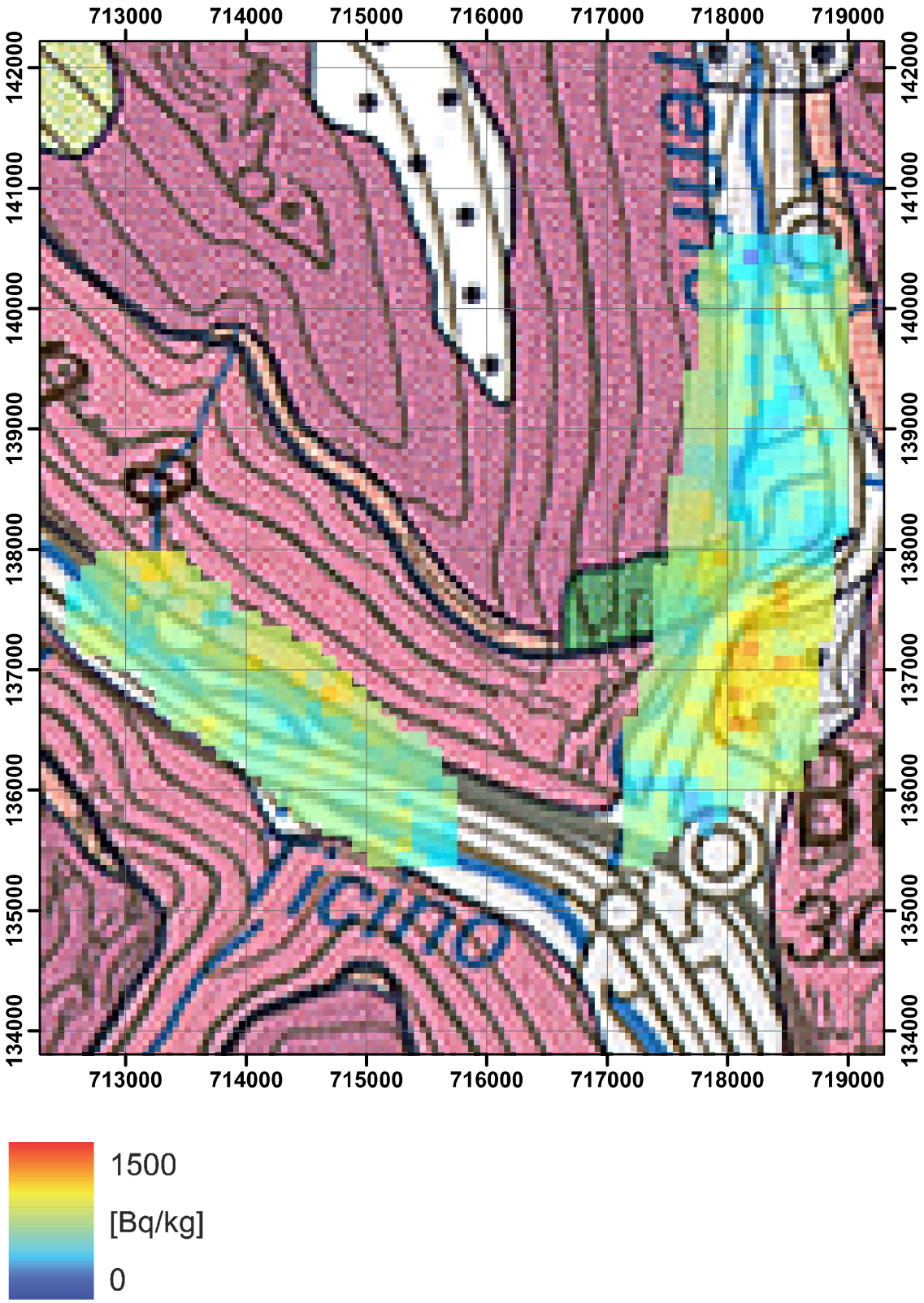

Figure 36: ^{40}K activity concentration and geology at the NRLA sites near Bodio and Biasca.
Geological atlas of Switzerland 1:500 000 © 2011 swisstopo (JD100043).

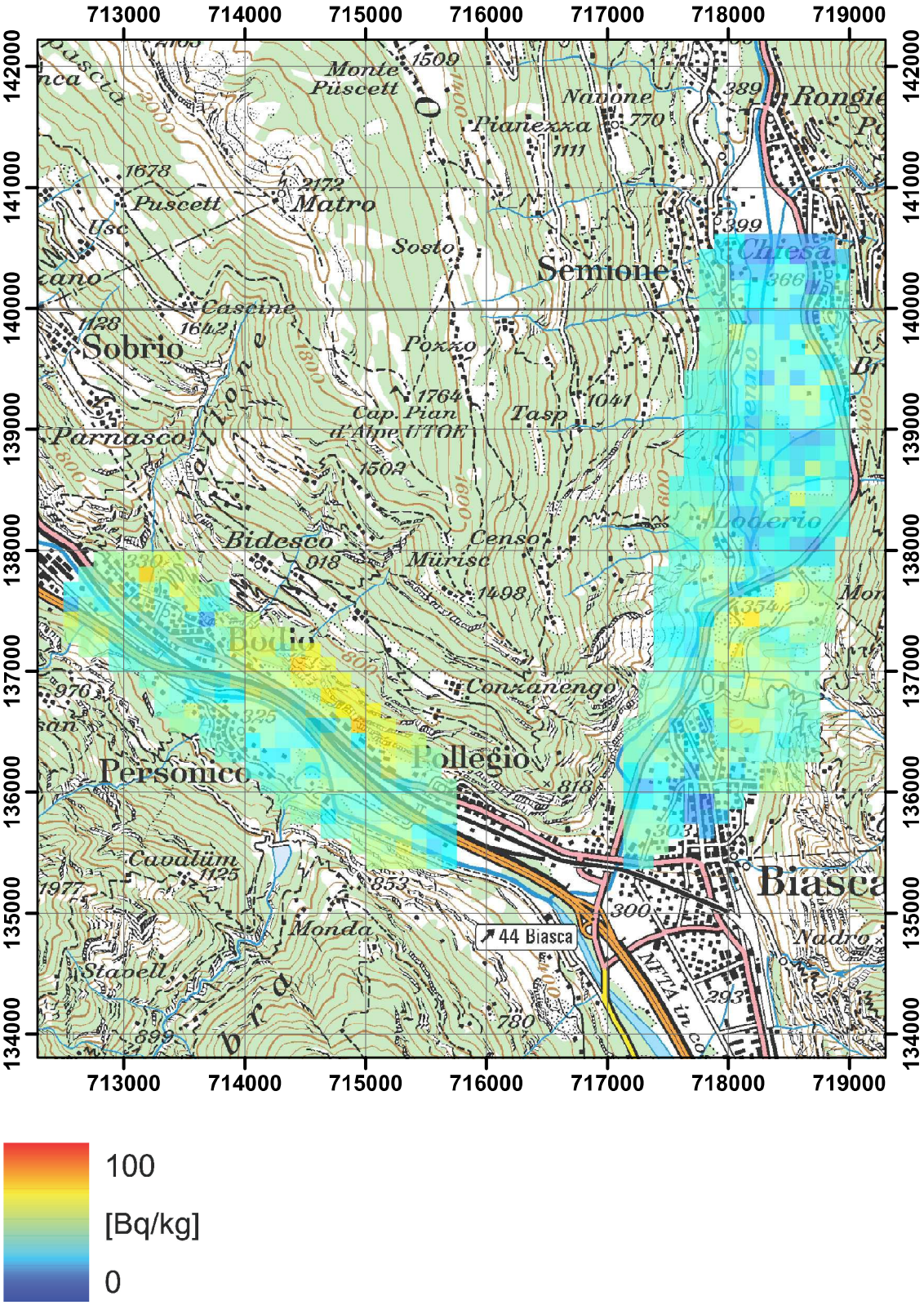

Figure 37: ^{232}Th activity concentration at the NRLA sites near Bodio and Biasca. PK100 © 2011 swisstopo (JD100043).

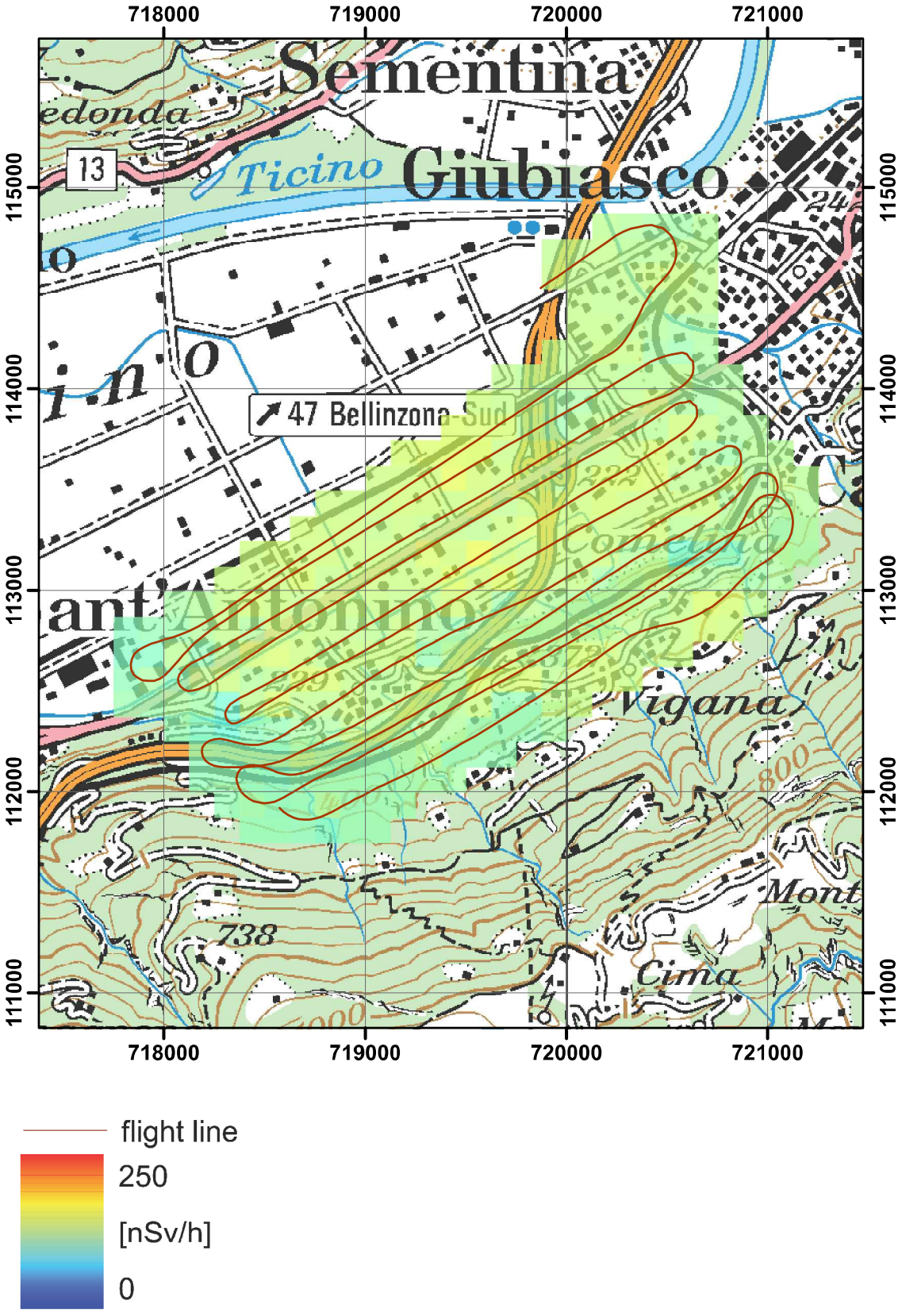

Figure 38: Dose rate near Camorino.
PK100 © 2011 swisstopo (JD100043).

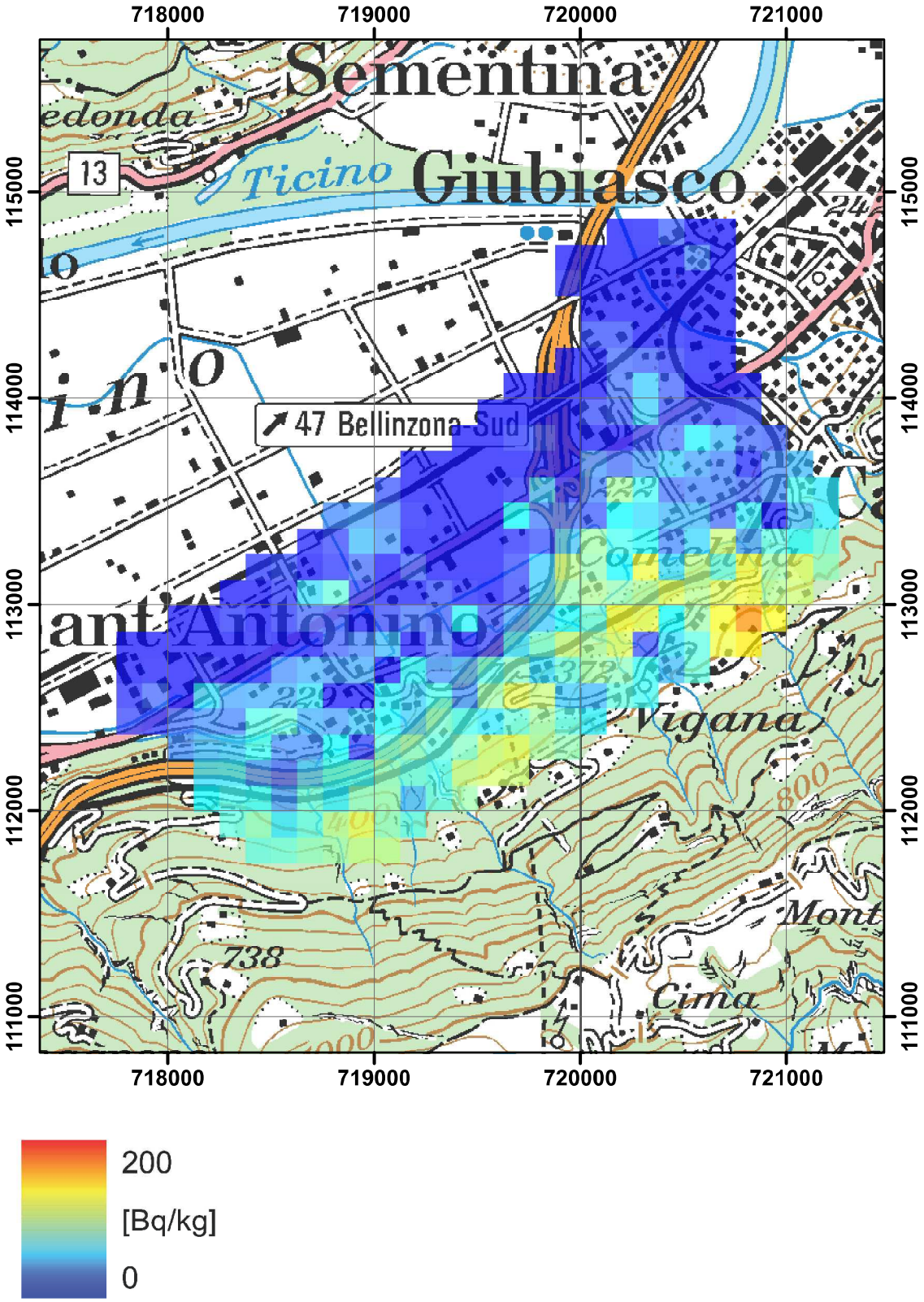

Figure 39: ^{137}Cs activity concentration near Camorino.
PK100 © 2011 swisstopo (JD100043).

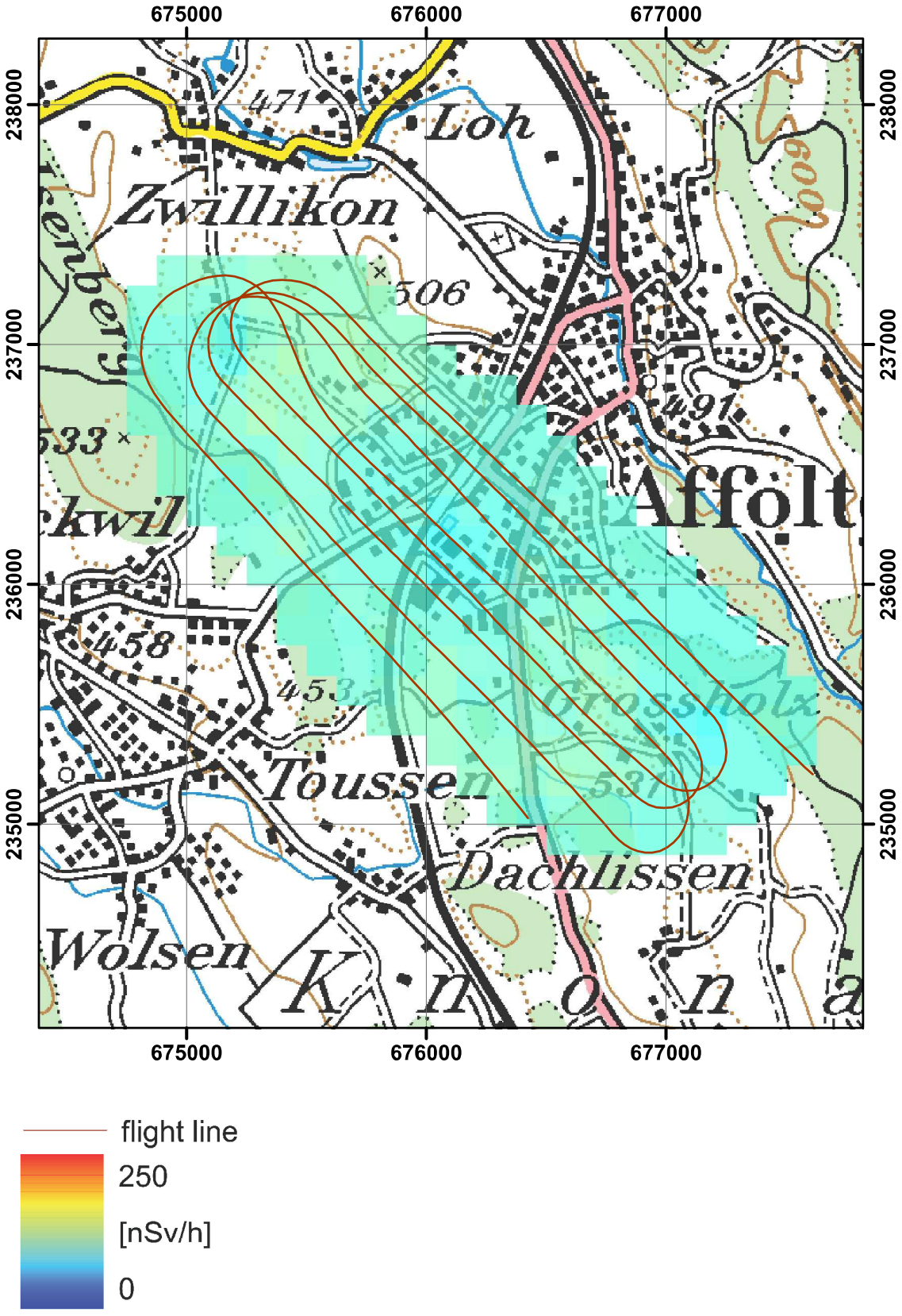

Figure 40: Dose rate at the NRLA deposit near Affoltern am Albis. PK100 © 2011 swisstopo (JD100043).

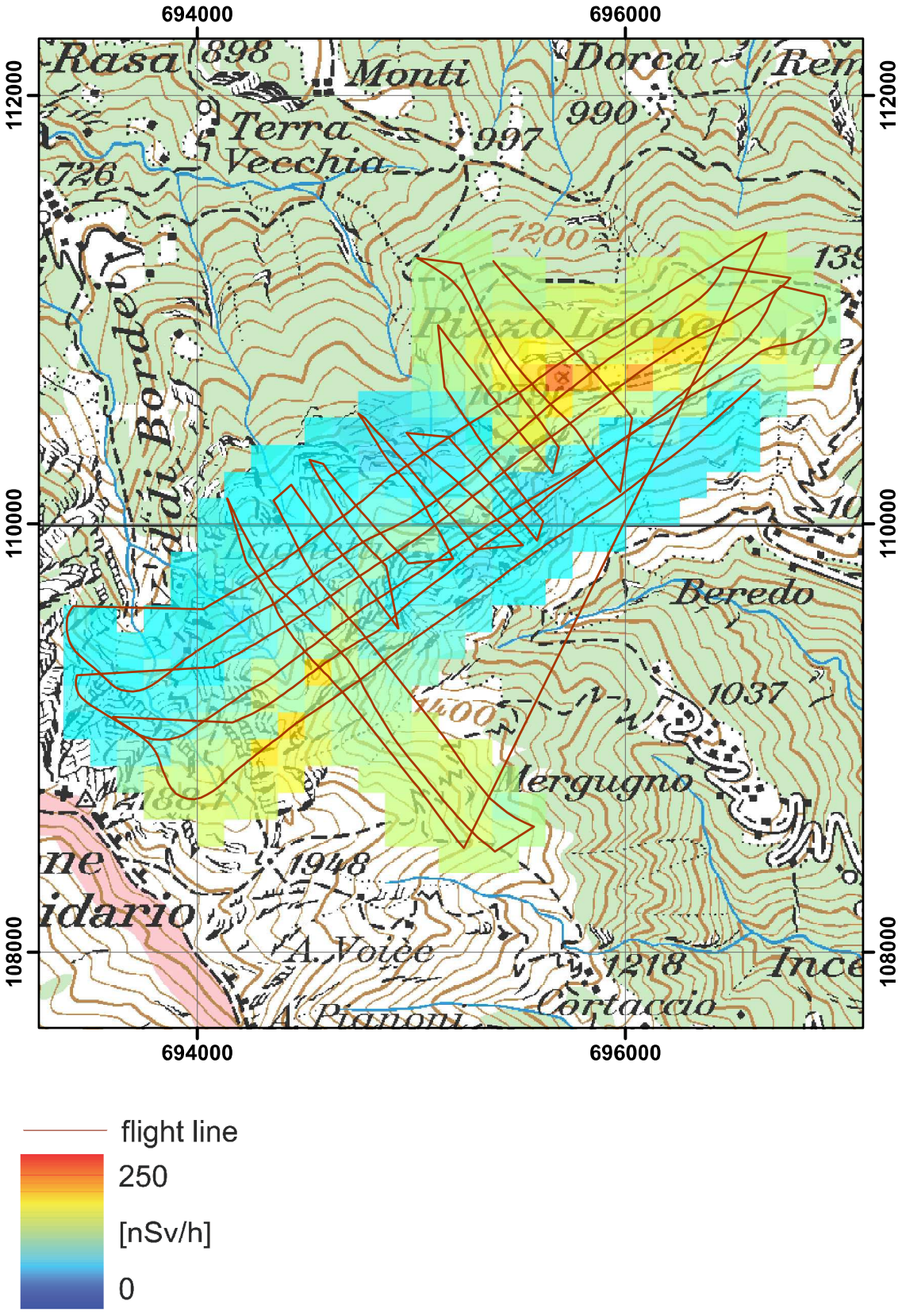

Figure 41: Dose rate at the Pizzo Ometto.
PK100 © 2011 swisstopo (JD100043).

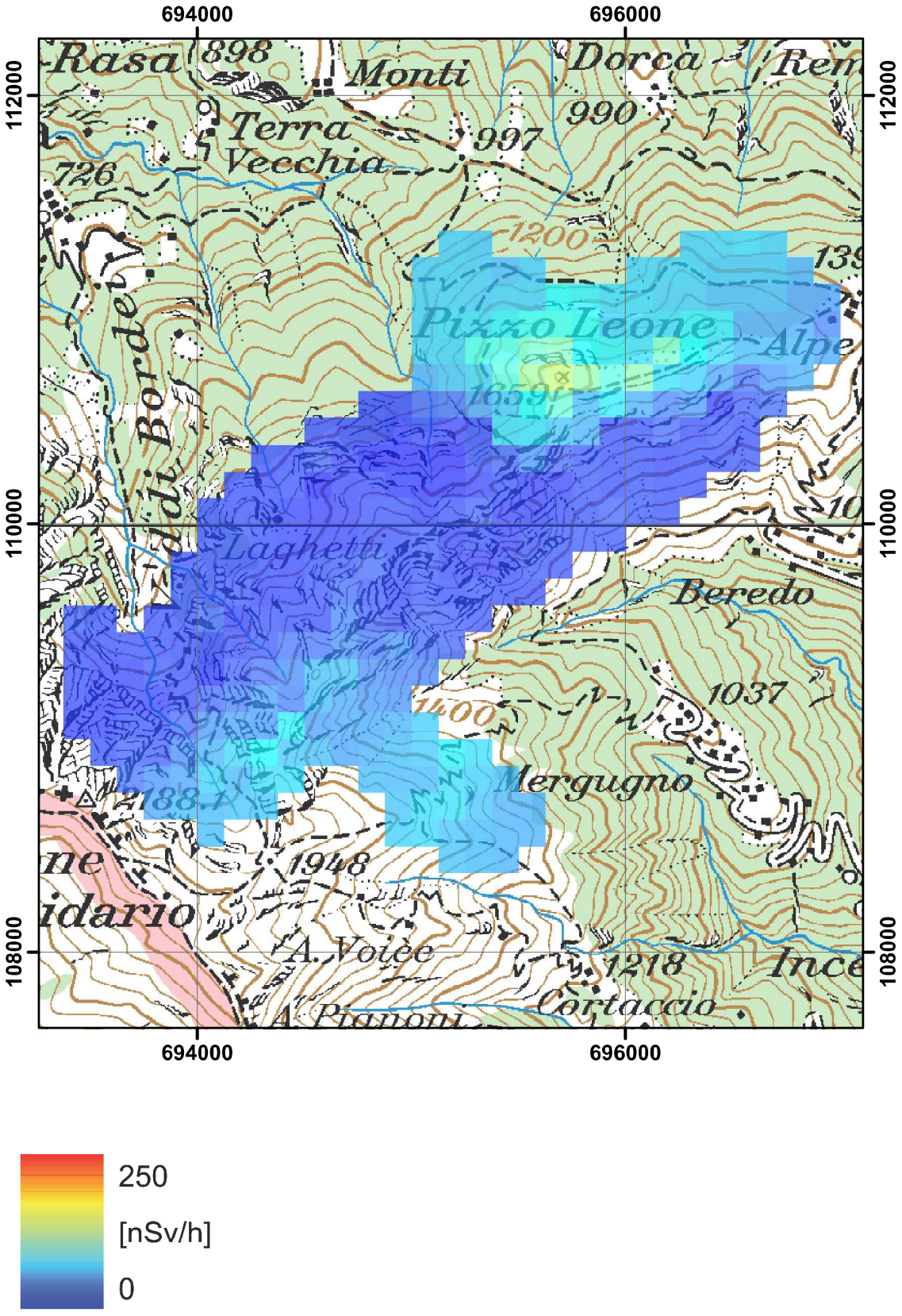

Figure 42: Terrestrial dose rate at the Pizzo Ometto.
PK100 © 2011 swisstopo (JD100043).

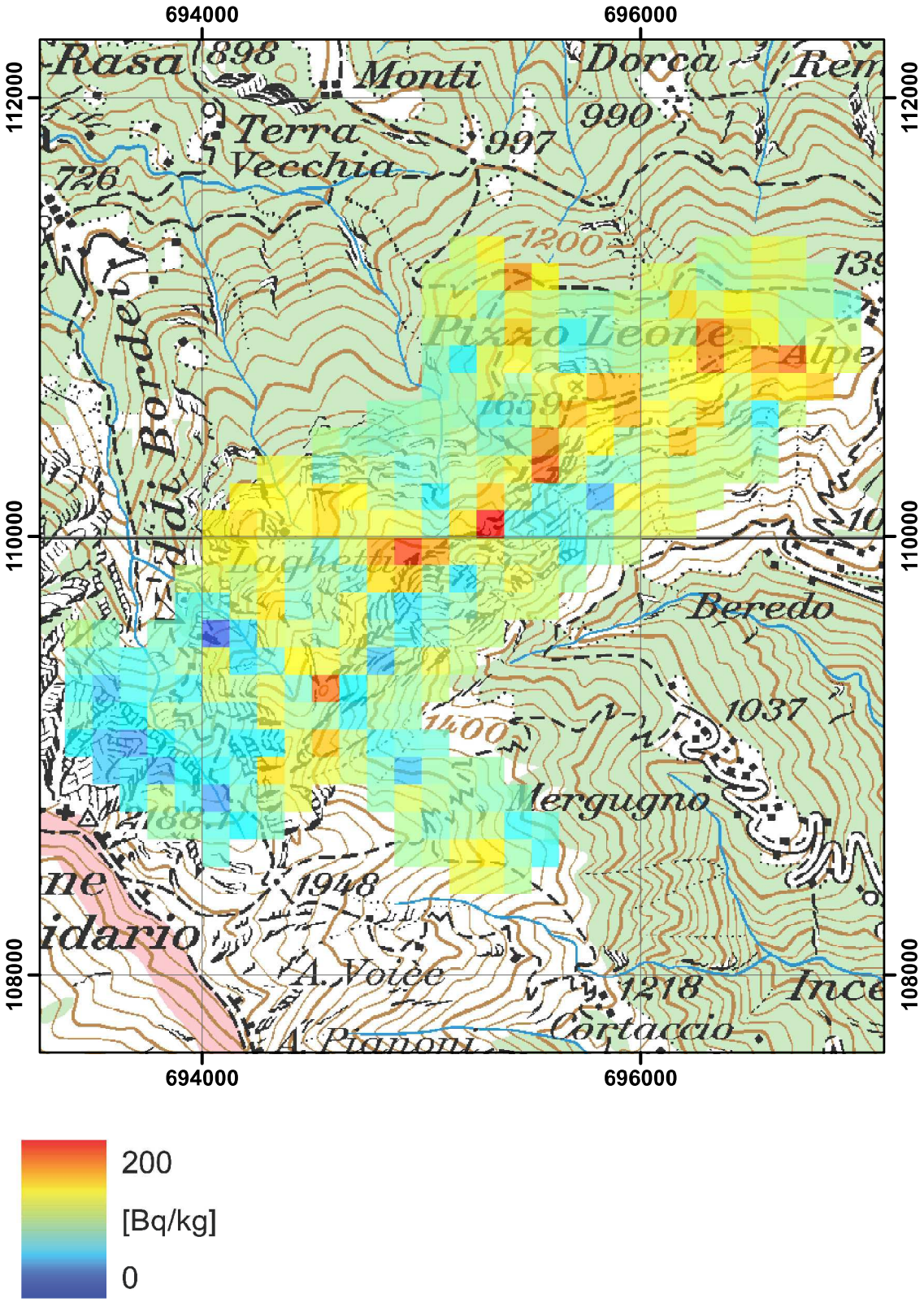

Figure 43: ^{137}Cs activity concentration at the Pizzo Ometto. PK100 © 2011 swisstopo (JD100043).

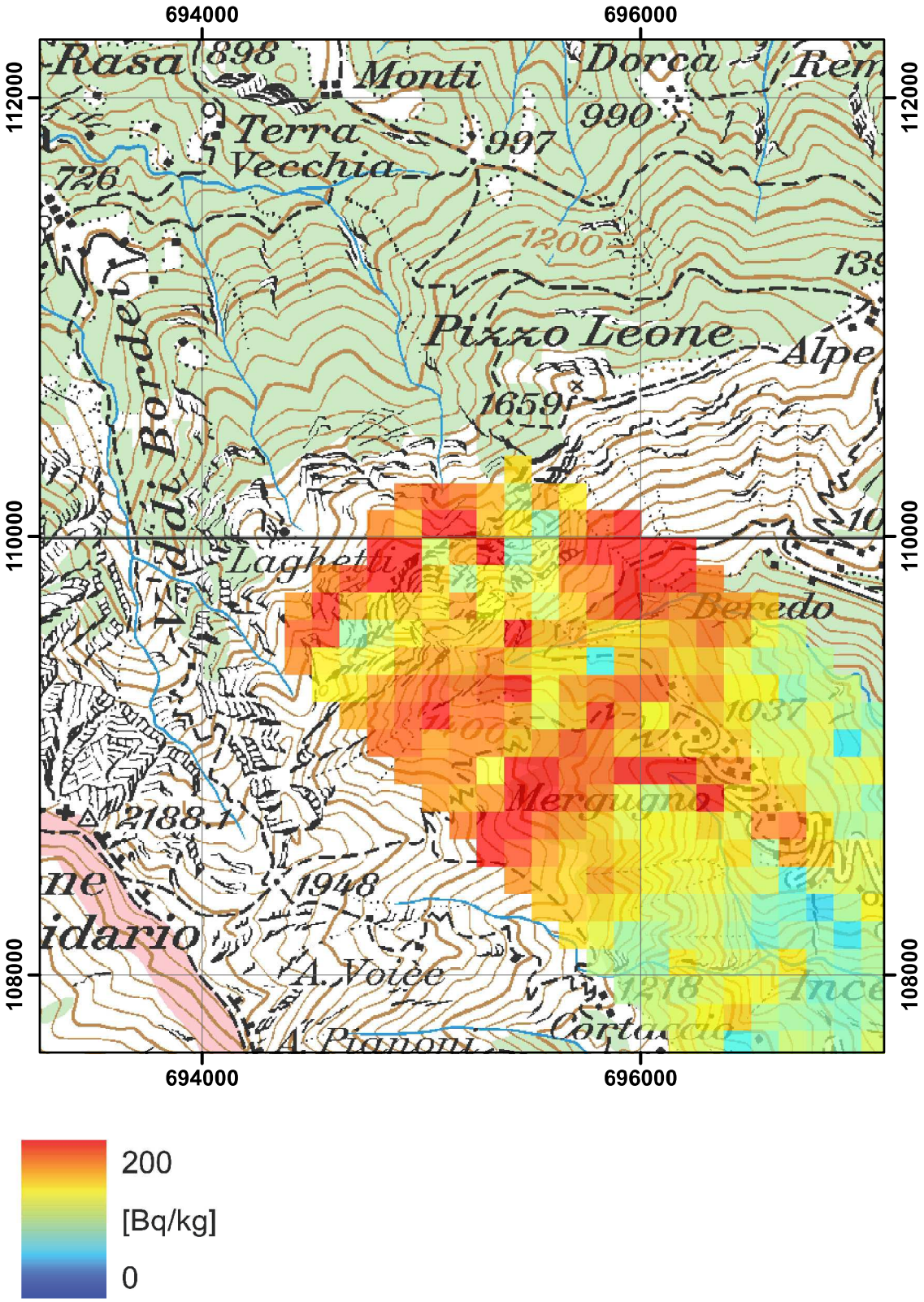

Figure 44: ^{137}Cs activity concentration measured 1999 at the Pizzo Ometto. PK100 © 2011 swisstopo (JD100043).

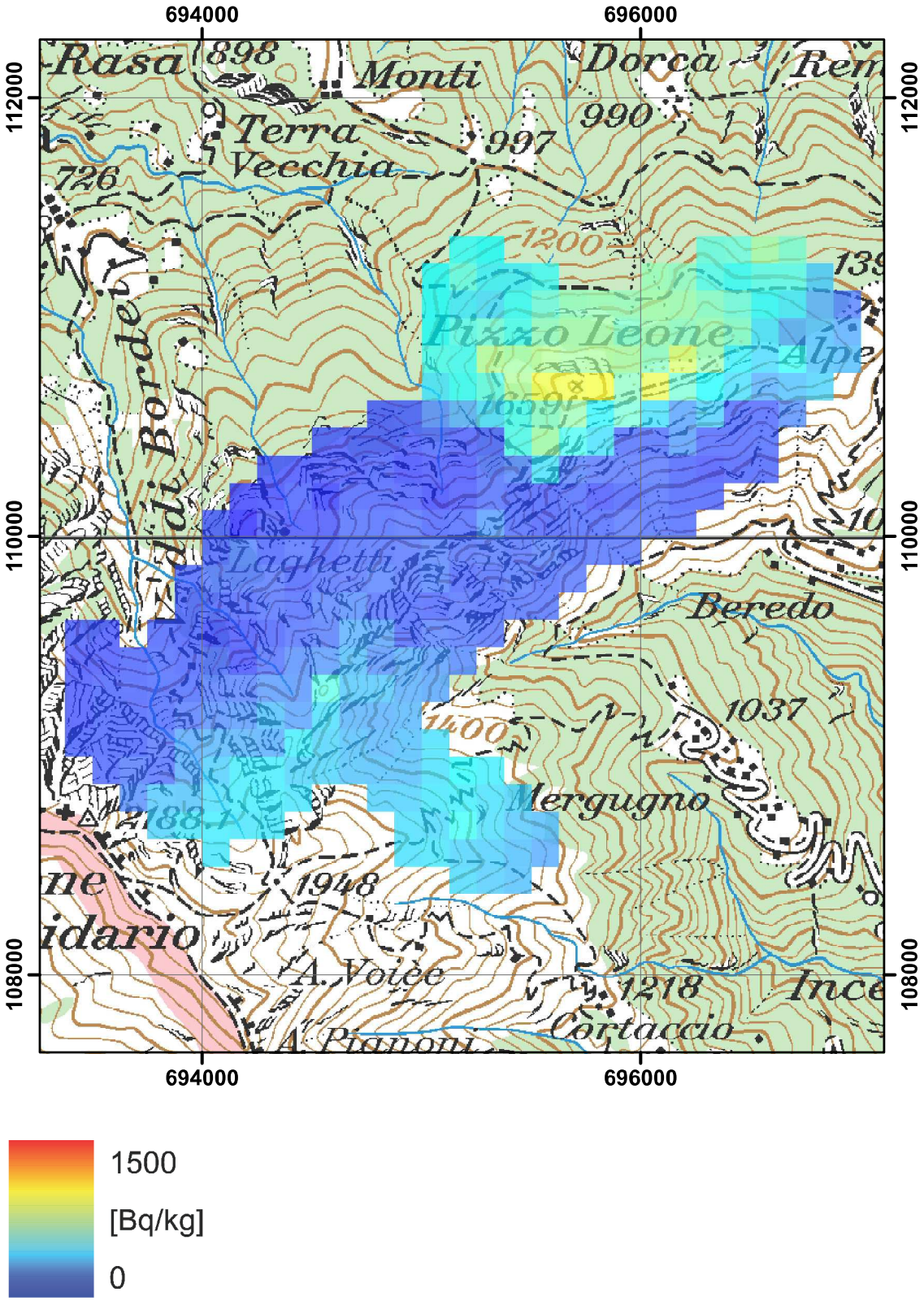

Figure 45: ^{40}K activity concentration at the Pizzo Ometto.
PK100 © 2011 swisstopo (JD100043).

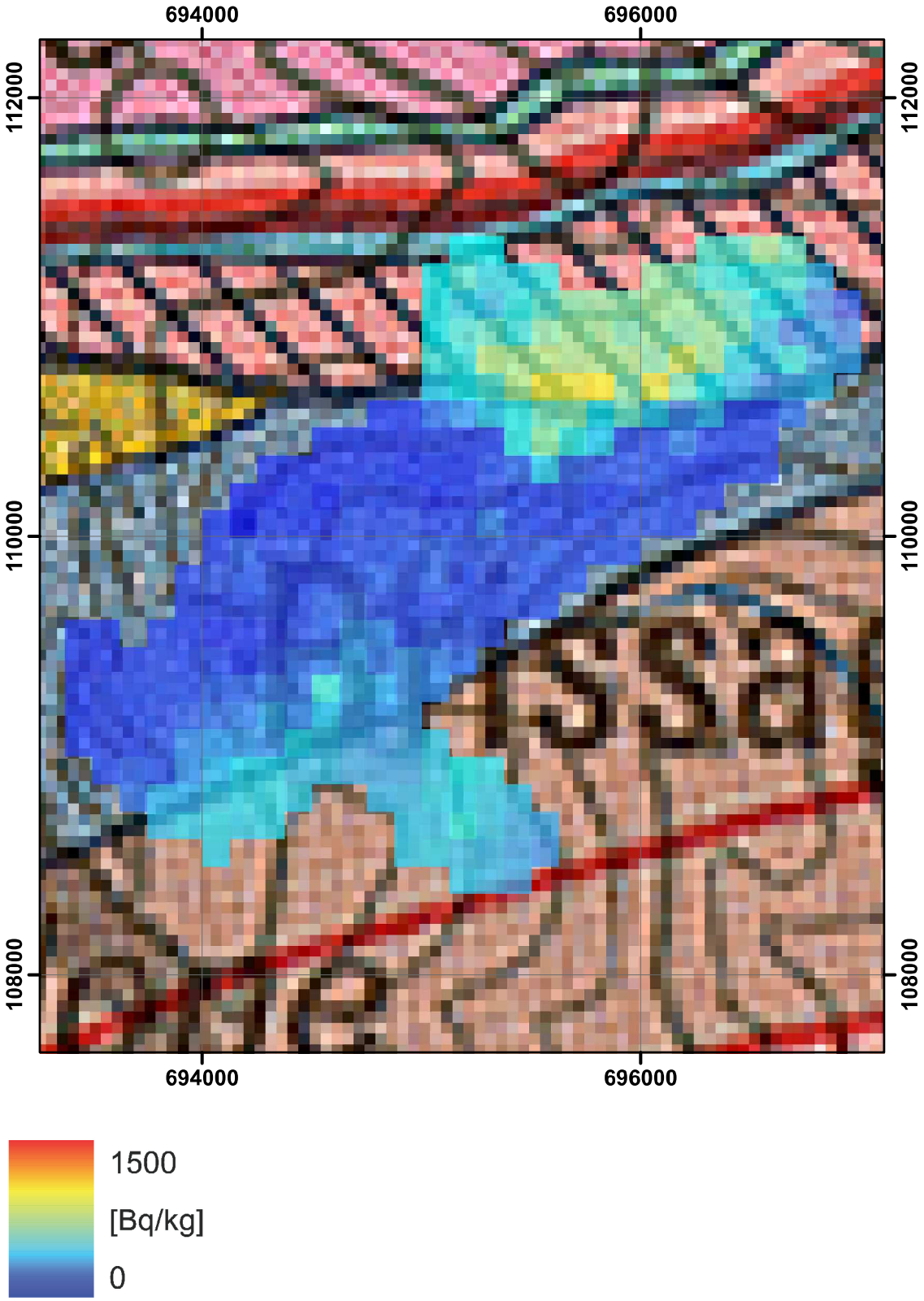

Figure 46: ^{40}K activity concentration and geology at the Pizzo Ometto. Geological atlas of Switzerland 1:500 000 © 2011 swisstopo (JD100043).

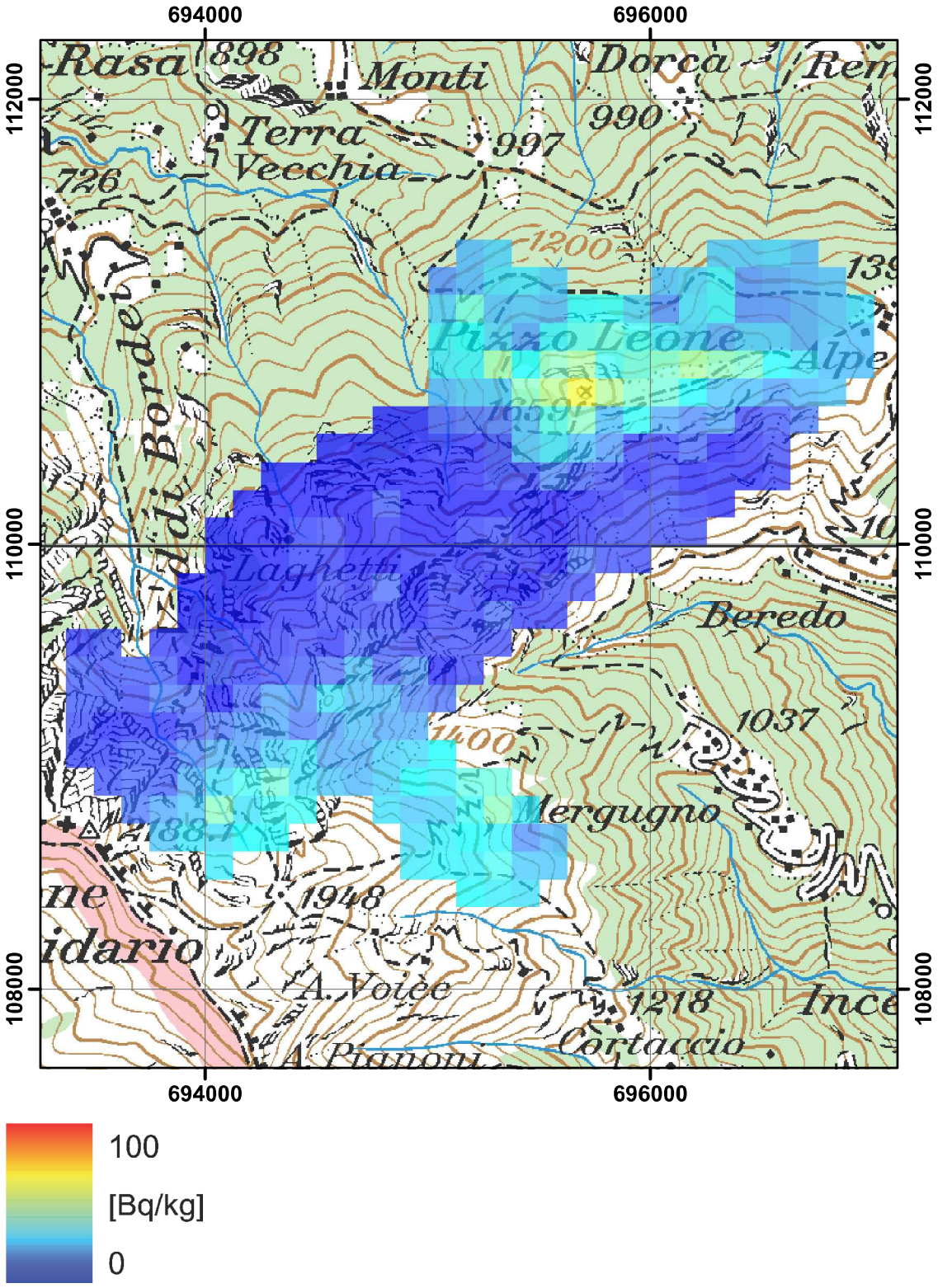

Figure 47: ^{232}Th activity concentration at the Pizzo Ometto.
PK100 © 2011 swisstopo (JD100043).

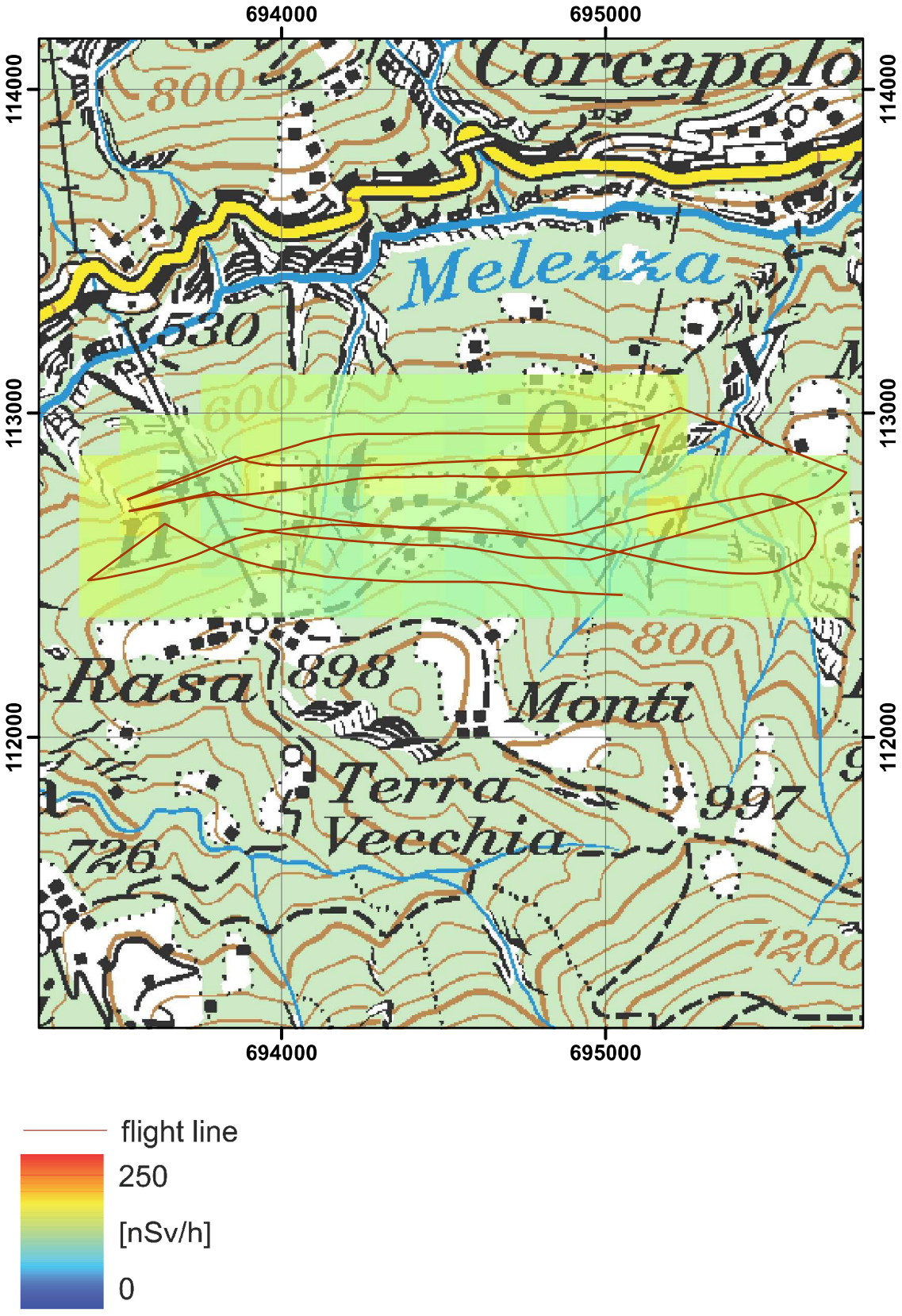

Figure 48: Dose rate in the vicinity of Rasa.
PK100 © 2011 swisstopo (JD100043).

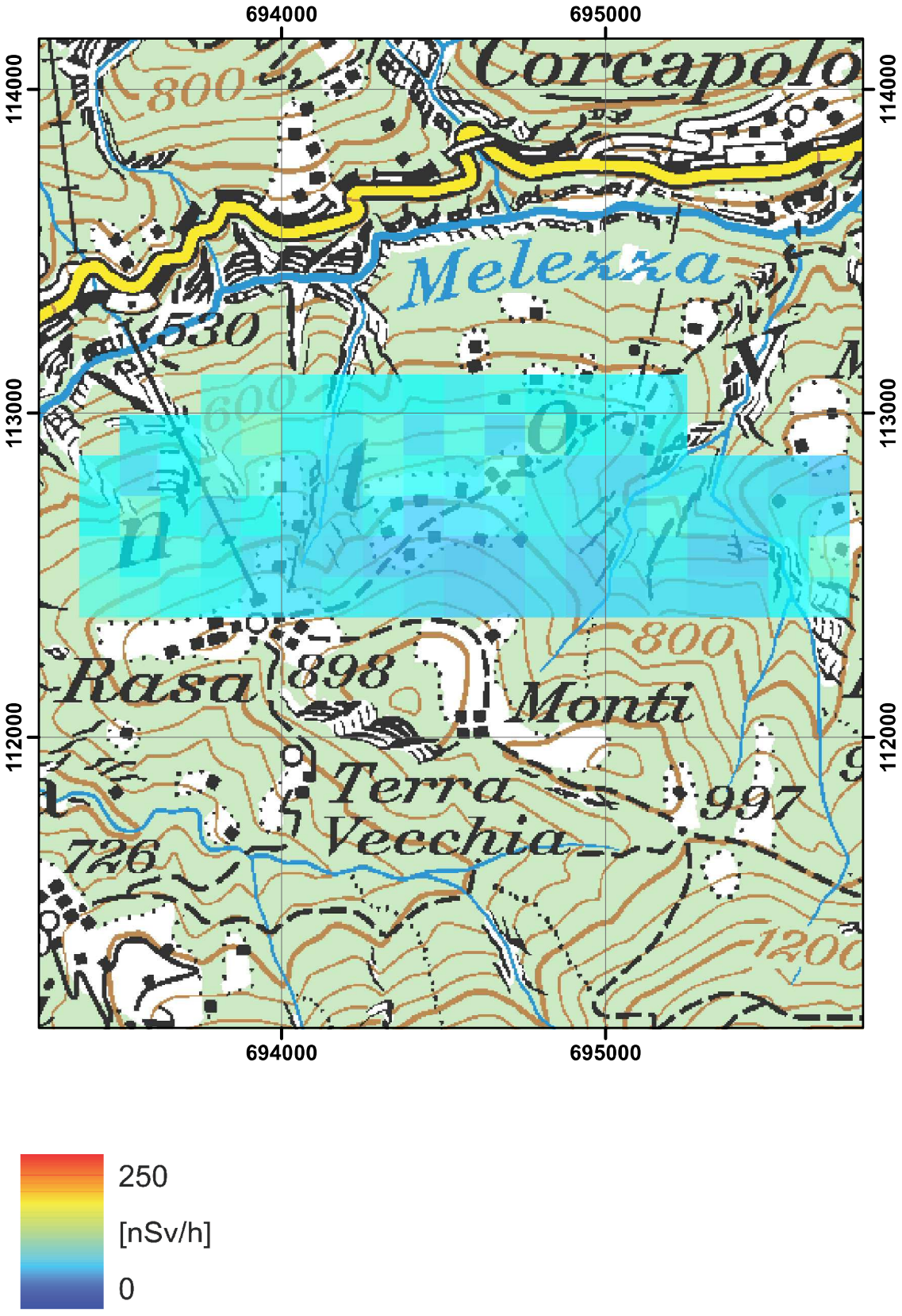

Figure 49: Terrestrial dose rate in the vicinity of Rasa.
PK100 © 2011 swisstopo (JD100043).

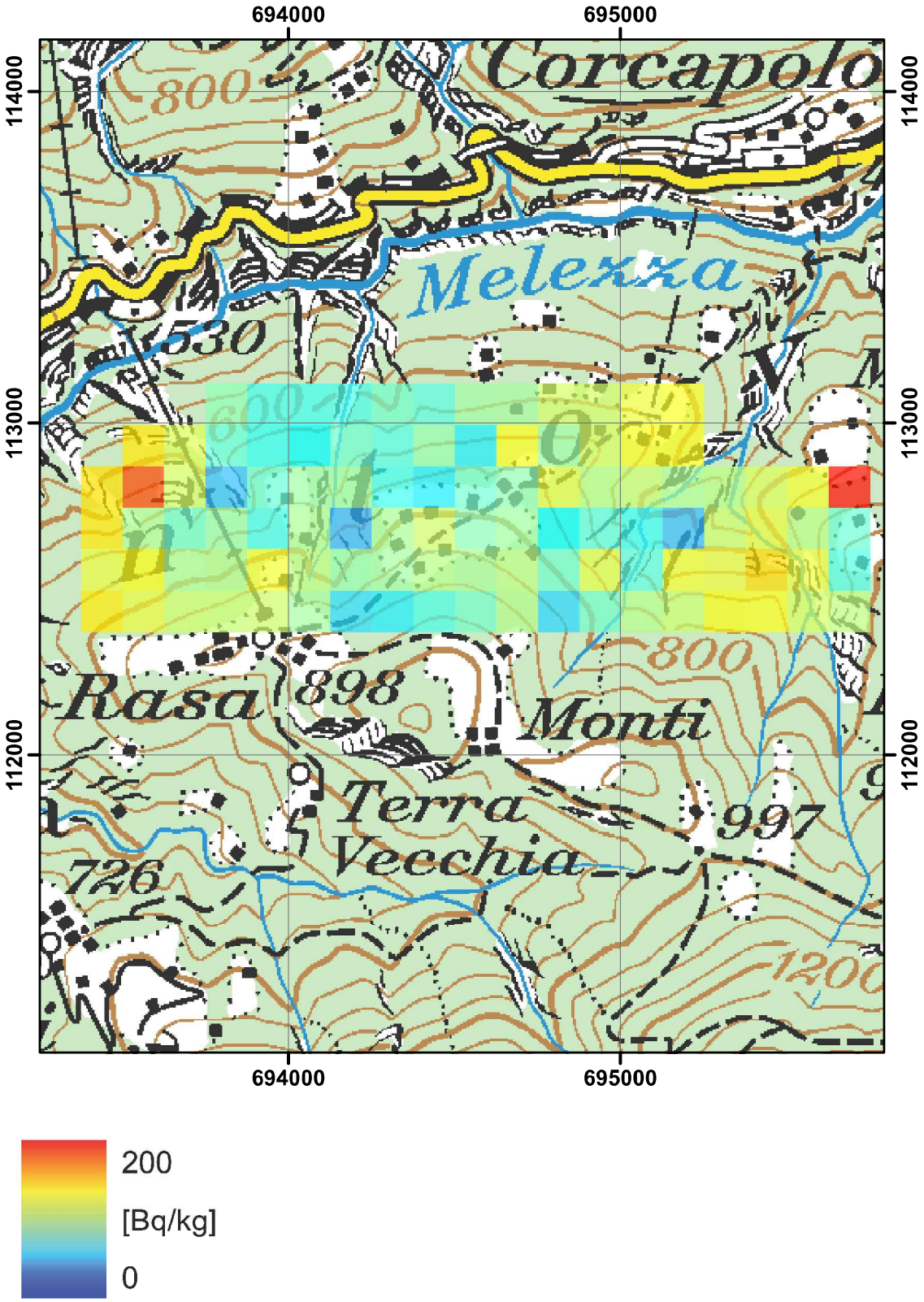

Figure 50: ^{137}Cs activity concentration in the vicinity of Rasa. PK100 © 2011 swisstopo (JD100043).

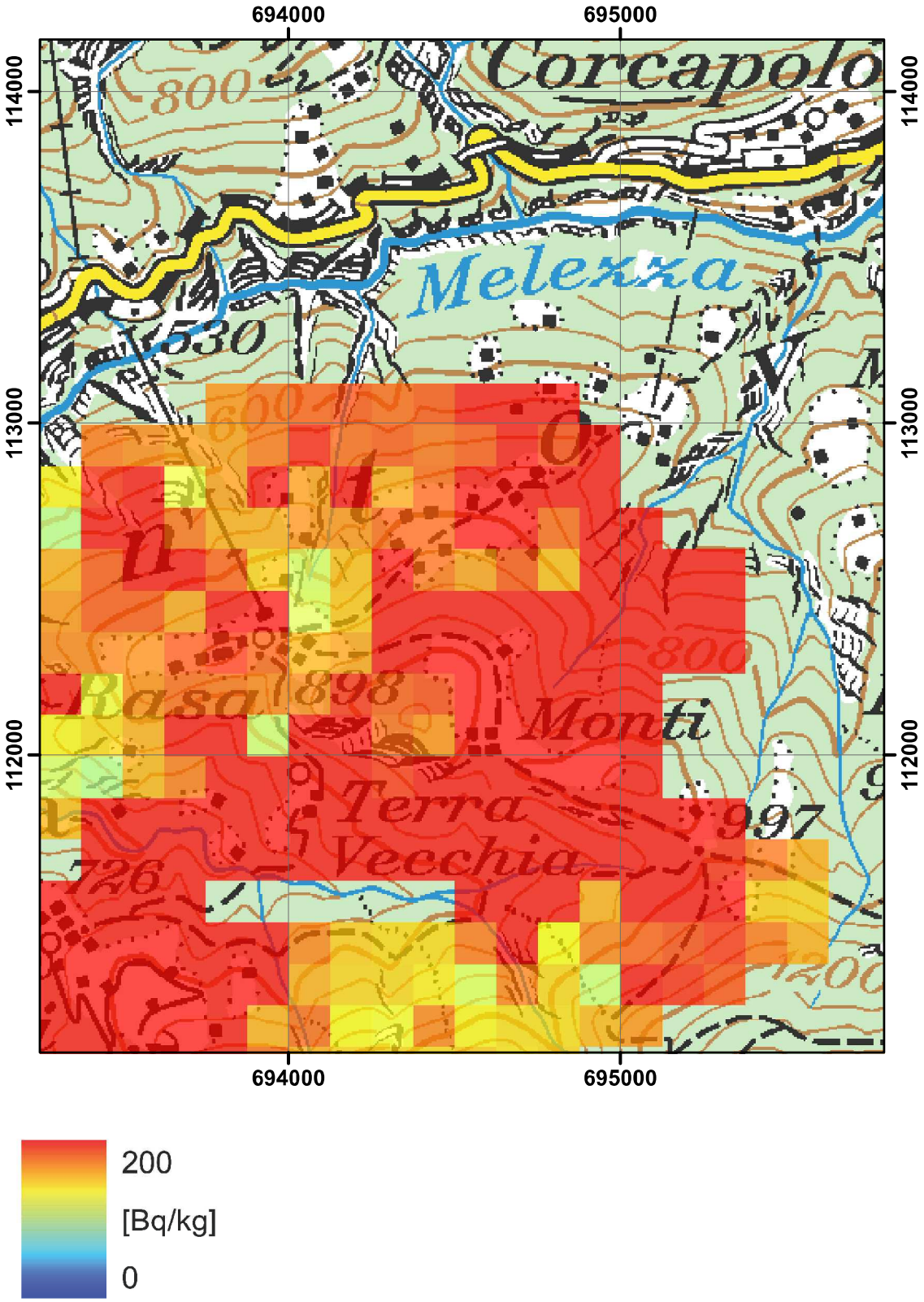

Figure 51: ^{137}Cs activity concentration measured 1998 in the vicinity of Rasa. PK100 © 2011 swisstopo (JD100043).

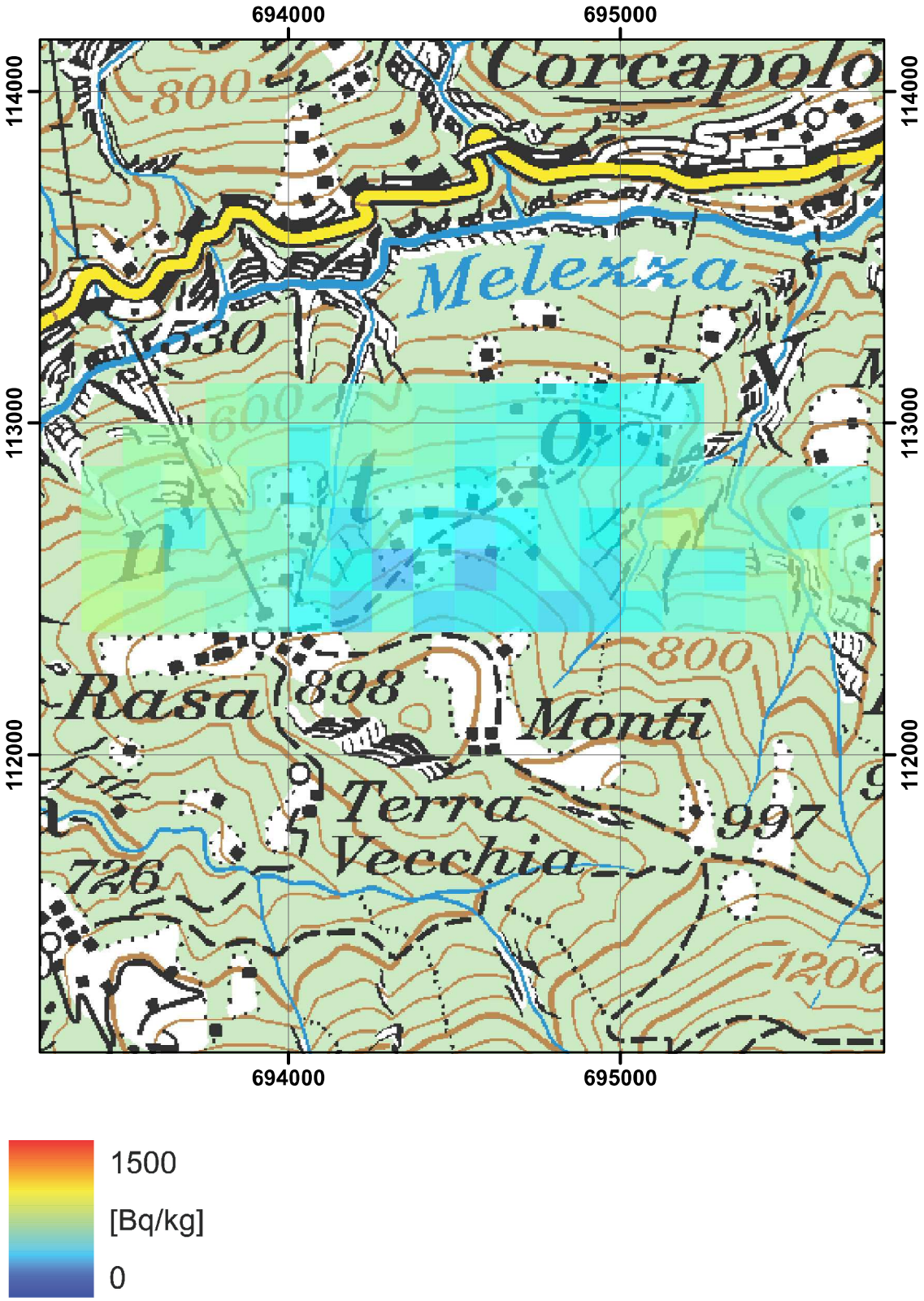

Figure 52: ^{40}K activity concentration in the vicinity of Rasa.
PK100 © 2011 swisstopo (JD100043).

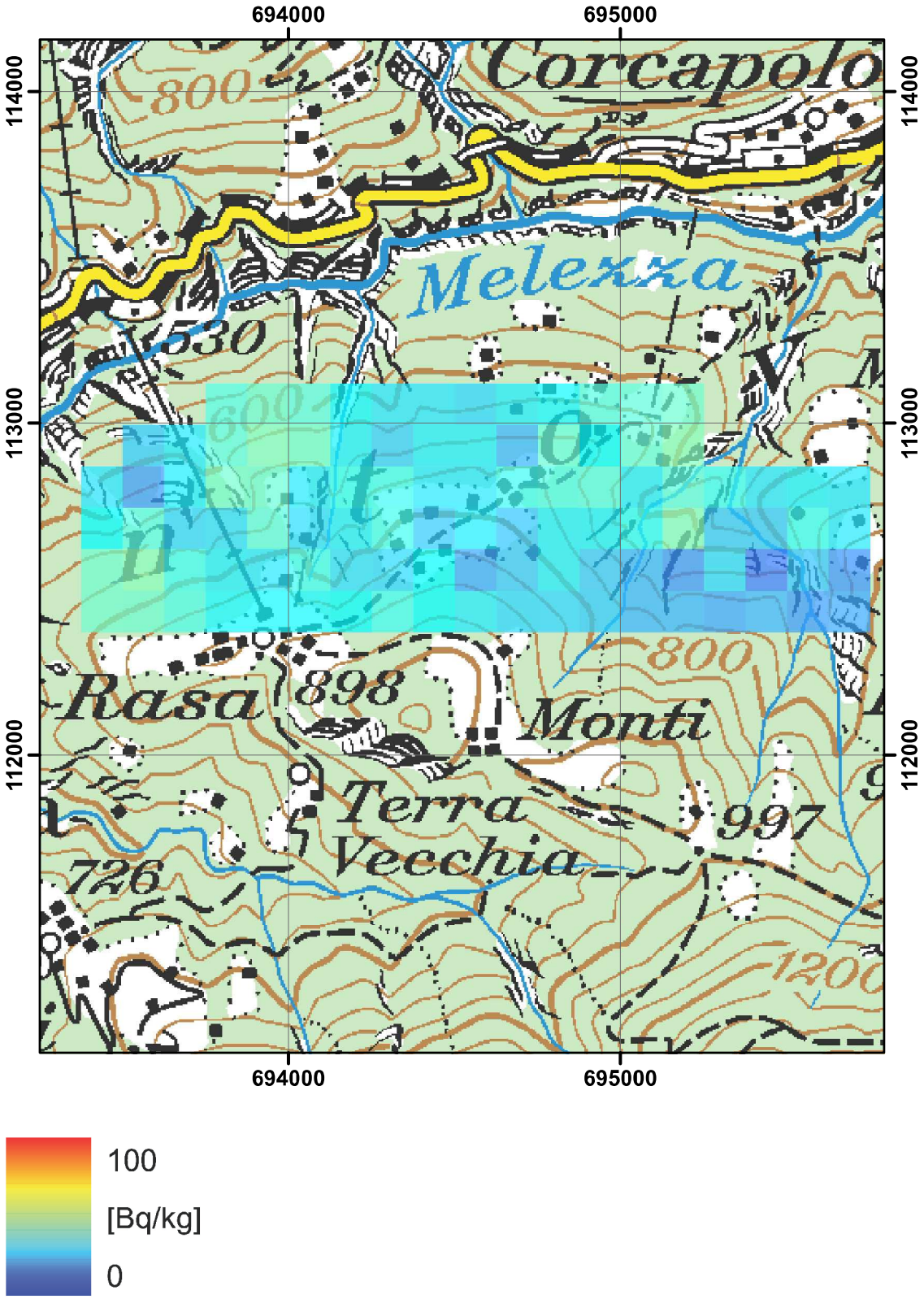

Figure 53: ^{232}Th activity concentration in the vicinity of Rasa. PK100 © 2011 swisstopo (JD100043).

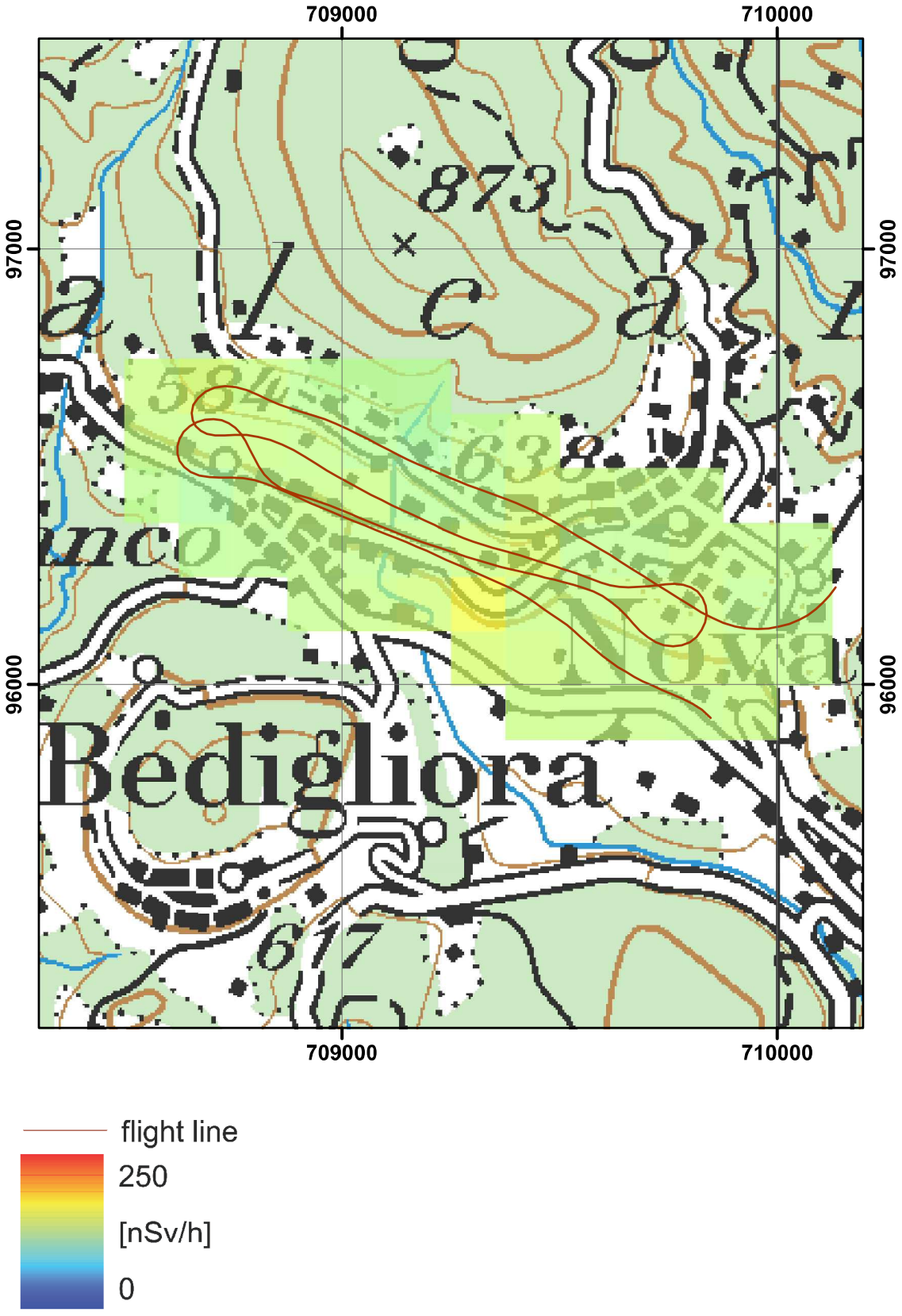

Figure 54: Dose rate near Novaggio.
PK100 © 2011 swisstopo (JD100043).

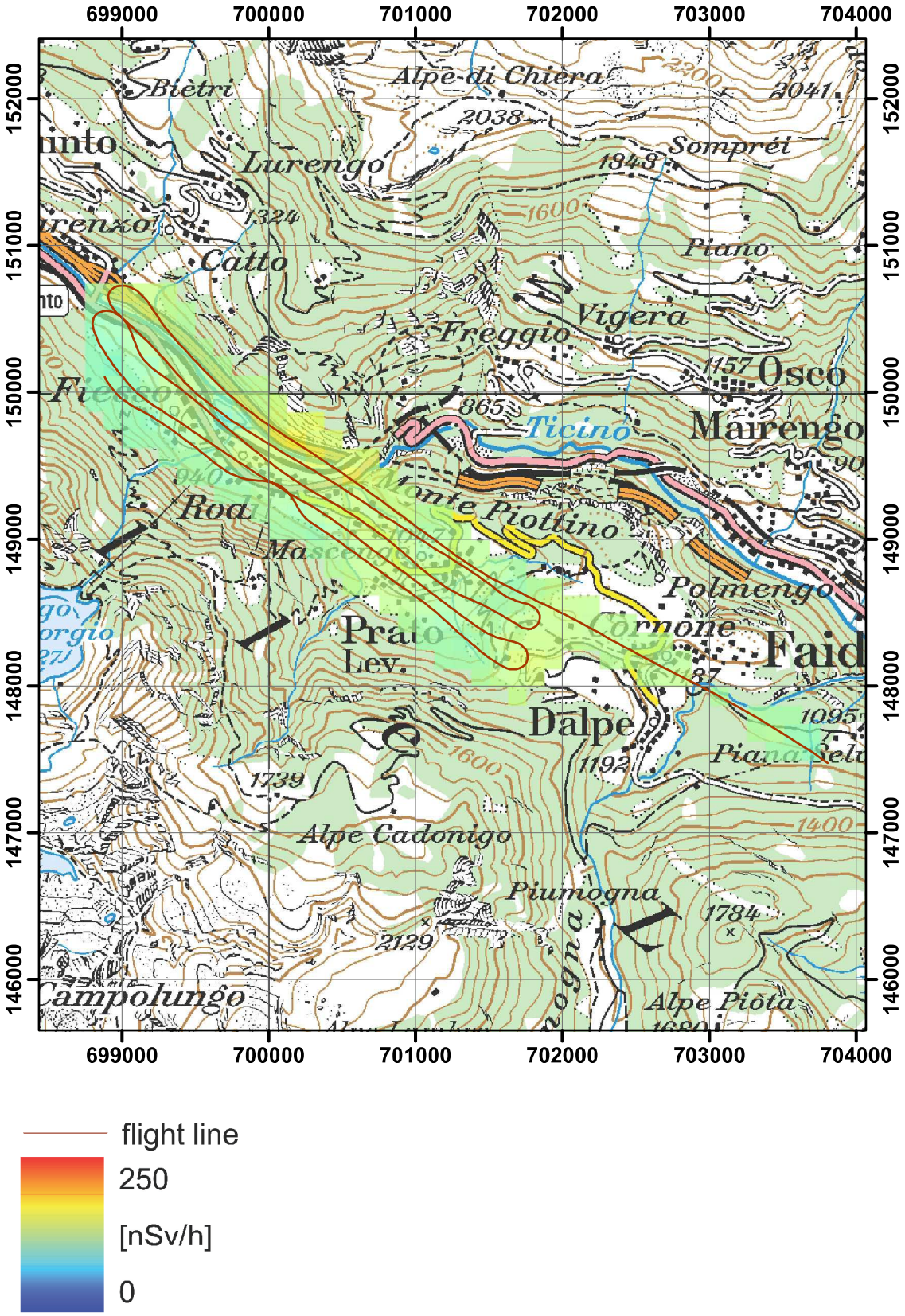

Figure 55: Dose rate near Rodi.
PK100 © 2011 swisstopo (JD100043).

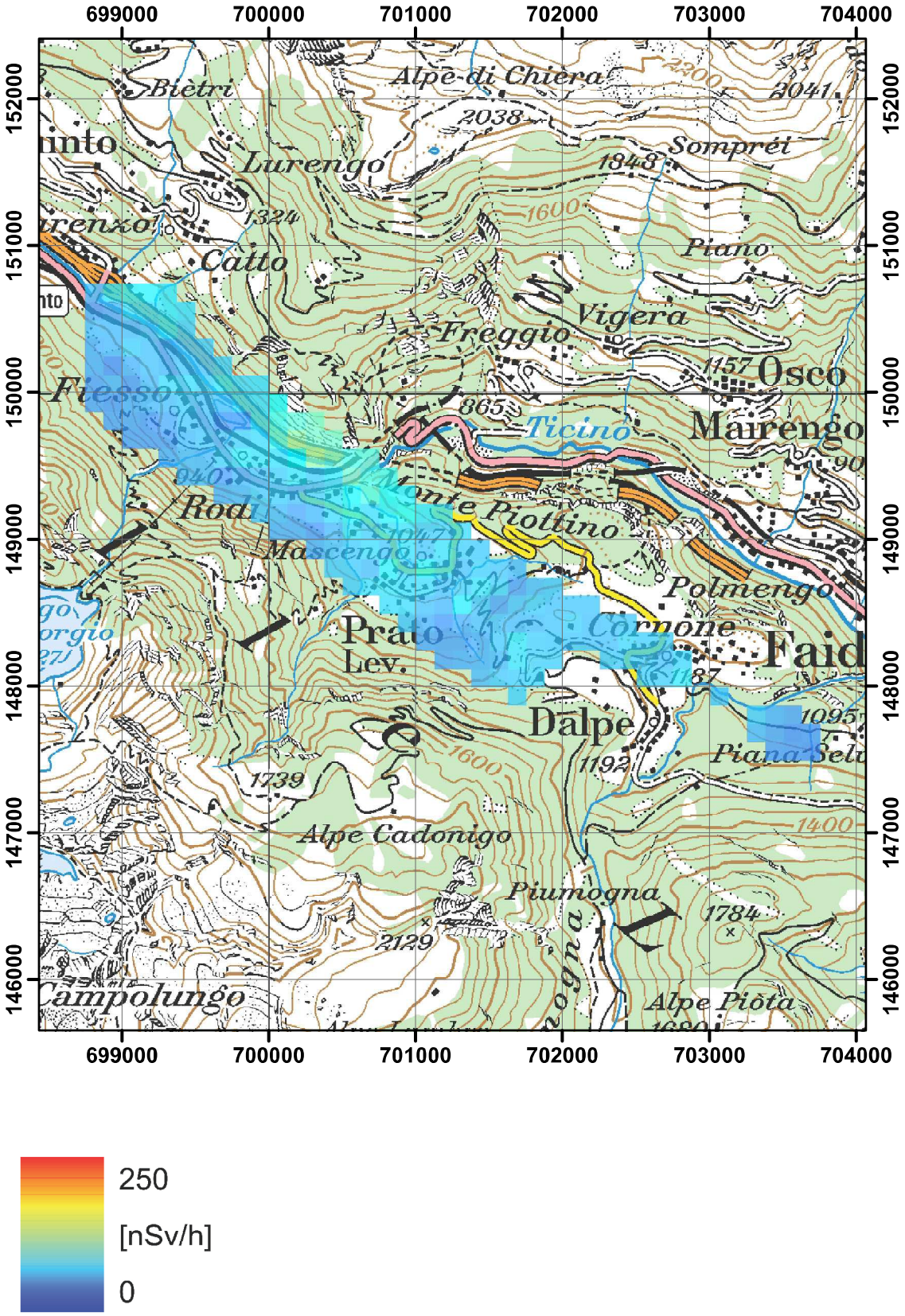

Figure 56: Terrestrial dose rate near Rodi.
PK100 © 2011 swisstopo (JD100043).

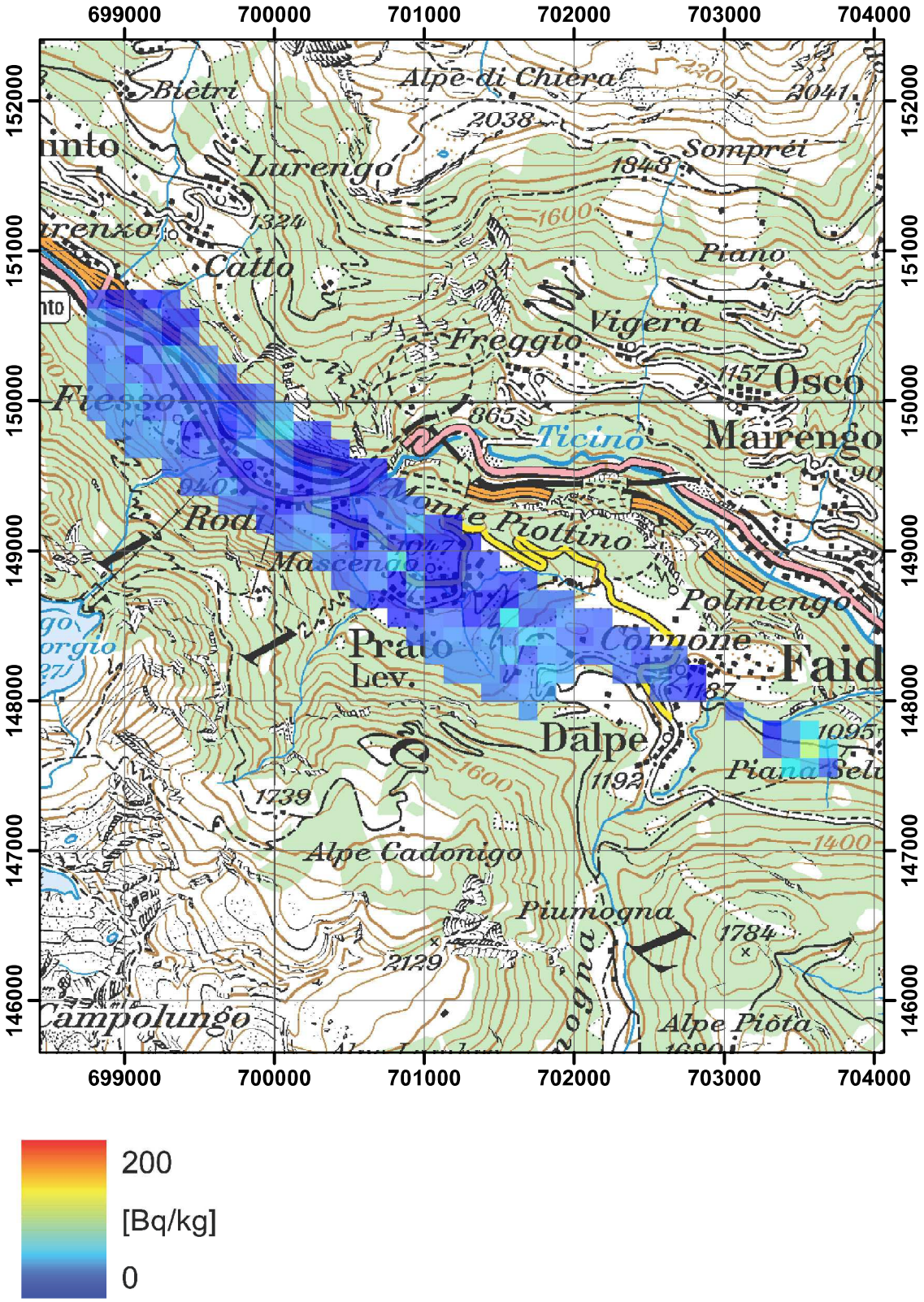

Figure 57: ^{137}Cs activity concentration near Rodi.
PK100 © 2011 swisstopo (JD100043).

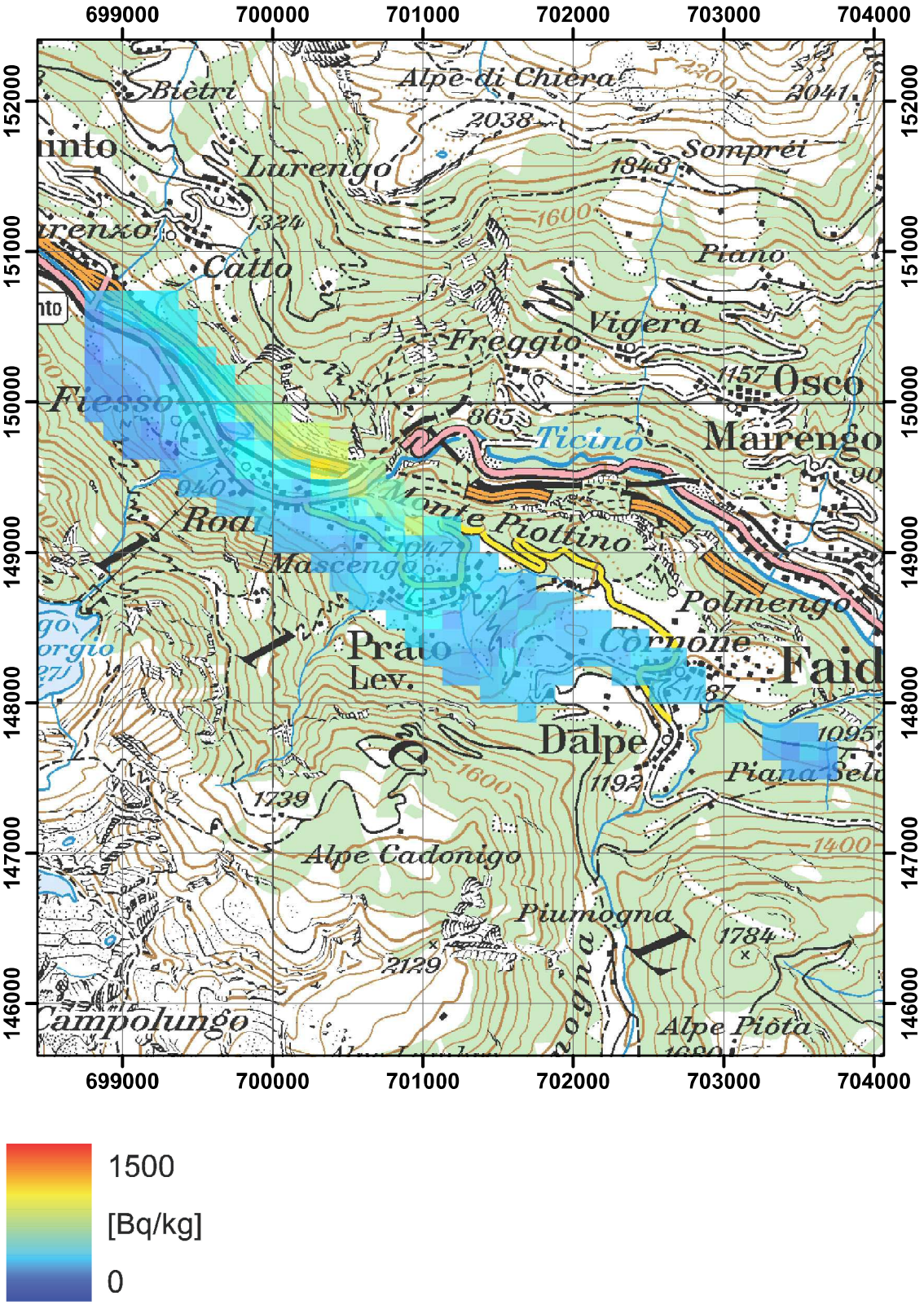

Figure 58: ^{40}K activity concentration near Rodi.
PK100 © 2011 swisstopo (JD100043).

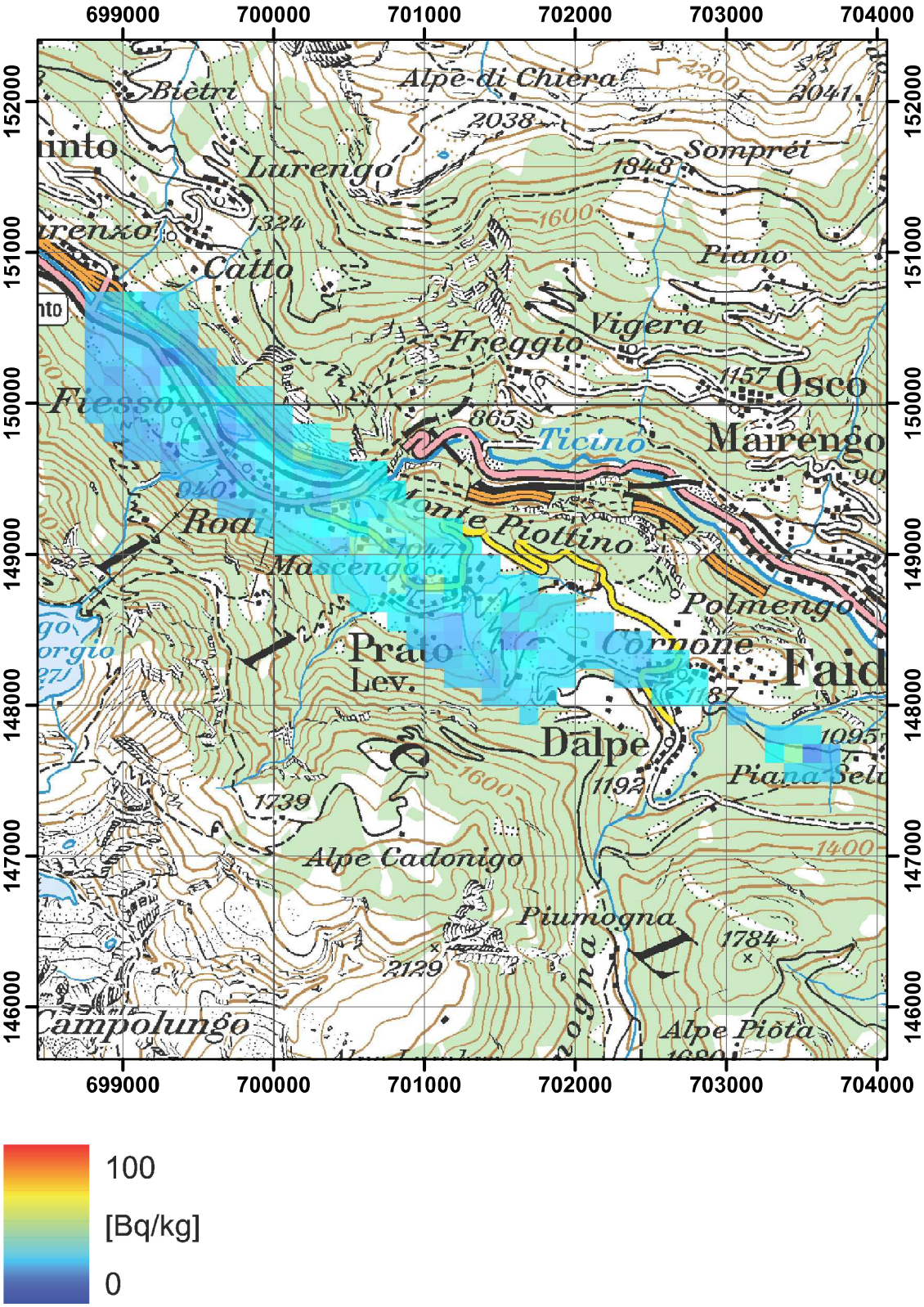

Figure 59: ^{232}Th activity concentration near Rodi.
PK100 © 2011 swisstopo (JD100043).

Figure 60: Geologic map of the Rodi area.
Geological atlas of Switzerland 1:500 000 © 2011 swisstopo (JD100043).

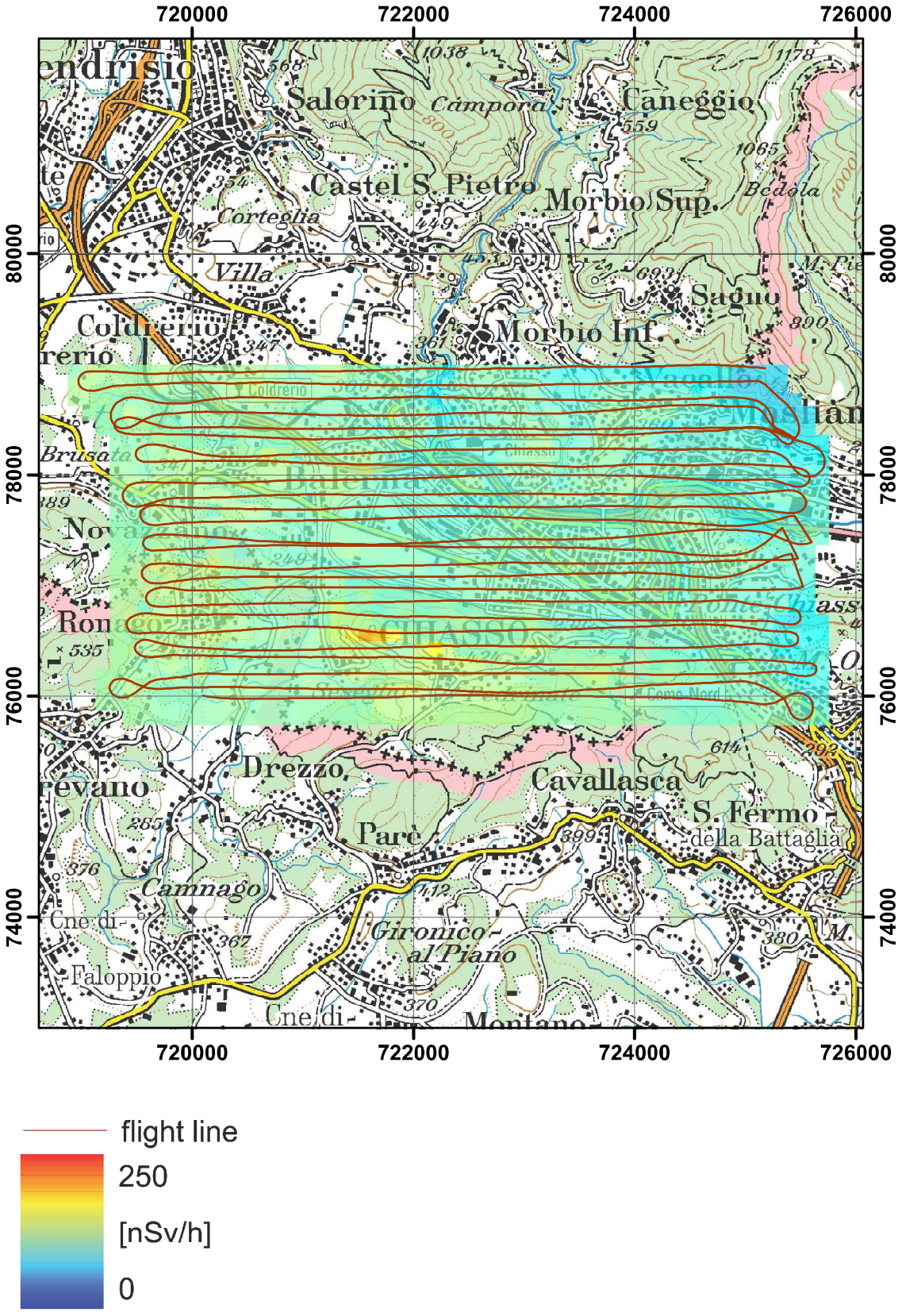

Figure 61: Dose rate at the town of Chiasso.
PK100 © 2011 swisstopo (JD100043).

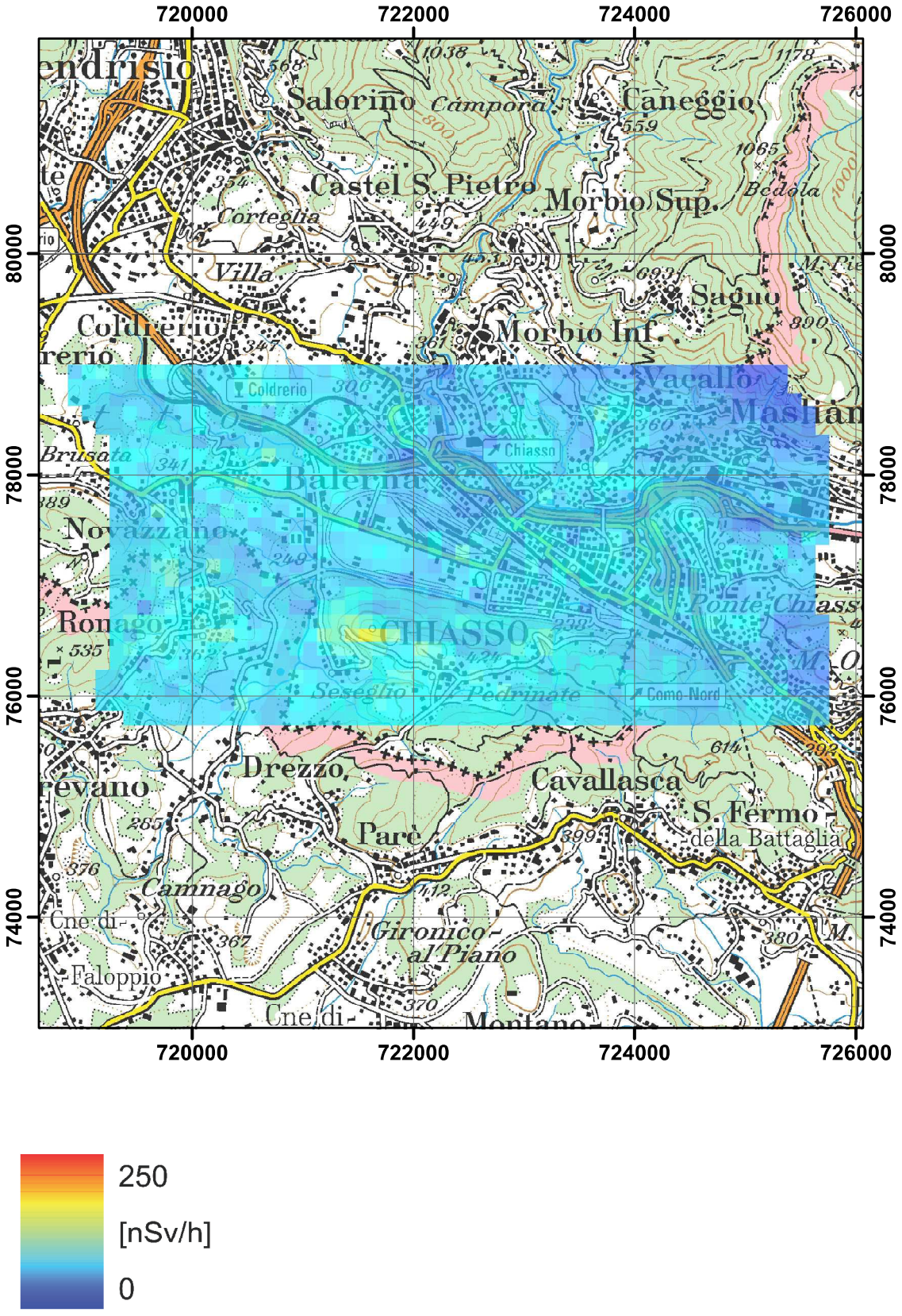

Figure 62: Terrestrial dose rate at the town of Chiasso.
PK100 © 2011 swisstopo (JD100043).

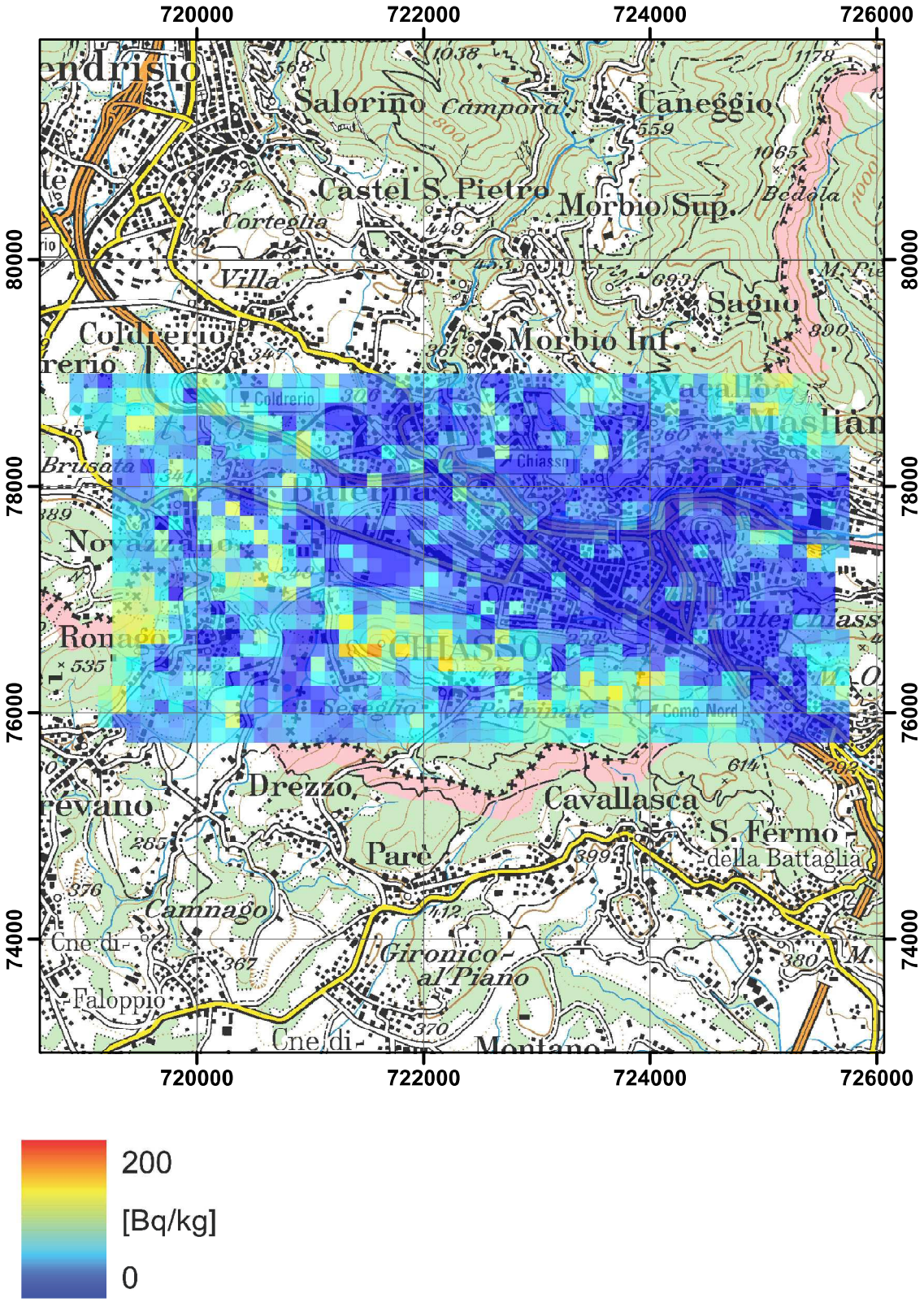

Figure 63: ^{137}Cs activity concentration at the town of Chiasso. PK100 © 2011 swisstopo (JD100043).

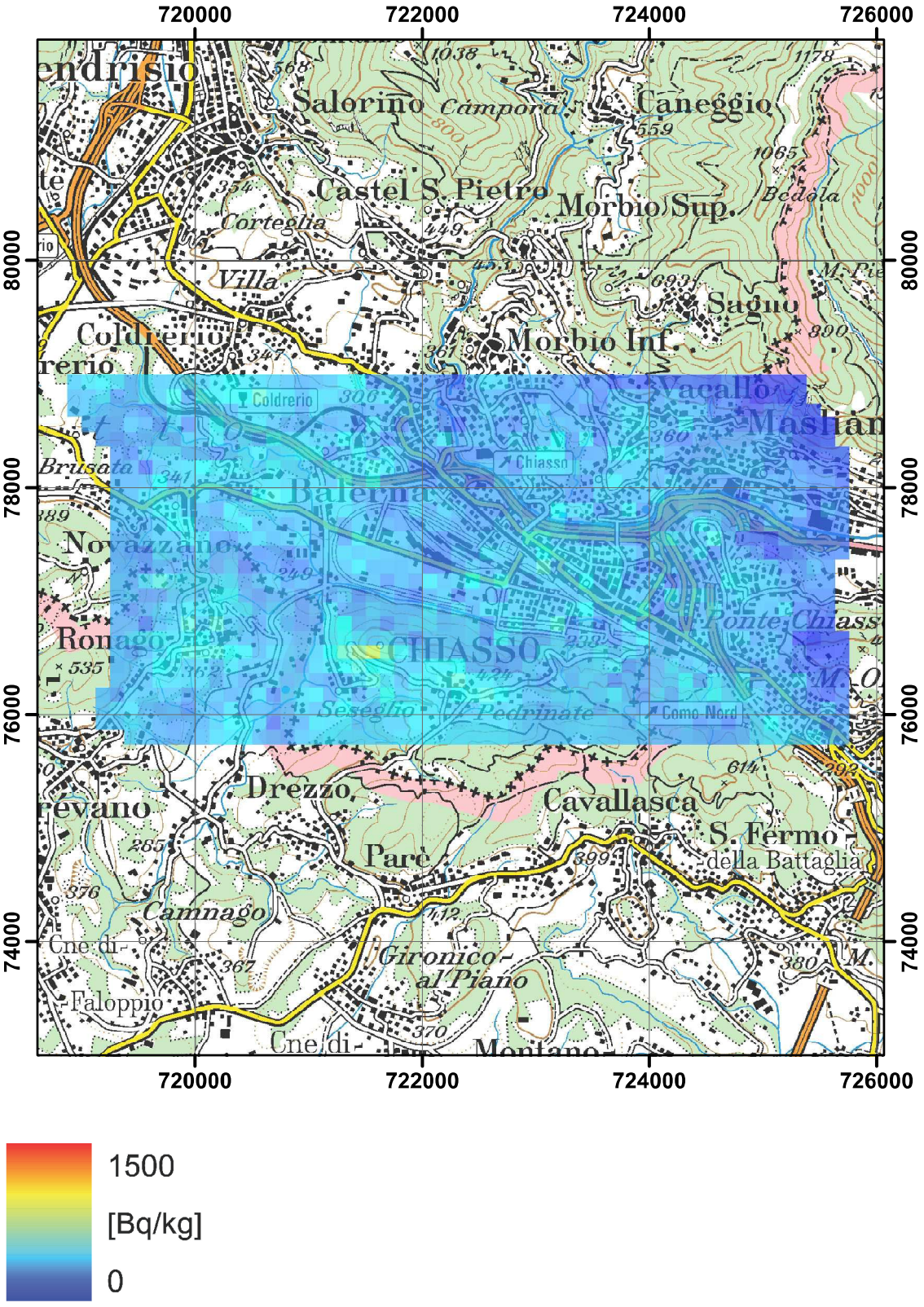

Figure 64: ^{40}K activity concentration at the town of Chiasso.
PK100 © 2011 swisstopo (JD100043).

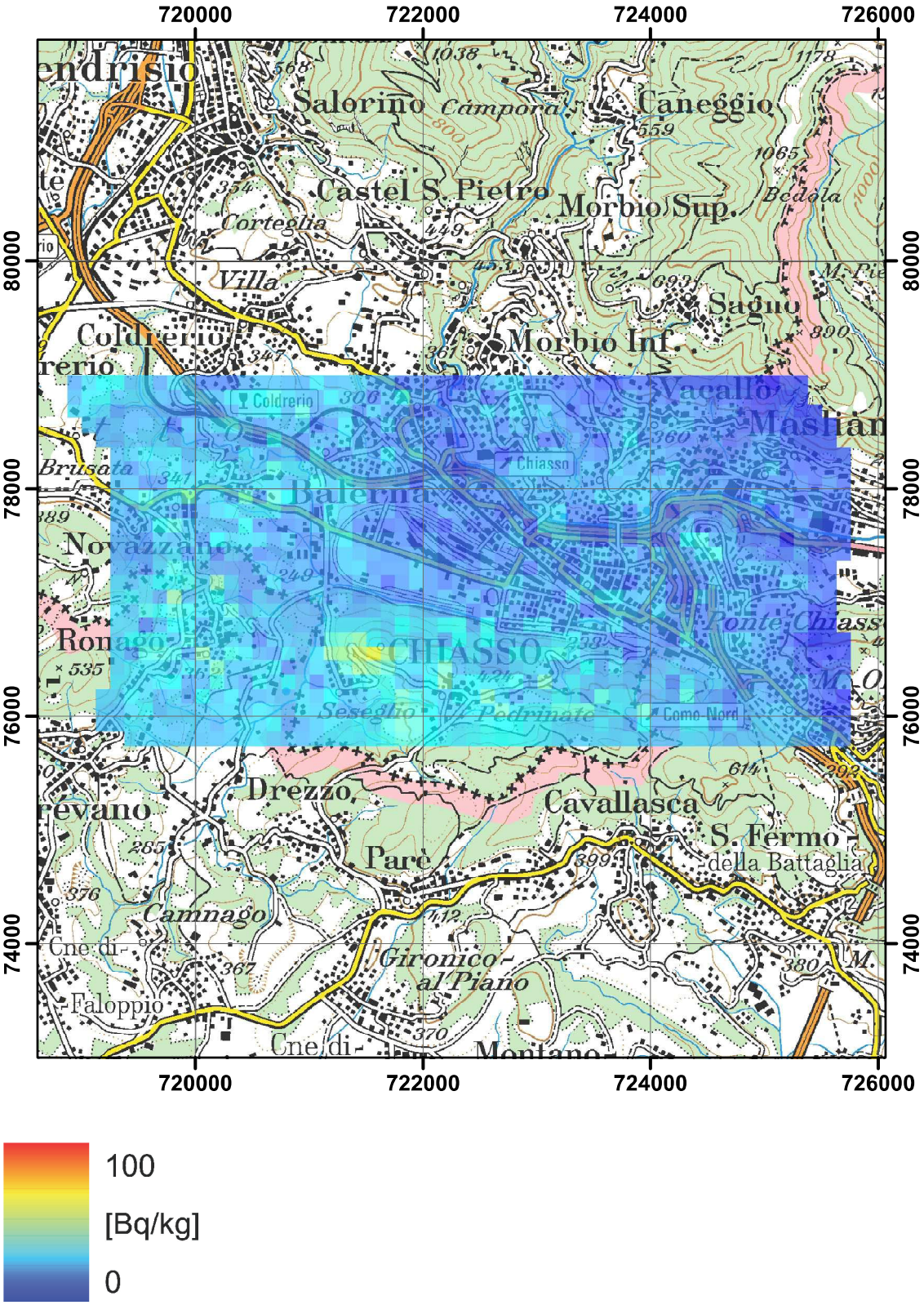

Figure 65: ^{232}Th activity concentration at the town of Chiasso.
PK100 © 2011 swisstopo (JD100043).

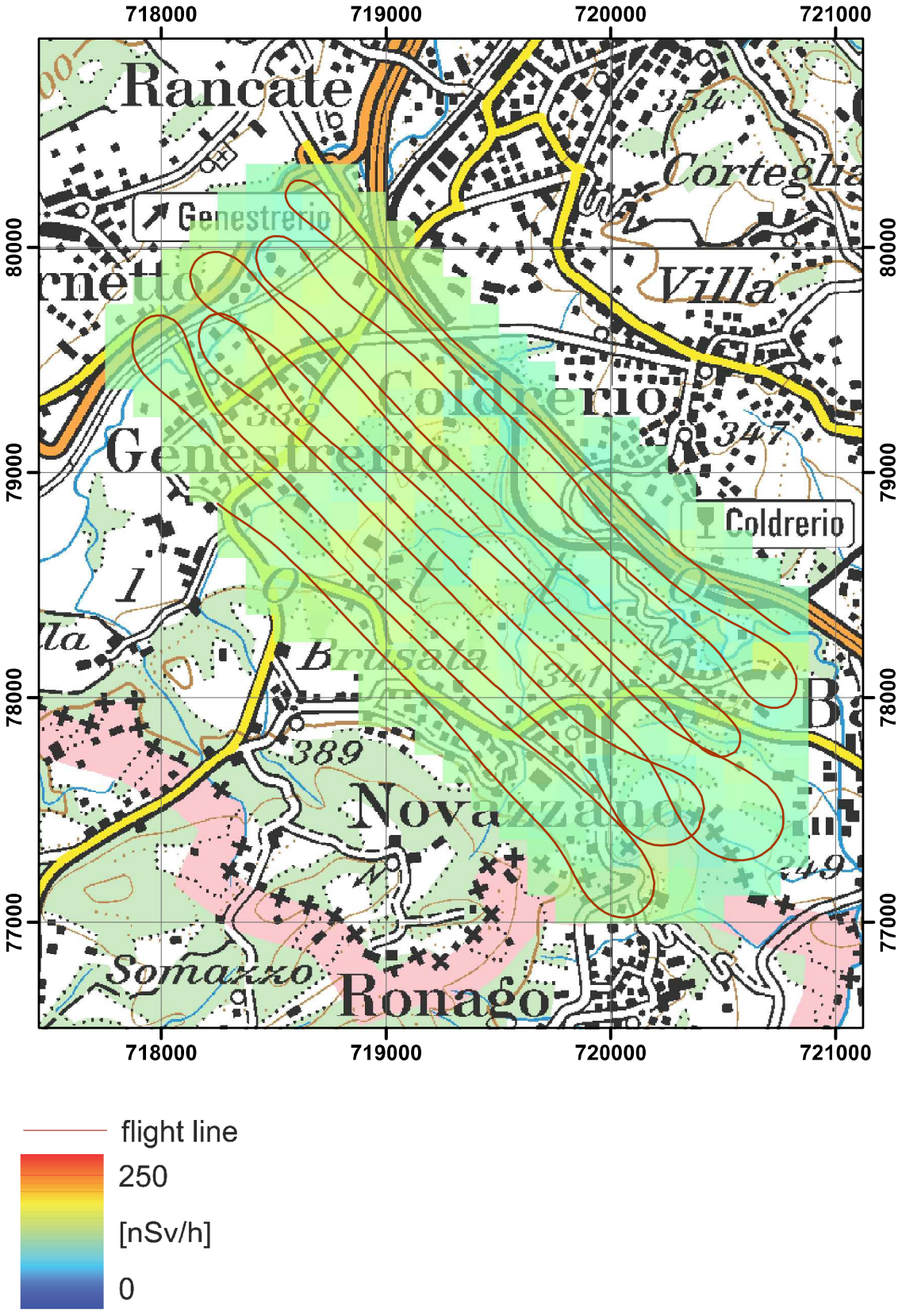

Figure 66: Dose rate between Genestrerio and Novazzano.
PK100 © 2011 swisstopo (JD100043).

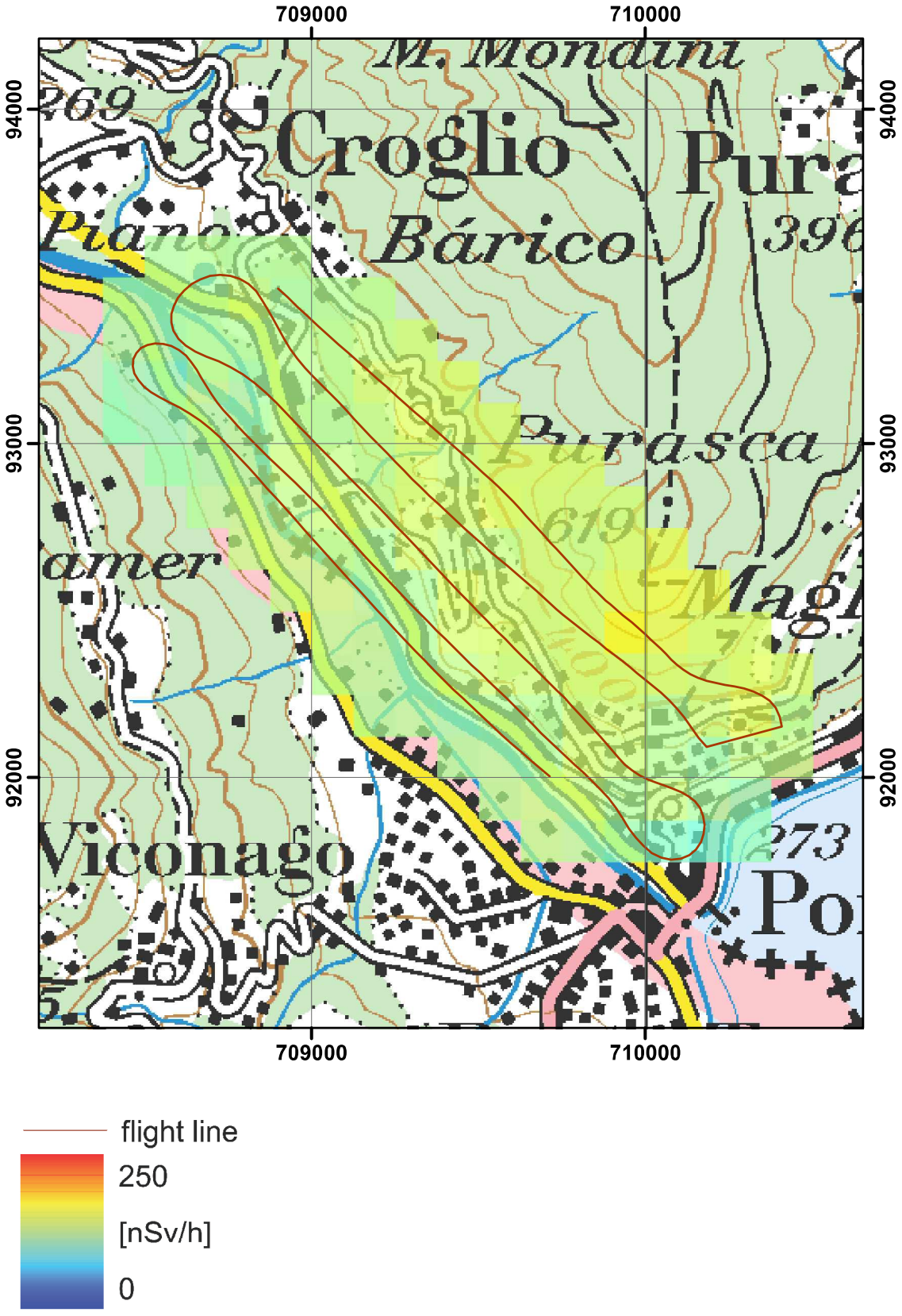

Figure 67: Dose rate near Croglio.
PK100 © 2011 swisstopo (JD100043).

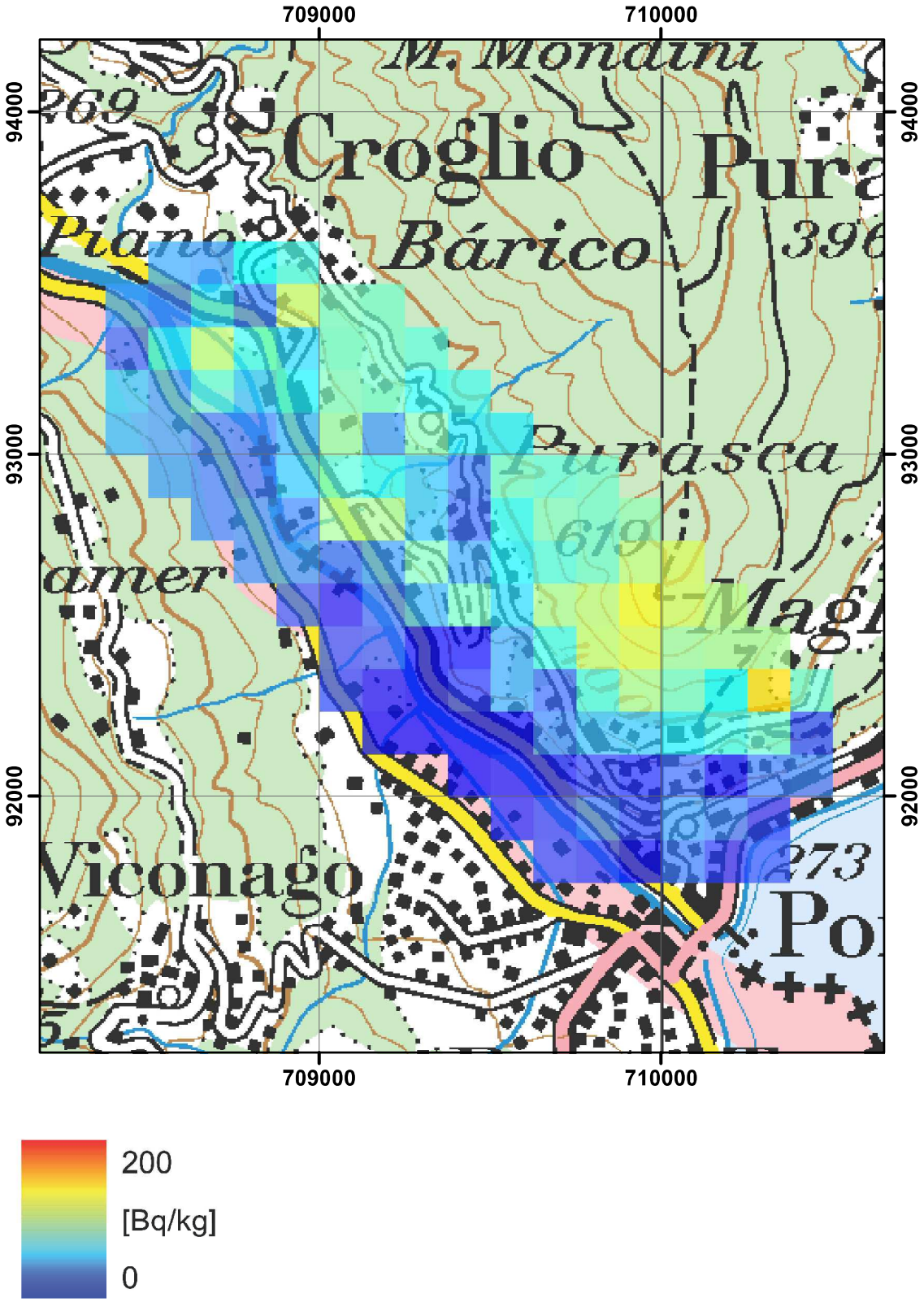

Figure 68: ^{137}Cs activity concentration near Croglio.
PK100 © 2011 swisstopo (JD100043).

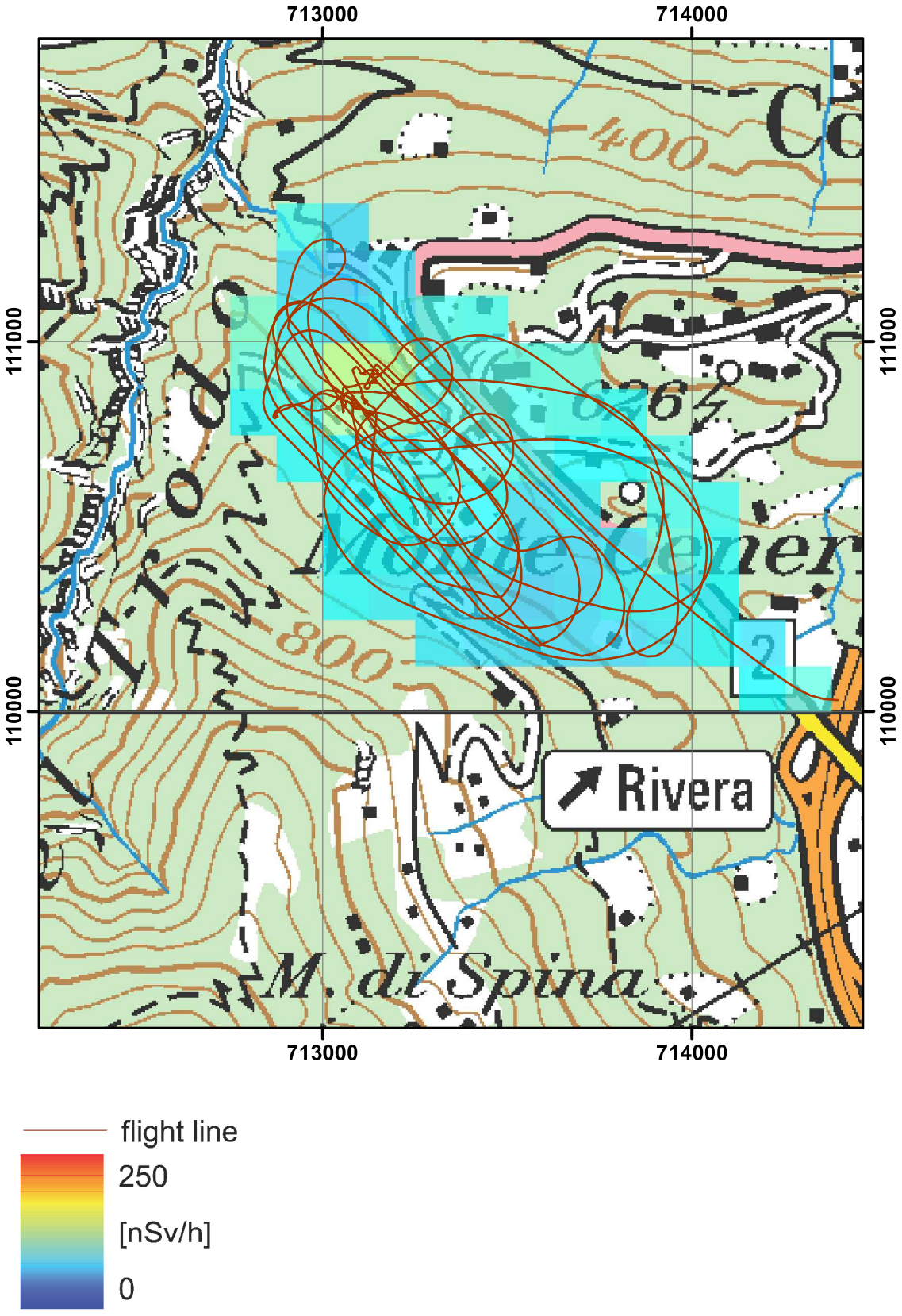

Figure 69: Dose rate in the vicinity of the exercise area near Monte Ceneri. PK100 © 2011 swisstopo (JD100043).

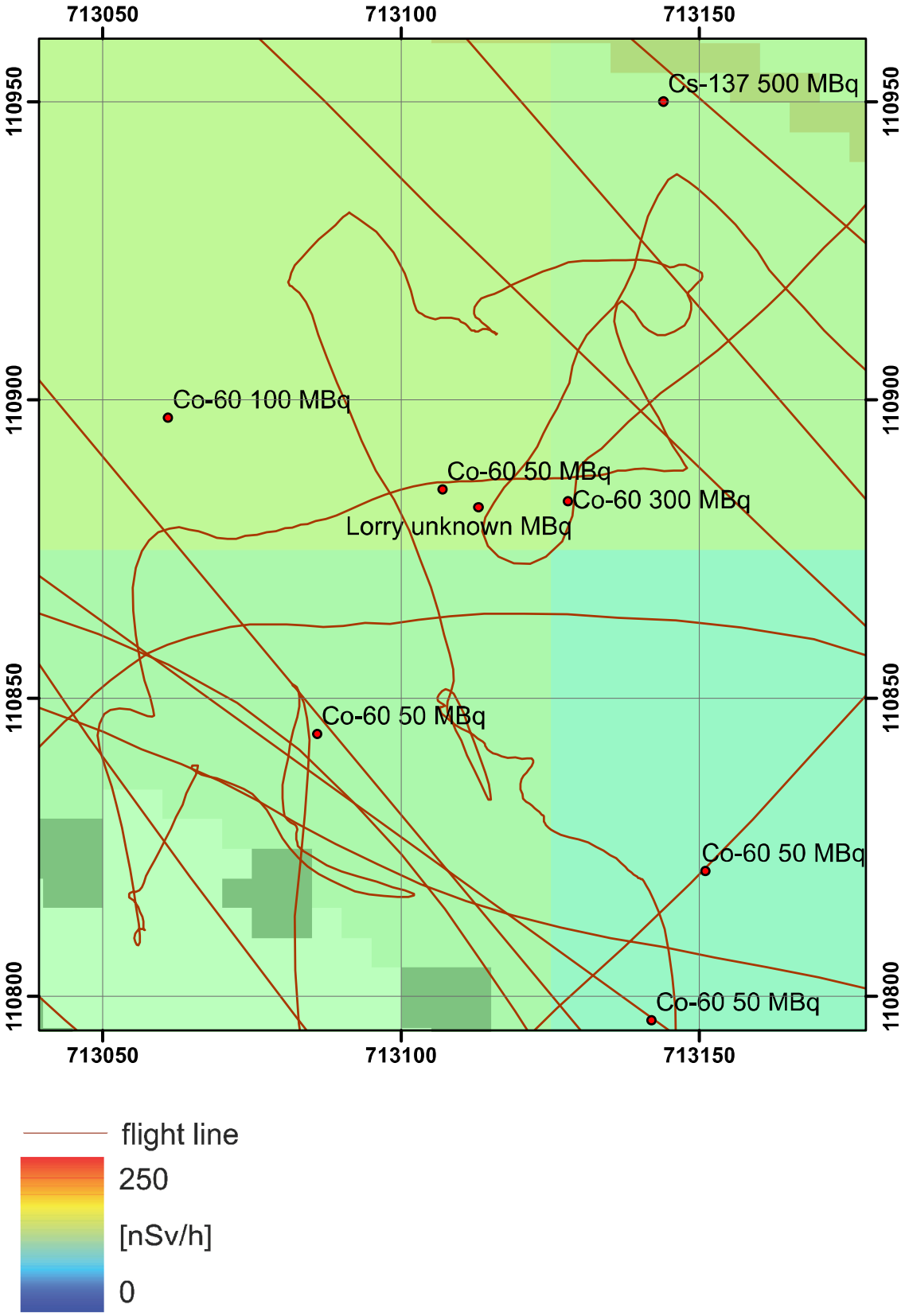

Figure 70: Dose rate and placed radioactive sources at the exercise area near Monte Ceneri. PK100 © 2011 swisstopo (JD100043).

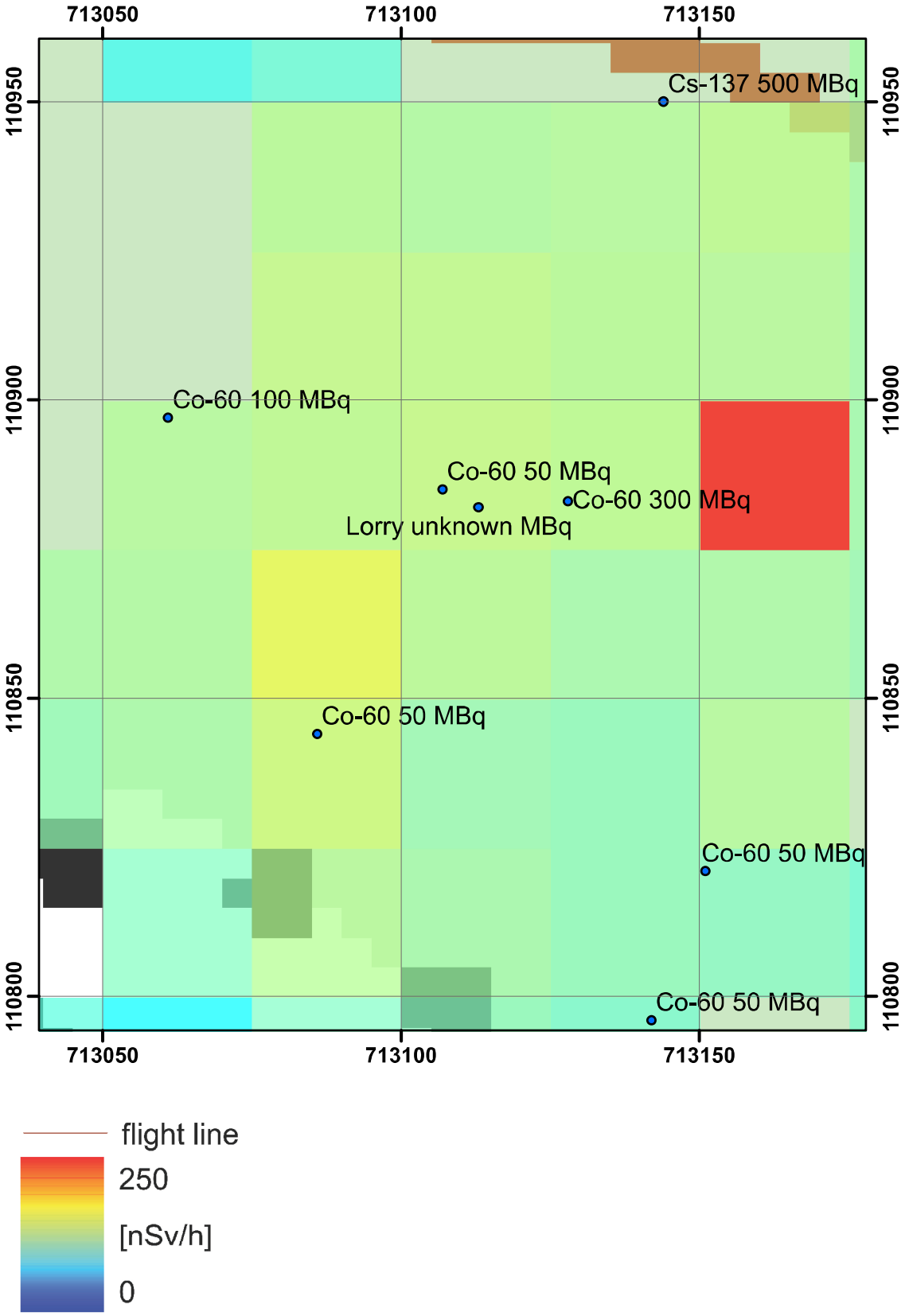

Figure 71: Dose rate at the exercise area near Monte Ceneri.
PK100 © 2011 swisstopo (JD100043).

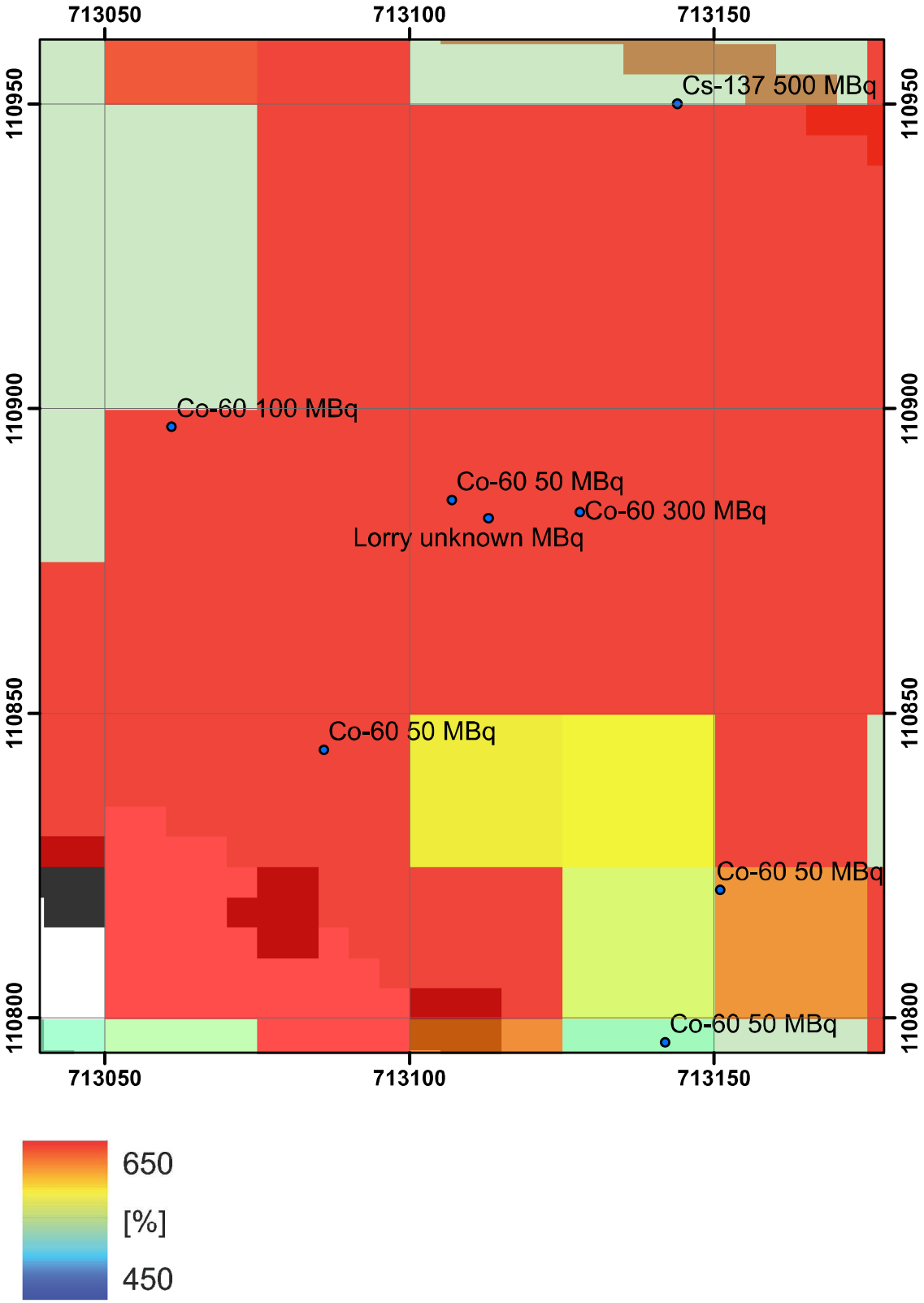

Figure 72: MMGC ratio at the exercise area near Monte Ceneri.
PK100 © 2011 swisstopo (JD100043).

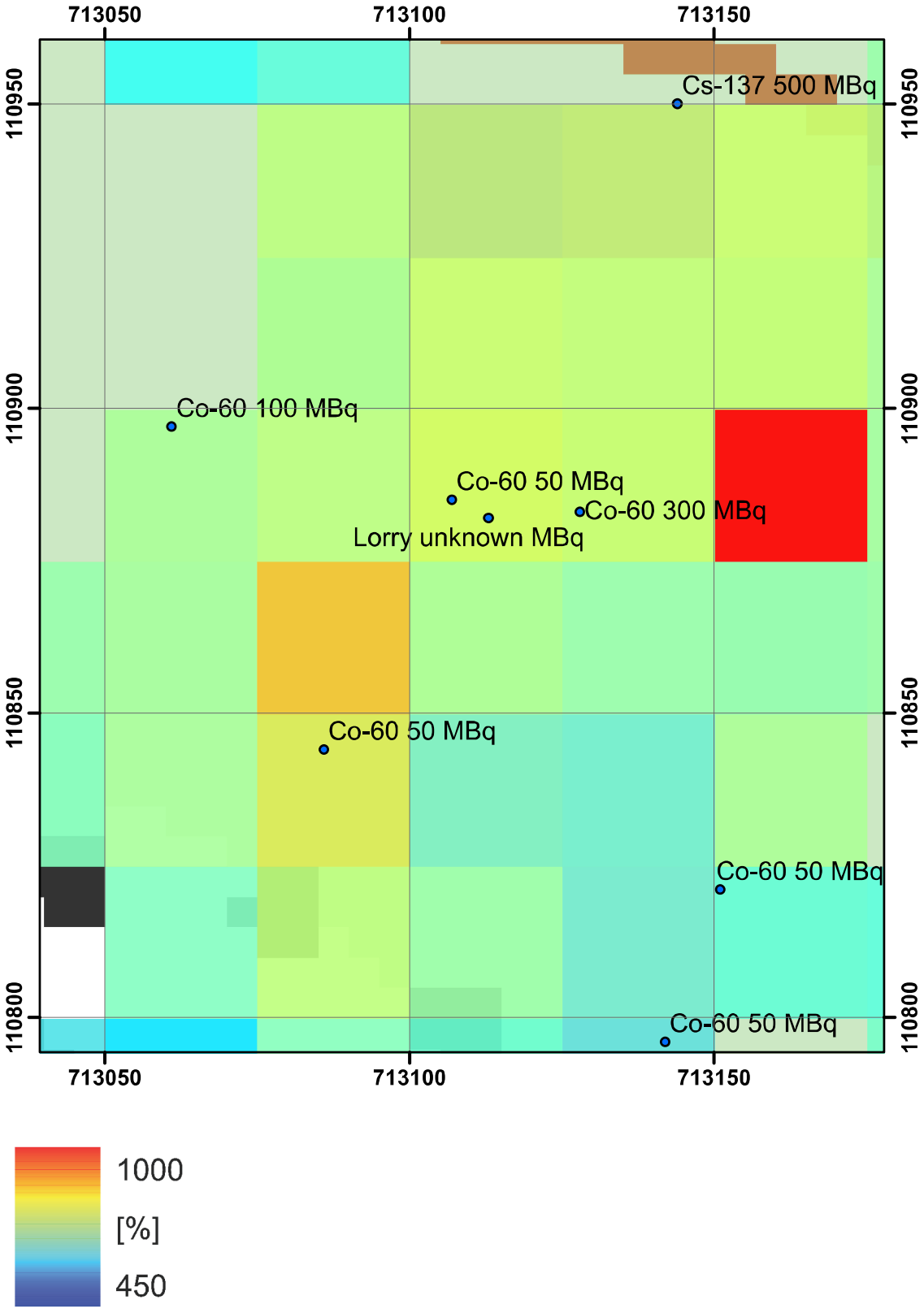

Figure 73: MMGC ratio at the exercise area near Monte Ceneri.
PK100 © 2011 swisstopo (JD100043).

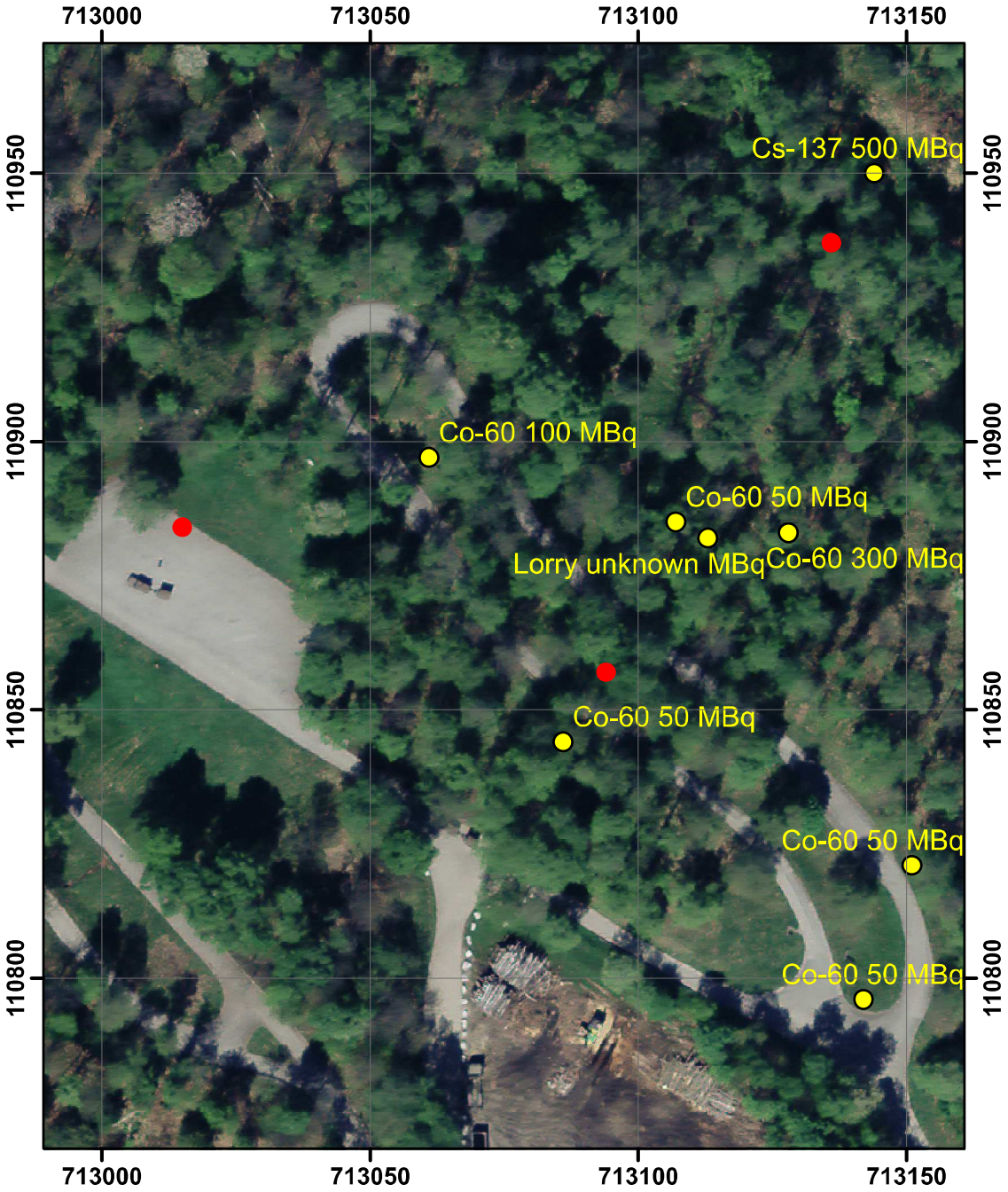

Figure 74: Aerial view of the exercise area near Monte Ceneri with markers at the location of placed (yellow circles) and suspected (red circles) radioactive sources. SwissImage © 2011 swisstopo (JD100043).

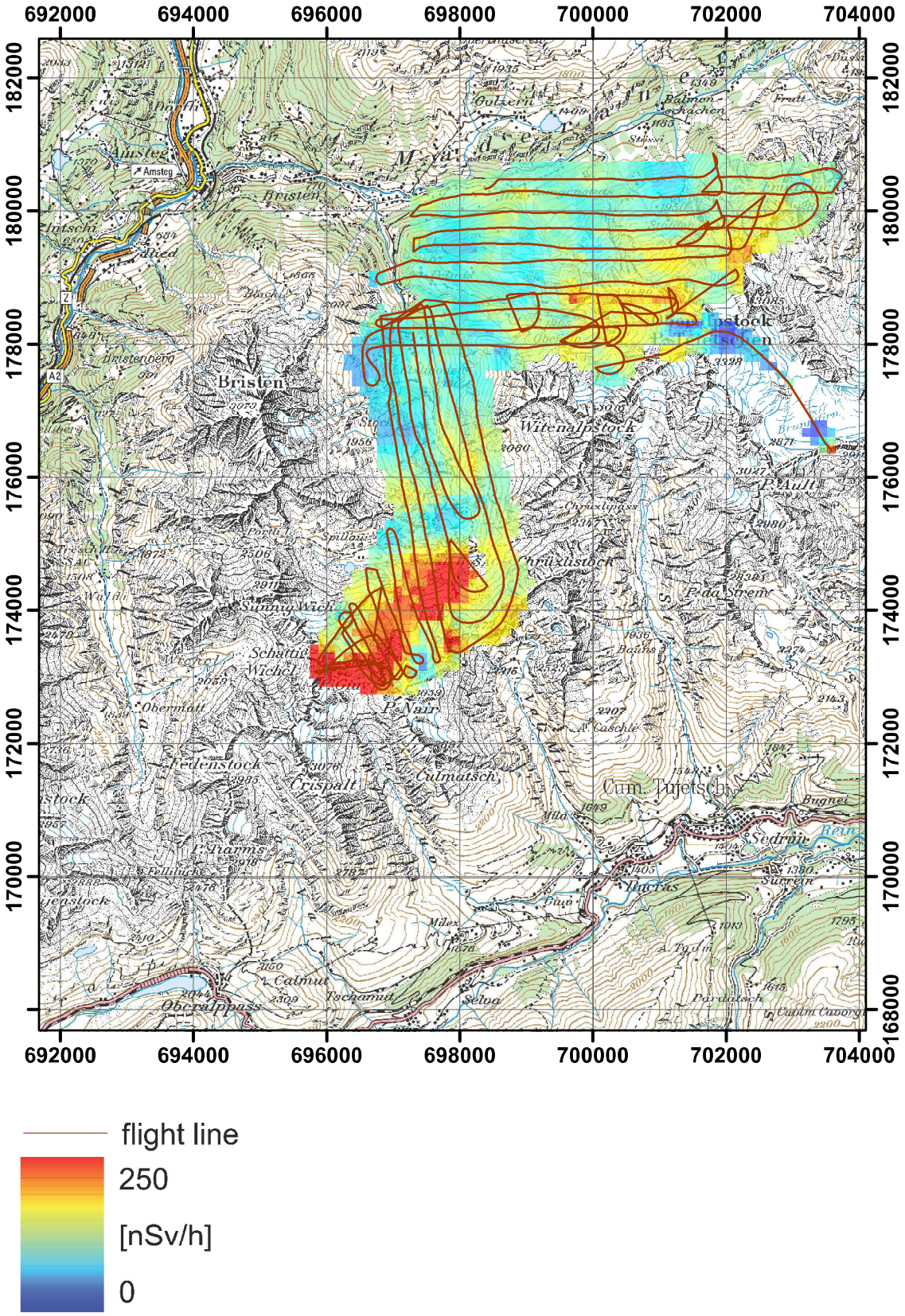

Figure 75: Terrestrial Dose rate in the vicinity of Piz Giuv.
PK200 © 2011 swisstopo (JD100043).

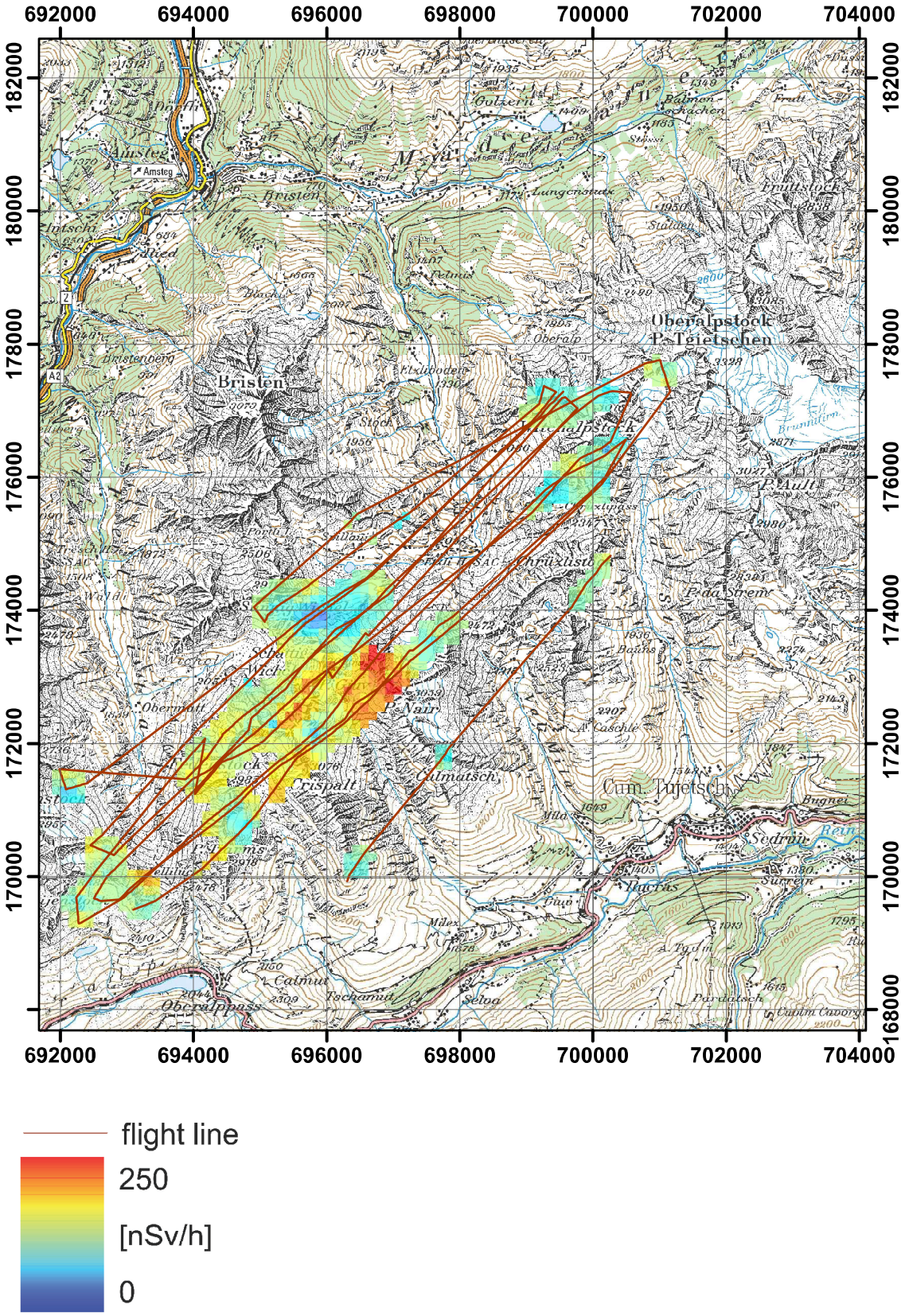

Figure 76: Terrestrial dose rate in the vicinity of Piz Giuv measured 1998. PK200 © 2011 swisstopo (JD100043).

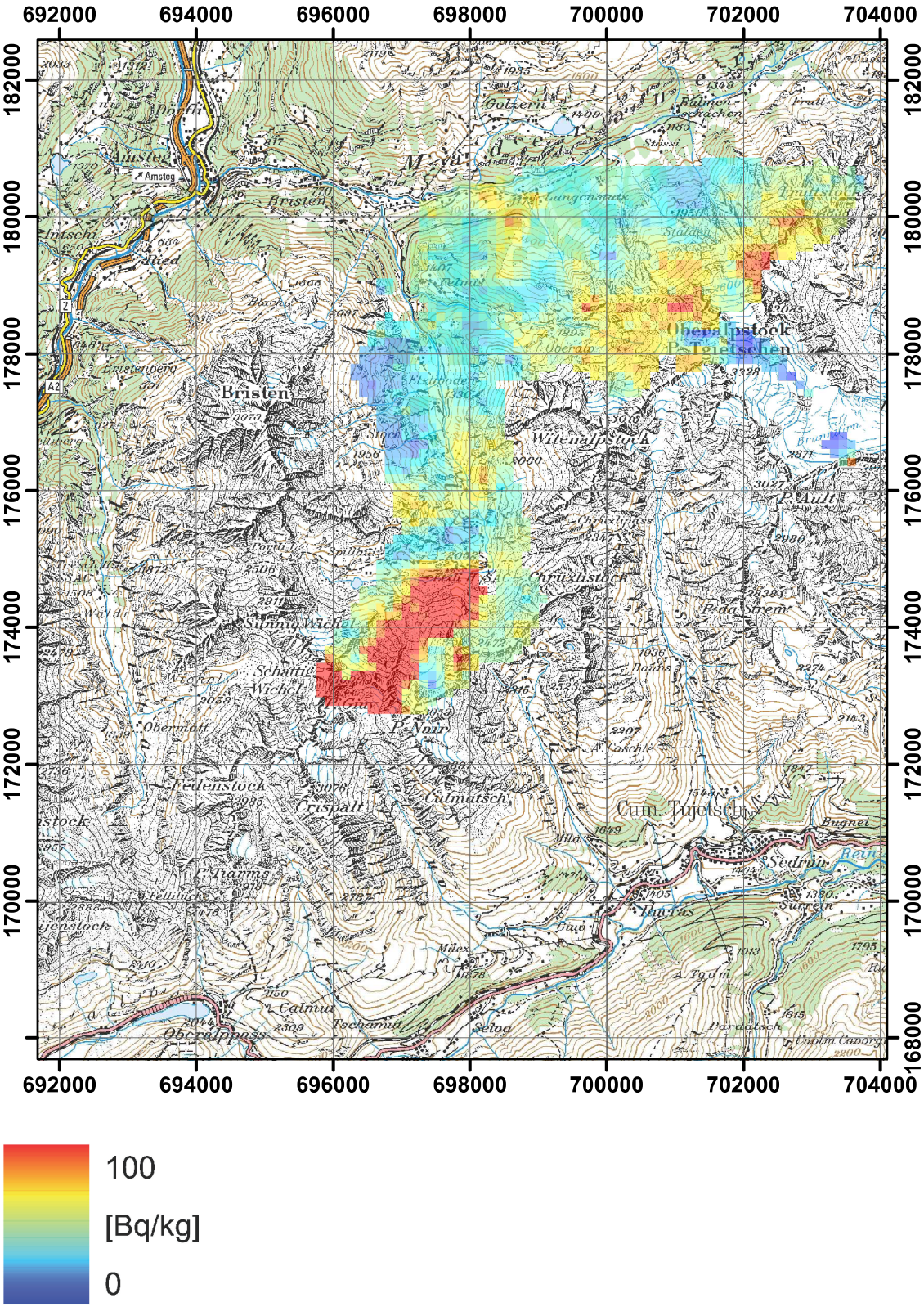

Figure 77: ^{232}Th activity concentration in the vicinity of Piz Giuv. PK200 © 2011 swisstopo (JD100043).

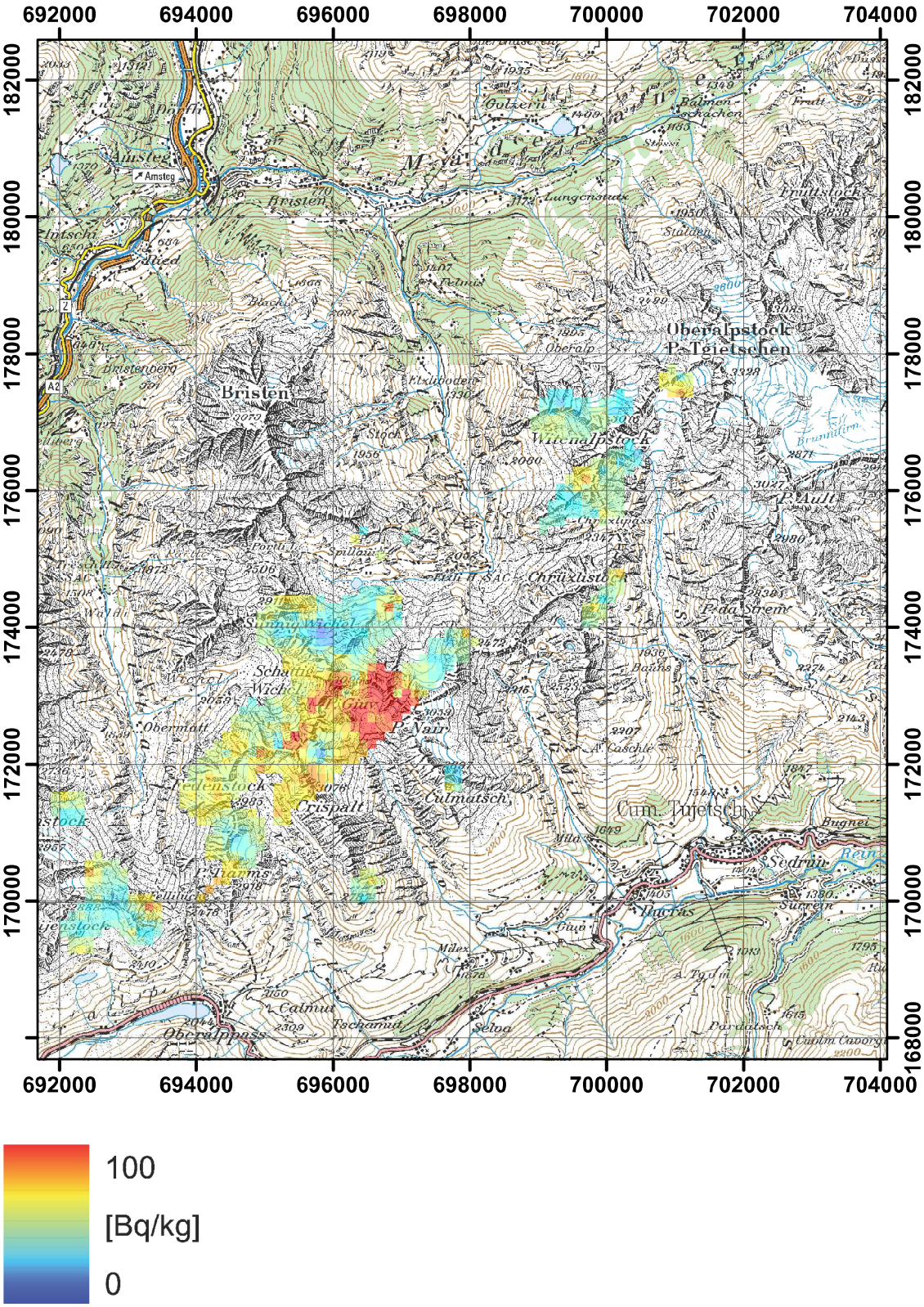

Figure 78: ^{232}Th activity concentration in the vicinity of Piz Giuv measured 1998. PK200 © 2011 swisstopo (JD100043).

Figure 79: Geological map in the vicinity of Piz Giuv.
Geological atlas of Switzerland 1:500 000 © 2011 swisstopo (JD100043).

Paul Scherrer Institut, 5232 Villigen PSI, Switzerland
Tel. +41 56 310 21 11, Fax +41 56 310 21 99
www.psi.ch